

Raskevicius T, 2017, Whole-rock d18O and d2H footprint of the Canadian Malartic Gold deposit, Pontiac subprovince, Quebec, Canada, MSc Thesis, U Laval, QC, 72 p.

NSERC-CMIC Mineral Exploration Footprints Project Contribution 157.



Whole-rock $\delta^{18}\text{O}$ and $\delta^2\text{H}$ footprint of the Canadian Malartic Gold deposit, Pontiac sub-province, Quebec, Canada

Mémoire

Thomas Raskevicius

Maîtrise interuniversitaire en sciences de la Terre
Maître ès sciences (M. Sc.)

Québec, Canada

© Thomas Raskevicius, 2017

**Whole-rock $\delta^{18}\text{O}$ and $\delta^2\text{H}$ footprint of the Canadian
Malartic Gold deposit, Abitibi sub-province, Quebec,
Canada**

Mémoire

Thomas Raskevicius

Sous la direction de :

Georges Beaudoin, directeur de recherche

Kurtis Kyser, codirecteur de recherche

Résumé

Le gisement aurifère de Canadian Malartic est le résultat d'un système hydrothermal qui a altéré les roches métasédimentaires du Groupe de Pontiac, les roches métavolcaniques du Groupe de Piché, les intrusions porphyriques, de même que des dykes mafiques tardifs. La minéralisation en or s'est mise en place par la circulation des fluides hydrothermaux et est responsable des réactions d'échange isotopiques de l'oxygène et de l'hydrogène. Ces réactions sont reflétées dans les valeurs en $\delta^{18}\text{O}$ and $\delta^2\text{H}$ qui peuvent être utilisées pour cartographier l'empreinte isotopique du système minéralisé.

L'empreinte isotopique des grauwackes du Groupe de Pontiac est marquée par une augmentation des valeurs de $\delta^2\text{H}$ de -91‰ jusqu'aux valeurs du bruit de fond d'environ -59‰ à mesure qu'on s'éloigne de la minéralisation. Les valeurs de $\delta^{18}\text{O}$ sont quant à elles relativement constantes à près de 10‰. Les dykes mafiques du secteur enregistrent eux aussi une empreinte isotopique marquée par une augmentation des valeurs de $\delta^2\text{H}$ de -84‰ près de la minéralisation jusqu'aux valeurs du bruit de fond d'environ -73‰, et une décroissance des valeurs en $\delta^{18}\text{O}$ de 9.8‰ jusqu'à 8.3‰ à mesure qu'on s'éloigne de la minéralisation. La composition isotopique du fluide métamorphique en équilibre avec le grauwacke moyen en dehors de l'empreinte, à la température estimée de la minéralisation (~475°C), est de $\delta^{18}\text{O} = 7.6\text{‰}$ et $\delta^2\text{H} = -12\text{‰}$. Ceci est très près des compositions des fluides minéralisateurs du gisement aurifère de Canadian Malartic reportées dans les études précédentes.

Le krigeage des variations régionales des compositions isotopiques en oxygène et hydrogène dans les roches encaissantes du gisement de Canadian Malartic permet de cartographier l'empreinte isotopique. Dans les grauwackes, l'isoplèthe de $\delta^2\text{H} = -59\text{‰}$ encercle le domaine minéralisé et montre un allongement nord-ouest – sud-est, tandis que l'isoplèthe de $\delta^{18}\text{O} = 9.9\text{‰}$ semble aussi contenir le domaine minéralisé bien que très près des valeurs de fond. Dans les dykes mafiques, l'isoplèthe de $\delta^2\text{H} = -73\text{‰}$ contient la minéralisation de même qu'un large secteur au sud-sud-est, tandis que l'isoplèthe $\delta^{18}\text{O} = 8.3\text{‰}$ contient le centre du domaine minéralisé et s'étend vers le sud-est. La géochimie isotopique de l'oxygène et de l'hydrogène des roches encaissantes permet donc de définir une empreinte d'altération cryptique jusqu'à 2,5 km à l'extérieur du gisement de Canadian Malartic.

Abstract

The Canadian Malartic gold deposit is the result of a hydrothermal system that altered the host metasedimentary rocks of the Pontiac Group, metavolcanic rocks of the Piché Group, porphyritic dykes and sills, and mafic dykes. Gold mineralization formed by hydrothermal fluids flowing through these rocks and resulted in exchange reactions of oxygen and hydrogen isotopes. These reactions are reflected in whole-rock $\delta^{18}\text{O}$ and $\delta^2\text{H}$ values of the rocks that can be used to map the isotopic footprint of the mineralized system.

The isotopic footprint in Pontiac greywackes is marked by an increase in $\delta^2\text{H}$ values away from mineralization from -91‰ to background values of ca. -59‰, whereas $\delta^{18}\text{O}$ values remain relatively constant near 10‰. Mafic dykes in the area also record a footprint marked by an increase in $\delta^2\text{H}$ values from -84‰ near mineralization to background values ca. -73‰ and a decrease in $\delta^{18}\text{O}$ values away from mineralization from 9.8‰ to background values of ca. 8.3‰. The isotopic composition of the metamorphic fluid in equilibrium with the average least altered greywacke at upper greenschist to amphibolite conditions of ca. 475°C is approximately $\delta^{18}\text{O} = 7.6\text{‰}$ and $\delta^2\text{H} = -12\text{‰}$. This is very near the compositions of the mineralizing fluid at the Canadian Malartic deposit reported by previous studies.

Kriging of regional variations in oxygen and hydrogen isotopic compositions in host rocks to the Canadian Malartic deposit enables the mapping of the isotopic footprint. In greywackes, the -59‰ $\delta^2\text{H}$ isopleth encircles the mineralized domain and is elongated towards the northwest and southeast, while the 9.9‰ $\delta^{18}\text{O}$ isopleth appears to encircle the mineralized domain, but, remains very close to the background values. In mafic dykes, the -73‰ $\delta^2\text{H}$ isopleth encircles the mineralized domain as well as a large area to the south and southeast while the 8.3‰ $\delta^{18}\text{O}$ isopleth encircles the centre of the mineralized domain and extends over an area towards the southeast. Host rock oxygen and hydrogen isotope compositions thus permit the identification of a cryptic alteration footprint up to 2.5 km outside of the Canadian Malartic.

Table of Contents

Résumé.....	iii
Abstract.....	iv
Table of Contents.....	v
Foreword	viii
Chapter 1 – Introduction	1
1.1 General Framework.....	1
1.2 Approach.....	2
1.3 Presentation of the manuscript.....	3
Chapter 2 – Whole-rock $\delta^{18}\text{O}$ and $\delta^2\text{H}$ footprint of the Canadian Malartic Gold deposit, Pontiac sub-province, Quebec, Canada	5
2.1 Introduction	5
2.2 Geological Framework.....	7
2.2.1 Regional Geology	7
2.2.2 Local Geology.....	8
2.2.3 Gold Mineralization	9
2.3 Methodology.....	9
2.3.1 Sampling methods	9
2.3.2 Analytical Methods.....	10
2.3.3 Data Transformation and Principal Component Analysis.....	11
2.3.4 Geostatistical Models and Kriging	12
2.4 Results.....	13
2.4.1 Whole-rock lithochemistry	13
2.4.2 Whole-rock stable isotopes.....	17
2.4.3 Petrography	20
2.4.4 Principal Component Analysis (PCA)	26
2.4.5 Isotopic variation along sections P1, P2, and P3.....	27
2.4.6 Regional mapping of whole-rock O-H isotopic composition	33
2.5 Discussion	37
2.5.1 Geochemical and isotopic relationships.....	37
2.5.2 Oxygen and hydrogen isotopic footprint.....	38
2.5.3 Fluid oxygen and hydrogen isotopic composition.....	40
2.5.4 Modeling of fluid/rock reactions	42
2.5.5 Canadian Malartic and disseminated gold deposits.....	45

2.5.4 Applications to Exploration.....	47
2.6 Conclusions	47
Acknowledgements	49
2.7 Tables	50
2.8 References.....	61
Chapter 3 – Comparison of company and research samples	65
3.1 Introduction	65
3.2 Methods	65
3.4 Results	66
3.5 Discussion	68
3.5.1 Implications for Exploration Footprint	68
3.6 Tables	69
3.6 References.....	69
Chapter 4 – Summary and Conclusion.....	71
Appendix A.....	73
Appendix B	79

<i>Figure 2.1: Geological Map of the Malartic area with sample locations.....</i>	<i>10</i>
<i>Figure 2.2: Geochemical classification of greywackes.....</i>	<i>14</i>
<i>Figure 2.3: Geochemical classification for mafic dykes after Wilson (2007).....</i>	<i>15</i>
<i>Figure 2.4: Geochemical classification for mafic dykes after Floyd and Winchester (1977).....</i>	<i>15</i>
<i>Figure 2.5: Histograms of oxygen and hydrogen isotopic data.....</i>	<i>18</i>
<i>Figure 2.6: Bivariate plots of whole-rock $\delta^{18}O$ and δ^2H values versus modal mineralogy.....</i>	<i>19</i>
<i>Figure 2.7: Photomicrographs of Pontiac metasedimentary greywackes.....</i>	<i>21</i>
<i>Figure 2.8: Bivariate plots of whole-rock lithochemistry versus greywacke mineralogy.....</i>	<i>22</i>
<i>Figure 2.9: Photomicrographs of isotopically anomalous mafic dykes.....</i>	<i>24</i>
<i>Figure 2.10: Bivariate plots of whole-rock lithochemistry versus mafic dyke mineralogy.....</i>	<i>25</i>
<i>Figure 2.11: PCA of greywacke data.....</i>	<i>26</i>
<i>Figure 2.12: PCA of mafic dyke data.....</i>	<i>27</i>
<i>Figure 2.13: Section P1.....</i>	<i>30</i>
<i>Figure 2.14: Section P2.....</i>	<i>31</i>
<i>Figure 2.15: Section P3.....</i>	<i>32</i>
<i>Figure 2.16: Semivariograms spatial of δ^2H and $\delta^{18}O$ data.....</i>	<i>34</i>
<i>Figure 2.17: Geostatistical models of whole-rock $\delta^{18}O$ and δ^2H values of greywackes.....</i>	<i>35</i>
<i>Figure 2.18: Geostatistical models of whole-rock $\delta^{18}O$ and δ^2H of mafic dykes.....</i>	<i>36</i>
<i>Figure 2.19: Ideal section showing changes in $\delta^{18}O$ and δ^2H.....</i>	<i>40</i>
<i>Figure 2.20: Isotopic compositions of Canadian Malartic waters and natural reservoirs.....</i>	<i>41</i>
<i>Figure 2.21: Fluid/rock isotopic exchange models.....</i>	<i>46</i>
<i>Figure 3.1: Comparison between $\delta^{18}O$ data from the Canadian Malartic and CMIC samples.....</i>	<i>67</i>
<i>Figure 3.2: Comparison between δ^2H data from the Canadian Malartic and CMIC samples.....</i>	<i>67</i>
<i>Figure 3.3: Comparison between the water content of Canadian Malartic and CMIC samples.....</i>	<i>67</i>

Foreword

This memoir entitled “Whole-rock $\delta^{18}\text{O}$ and $\delta^2\text{H}$ footprint of the Canadian Malartic Gold deposit, Abitibi sub-province, Quebec, Canada, is a contribution to the NSERC-CMIC research investigating the footprint of the Canadian Malartic disseminated gold deposit.

The work focuses on the delineation of the fossil hydrothermal footprint surrounding the low grade and bulk tonnage Canadian Malartic deposit through the analysis of whole-rock isotopic and geochemical data collected from rocks in the surrounding area. Isotopic data are particularly useful in the understanding of geological processes as it gives insight into the conditions at which sensitive fluid/rock exchange reactions took place. This, coupled with the geochemical signatures of the hydrothermally altered rocks throughout to footprint can be used to develop regional scale ore deposit models.

The following chapters in this work suggest possible conceptual models that may explain the isotopic and geochemical data that are presented. However, the focus of this work is entirely pragmatic, and in this sense the identification of the isotopic footprint surrounding the Canadian Malartic deposit is an exciting accomplishment. In particular, the $\delta^2\text{H}$ footprint to the deposit may prove especially practical in the application to exploration programs searching for hydrothermal ore deposits. As hydrogen isotope data are significantly less costly to attain, and remains sensitive to isotope exchange reactions down to very low fluid/rock ratios.

The work presented herein is only possible thanks to the support from my supervisors Georges Beaudoin (Université Laval) and Kurt Kyser (Queen’s University). The research associate Stephane Perrouty (Western University) to the Canadian Malartic footprints project and PhD candidate Nicolas Gaillard (McGill University) who is working on a sister project to this work have also made substantial contributions to this work. Discussions and reviews from many others involved with the Canadian Malartic footprints project have also helped shape this memoir. Financial aid from both NSERC and industry sponsors as well as a SEG graduate student fellowship award has made this research possible.

Finally, I would like to thank the encouragement of my friends Clovis, Sheida, Nelly, Erik, Neal, Brady and Jessica.

Chapter 1 – Introduction

1.1 General Framework

The Canadian Malartic gold mine is owned by the Canadian Malartic General Partnership a 50/50 joint venture between Agnico Eagle Mines Ltd. and Yamana Gold Inc. in the town of Malartic, Quebec in the Abitibi subprovince of the Canadian Shield. The region is part of the world's largest greenstone belt covering an area in excess of 85 000² km between Ontario and Quebec (Card, 1990). The Abitibi greenstone belt has been producing gold as well as other metals since the beginning of the twentieth century. As such, over the past hundred years, the area has given rise to countless mining ventures primarily focused on exploiting high grade structurally delineated gold veins and leaving behind much more extensive sub-economic disseminated haloes. In recent years, advancements in technology as well as changes on the global economic stage have proved that once sub-economic gold resources can be mined at a profit in the Abitibi greenstone belt. The Canadian Malartic mine is an example of this rejuvenated interest in disseminated mineralization previously not considered for its economic potential. Throughout the Abitibi greenstone belt, many of these disseminated gold deposits are found in association with Timiskaming-age (2,680-2,672 Ma) syenitic to monzonitic porphyritic stocks (Robert 2001). The spatial association with these stocks, geochemical alteration, and metallic signature of mineralization have suggested that at least some of these disseminated gold deposits are genetically linked with the porphyritic intrusions (Thompson and Newberry 2000; Robert 2001; Helt et al. 2014; De Souza et al. 2015; Perrouty et al. 2017).

The deposit being mined at Canadian Malartic has measured and indicated ore reserves of 314.2 Mt with an average grade of 1.07 g/t for 10.8 Moz of gold (Gervais et al. 2014). The original Canadian Malartic mine was discovered in 1925, but work on the property quickly stopped due to a lack of financing. Subsequent geophysical work revived interest in the property in the early 1930's. Drilling began in 1936 followed by the sinking of a shaft and construction of a mill in 1939 (Halet, 1944). Production and exploration continued intermittently throughout the latter half of the twentieth century with ownership changing hands a number of times. In 2004, Osisko Mining corp. purchased the bulk of the property's mining claims with the specific intent to explore the area for low grade and high tonnage mineralization envisioned as an Archean porphyry deposit type (Wares and Burzynski, 2011). Diamond drilling by Osisko soon after defined the current Canadian Malartic ore body and production began again in 2011.

Mineral explorationists are constantly searching for the next undiscovered ore body. These discoveries however, are becoming increasingly harder to make as prospective areas become thoroughly explored. The Natural Sciences and Engineering Research Council and the Canada Mining Innovation Council (NSERC-CMIC) is a joint national research network focused on developing new integrated vectors towards mineralization. The NSERC-CMIC network is collecting multiparameter data sets on Canada's most significant ore deposits. The data are then being holistically integrated in order to define the most distal signature footprint to the deposits and vector in towards the mineralized core.

This study is a contribution to the investigation into the footprint of the Canadian Malartic disseminated gold deposit. As part of the NSERC-CMIC team working at the Canadian Malartic site, the focus of this project is to define the footprint to the Canadian Malartic deposit with respect to fluid flow pathways and fluid/rock reactions using geochemistry combined with whole-rock oxygen and hydrogen isotopic data. All data will be integrated with the work of other researchers investigating the mineralogy, geochemistry, geology, geophysics, and petrophysics of the footprint. Findings from this project as well as the complimentary research by the NSERC-CMIC team have implications on both district scale ore forming processes as well as the determination of the largest possible exploration target attributable to the deposit. Identifying the Canadian Malartic footprint will aid in the discovery of analogous deposits at depth or in poorly exposed terrains.

1.2 Approach

This project is focused on mapping and understanding the fossil hydrothermal footprint associated with the Canadian Malartic deposit. The hydrogen and oxygen isotopic variations throughout the footprint of the Canadian Malartic deposit are expected to yield fundamental insights into district scale ore deposit models as well as exploration vectors for the search of similar types of ore deposits. The $\delta^{18}\text{O}$ and $\delta^2\text{H}$ values of hydrothermally altered rocks preserve evidence of isotopic exchange reactions that are extremely sensitive to fluid/rock interaction. Unlike other geochemical tracers, whole-rock isotopic compositions can be used to model these exchange reactions between the fluids and host rocks. Therefore, this study offers insight into the actual fluid/rock history that has affected the mineralized rocks. With isotopic data, it is possible to fingerprint fluid sources, quantify fluid/rock interaction, and deduce the temperature of alteration. Isotopic data, when integrated with whole-rock geochemical data and constrained by geological context, can provide important constraints on the processes affecting the host rocks to the Canadian Malartic disseminated gold deposit. The main objectives of this project are outlined here:

1. Outline the oxygen and hydrogen isotopic footprint to the Canadian Malartic deposit
2. Advance exploration methods by effectively increasing the exploration target beyond the shell of mineralization and assessing the appropriate type of sampling methods to be used in mineral exploration.
3. Model the oxygen and hydrogen isotope exchange in the Canadian Malartic country rocks
4. Understand the fluid/rock interaction throughout the footprint of the Canadian Malartic deposit

These objectives are attained by the consideration and integration of whole-rock oxygen and hydrogen isotope and geochemical data over a two-dimensional 5 x 4 km surface, dominantly south of the Canadian Malartic deposit. The mapping is facilitated by three sections, two of which are approximately 3 km in length and are labeled P1 and P2 originating in the Canadian Malartic deposit and extending due south. The third section labeled P3 cuts through the deposit from the weakly mineralized Cartier zone to the northwest and ending near the weakly mineralized Bravo zone towards the southeastern margin of the mapping area (Fig. 2.1). Additional samples are taken from off-section diamond drill cores and outcrops in order to model regional distribution. Integration of oxygen and hydrogen isotope composition with geochemical data collected from these samples relates fluid/rock interaction with the chemical signature of alteration throughout the footprint. Also, the use of standard isotopic fractionation equations and the isotopic composition of natural water reservoirs aids in the understanding of the isotopic variation and constrains quantitative fluid/rock interaction models. The hydrothermal alteration evident with increasing fluid/rock interaction is also reflected in changes in other rock properties such as mineralogy and density. Therefore, these relationships will be important to the integration of data across NSERC-CMIC subprojects.

1.3 Presentation of the manuscript

The preceding chapters of this manuscript document the research into the oxygen and hydrogen isotopic footprint of the Canadian Malartic deposit. The manuscript includes 4 chapters. Chapter 1 (this chapter) outlines the research problems, objectives, and structure of the thesis. Chapter 2 is written as a stand-alone article to be submitted to the peer-reviewed scientific journal *Mineralium Deposita*. The article making up Chapter 2 first presents the geology of the Canadian Malartic deposit and surrounding area. This article goes on to discuss the analytical methods and results of the whole-rock isotopic and geochemical analysis used to determine the footprint to the Canadian Malartic deposit. The article ends by discussing computed models of fluid/rock isotopic exchange and how these models compare with empirical data collected from the footprint of Canadian Malartic deposit and how this fits in with global models for the formation of disseminated gold deposits. Chapter 3 presents a comparison of oxygen and

hydrogen isotopic data collected from two batches of samples. The first batches of samples were collected ca. 2008 as part of a diamond drilling program defining the deposit. The second batch was collected as part of the NSERC-CMIC footprints research. This chapter assesses the application of pre-existing sample libraries for the use in exploration programs using oxygen and hydrogen isotopic data. The final chapter (Chapter 4) presents general conclusions determined by this study and an overall summary of the manuscript.

This research was primarily carried out by the principal author with the support of his supervisors, Georges Beaudoin (Université Laval) and Kurt Kyser (Queens University). This research has also been made possible due to the efforts of other NSERC-CMIC team members including research associate Stephane Perrouty (Western University) and PhD candidate Nicolas Gaillard (McGill University).

Chapter 2 – Whole-rock $\delta^{18}\text{O}$ and $\delta^2\text{H}$ footprint of the Canadian Malartic Gold deposit, Pontiac sub-province, Quebec, Canada.

Abstract

The Canadian Malartic gold deposit is the result of a hydrothermal system that altered the host metasedimentary rocks of the Pontiac Group, metavolcanic rocks of the Piché Group, porphyritic dykes and sills, and mafic dykes. Gold mineralization formed by hydrothermal fluids flowing through these rocks and resulted in exchange reactions of oxygen and hydrogen isotopes. These reactions are reflected in whole-rock $\delta^{18}\text{O}$ and $\delta^2\text{H}$ values of the rocks that can be used to map the isotopic footprint of the mineralized system.

The isotopic footprint in Pontiac greywackes is marked by an increase in $\delta^2\text{H}$ values away from mineralization from -91‰ to background values of ca. -59‰, whereas $\delta^{18}\text{O}$ values remain relatively constant near 10‰. Mafic dykes in the area also record a footprint marked by an increase in $\delta^2\text{H}$ values from -84‰ near mineralization to background values ca. -73‰ and a decrease in $\delta^{18}\text{O}$ values away from mineralization from 9.8‰ to background values of ca. 8.3‰. The isotopic composition of the metamorphic fluid in equilibrium with the average least altered greywacke at upper greenschist to amphibolite conditions of ca. 475°C is approximately $\delta^{18}\text{O} = 7.6‰$ and $\delta^2\text{H} = -12‰$. This is very near the compositions of the mineralizing fluid at the Canadian Malartic deposit reported by previous studies.

Kriging of regional variations in oxygen and hydrogen isotopic compositions in host rocks to the Canadian Malartic deposit enables the mapping of the isotopic footprint. In greywackes, the -59‰ $\delta^2\text{H}$ isopleth encircles the mineralized domain and is elongated towards the northwest and southeast, while the 9.9‰ $\delta^{18}\text{O}$ isopleth appears to encircle the mineralized domain, but, remains very close to the background values. In mafic dykes, the -73‰ $\delta^2\text{H}$ isopleth encircles the mineralized domain as well as a large area to the south and southeast while the 8.3‰ $\delta^{18}\text{O}$ isopleth encircles the centre of the mineralized domain and extends over an area towards the southeast. In all, whole-rock isotopes have been used to identify a cryptic alteration footprint up to 1 and 2.5 km outside of the Canadian Malartic deposit for O and H isotopic values respectively.

2.1 Introduction

Canadian Malartic is a world-class low-grade disseminated gold deposit situated in the Superior province of northern Quebec. Current measured and indicated resources and reserves of the deposit are 10.8 Moz in

314.2 Mt with an average grade of 1.07g/t (Gervais et al. 2014). Several authors have studied this deposit in an effort to understand the nature and origin of the mineralization. Descriptions of geology, petrology, mineralogy, and structure have been used to delineate gold mineralization (e.g. Beaulieu 2010; Derry 1939; Halet 1944; Sansfacon and Hubert 1990). The Canadian Malartic deposit is similar to many other Archean orogenic gold deposits throughout the Abitibi greenstone belt in terms of structural relationships, timing of mineralization, and alteration styles (Bateman et al. 2008). Some workers have suggested that the mineralizing fluids at the Canadian Malartic deposit were at least in part exsolved from a fractionally crystallizing igneous melt (e.g. Issigonis 1980; Helt et al. 2014; Perrouty et al. 2017). However, the magmatic water source was challenged by Beaudoin and Raskevicius (2014) who showed the oxygen and hydrogen isotopic ratios of biotite from veins are in equilibrium with metamorphic water. Subsequent studies have also proposed a hybrid model, whereby, characteristics of the Canadian Malartic deposit are explained by an early magmatic-hydrothermal event superimposed by a later hydrothermal event synchronous with the second stage of regional deformation (De Souza et al. 2015). Despite the controversy over the source of the mineralizing fluid, all workers accept that fluid/rock interactions were responsible for the extensive alteration associated with the gold mineralization at the Canadian Malartic deposit. Moreover, the exchange of oxygen and hydrogen isotopes between the rock and the hydrothermal fluid is recorded in subtle mass changes that are reflected in the $\delta^{18}\text{O}$ and $\delta^2\text{H}$ values in the host rocks surrounding the deposit. Using the $\delta^{18}\text{O}$ and $\delta^2\text{H}$ values from the host rocks it is possible to quantify the fluid/rock interaction, and by mapping these data it is possible to gain a detailed understanding of the fossil hydrothermal system defining the isotopic footprint to the Canadian Malartic deposit.

Mapping the hydrothermal fluid flow systems related to mineral deposits using oxygen and hydrogen isotopes has been used to understand ore deposit genesis (Taylor 1974). Mapping the hydrothermal footprints of ore deposits have shown that the isotopic footprint can generate an exploration target orders of magnitude greater than the deposit itself (e.g. Cathles et al. 1993). Also, these methods provide tools effective on a regional scale that help study and understand hydrothermal processes. Regional variations in $\delta^{18}\text{O}$ of vein minerals and the sources of their parental fluids around the Val-d'Or orogenic vein field are presented in Beaudoin and Pitre (2005). A numerical model of the isotopic data showed that fluid flow throughout the region was controlled by a lower permeable boundary corresponding with middle to deep crustal rocks volatilizing metamorphic fluids, and an upper impermeable boundary breached by deeply rooted crustal structures which focus the upward migration of the auriferous fluids (Beaudoin et al. 2006). Elsewhere in the Abitibi greenstone belt, studies have examined the control of fluid flow pathways on the formation of volcanogenic massive sulfide (VMS) mineralization in the Noranda camp (e.g. Cathles et al. 1993; Taylor et al. 2014). Examples of oxygen and hydrogen isotope mapping have also been used on

much younger epithermal systems of the American Cordillera (Criss and Fleck, 1990; Criss et al. 2000; Rice et al. 2001). In general, these studies have shown that mass exchange reactions recorded in whole-rock isotope compositions have the potential not only to identify a cryptic or invisible alteration footprint, but, also provide insight into the mineralizing process. The mapping of oxygen and hydrogen isotopic data integrated with whole-rock geochemical data at the Canadian Malartic deposit provides evidence to understand the hydrothermal processes affecting the host rocks to the deposit.

This paper presents new oxygen and hydrogen isotopic and geochemical data from the rocks that host the Canadian Malartic deposit. The purpose of this study is to: (1) understand the fluid/rock interaction throughout the footprint of the deposit, (2) model the oxygen and hydrogen isotope exchange reactions between the mineralizing fluid and host rocks, and (3) provide a foundation for the application of oxygen and hydrogen isotopic data to real world exploration methods. To achieve these goals the major sources of geochemical and isotopic variation throughout the host rocks have been extracted by means of principal component analysis (PCA) and their geological context is discussed. The oxygen and hydrogen isotopic data are used to map in plan and in sections the stable isotopic variations throughout the study area. Finally, fluid/rock exchange is used to model the variation in oxygen and hydrogen isotopic compositions throughout the host rocks to understand the fluid flow history throughout the footprint of the deposit.

2.2 Geological Framework

2.2.1 Regional Geology

The Canadian Malartic deposit is located in the Archean Superior province south of the Cadillac-Larder Lake Tectonic Zone (CLLTZ). The CLLTZ is a crustal scale fault zone that marks the contact between the Abitibi and Pontiac subprovinces. The Abitibi greenstone belt is dominantly comprised of greenschist facies volcano-sedimentary rocks intruded by syn- to late plutonic supracrustal assemblages (Card, 1990). Throughout the southern Abitibi greenstone belt, volcanic rocks typically alternate through the stratigraphy from komatiitic and tholeiitic basalt, rhyolite, and calc-alkaline andesite, reflecting the protracted interplay between an evolving volcanic arc and a subjacent mantle plume (Ayer et al. 2002; Scott, 2002; Wyman et al. 2002). The volcanism that constructed the southern Abitibi greenstone belt occurred between 2750 Ma and 2675 Ma (Ayer et al. 2002) and erosion of the volcanic edifices resulted in deposition of the turbiditic mudstones, greywackes, and volumetrically minor conglomerates of the Pontiac Group as a synorogenic distal flysch facies in a foreland basin (Feng et al. 1993; Davis 2002). Ongoing convergent plate tectonics eventually led to the development of an accretionary wedge and the

docking of the Pontiac group to the southern Abitibi greenstone belt south of the CLLTZ (Card, 1990; Daigneault et al. 2002). A first phase of deformation (D_1) is recorded as a regional northeast-southwest shortening event leading to folding and faulting of strata throughout the area (Desrochers and Hubert, 1996; Robert, 2001). The second phase of deformation (D_2) commenced as an overall north-south shortening event responsible for the dominantly east-west but locally rotated foliation throughout the area. During D_2 , the principal direction of compression gradually rotated incorporating a dextral shear component, culminating with a relatively minor east-west oriented transpressional event (D_3) (Desrochers and Hubert, 1996). The east-west transpression during the late- D_2 and D_3 events opened pull-apart basins along major tectonic zones such as the CLLTZ, in which deposition of the Timiskaming Group took place (Thurston and Chivers 1990). The Timiskaming Group is typified by pebble-cobble conglomerates of a fluvial setting has been dated to be < 2680 Ma and unconformably overlies all older units in the Abitibi greenstone belt (Hyde 1980; Corfu et al. 1991).

2.2.2 Local Geology

The Canadian Malartic deposit is hosted by metavolcanic rocks of the Piché Group, clastic metasedimentary rocks of the Pontiac Group, and monzo- to granodioritic porphyries intruded into the Pontiac Group. The Piché Group consists of mafic to ultramafic rocks confined to a corridor <1 km wide within the highly strained CLLTZ (Sansfacon and Hubert, 1990). Sporadically in the Piché Group, komatiitic flows display relict spinifex textures. However, most of the Piché Group rocks in the Malartic area are pervasively metamorphosed to serpentine and locally, chlorite-carbonate-talc schists (Issigonis, 1980; Sansfacon and Hubert, 1990). The Pontiac Group, south of the CLLTZ hosts the bulk of the Canadian Malartic deposit. The Pontiac Group is volumetrically dominated by metaturbaditic greywacke with a lesser proportion of mudstone and conglomerate (Daigneault et al. 2002; Davis, 2002). Deposition of the Pontiac Group has been constrained from detrital zircons and the Lac Fournière pluton to a maximum age of 2685 ± 3 Ma and a minimum of 2682 ± 1 Ma (Davis, 2002). Near the Canadian Malartic deposit, the metamorphic grade increases from a chlorite-biotite domain in the north near the CLLTZ, to reach garnet and staurolite isograds approximately 3 km south. The Pontiac Group is intruded by thin, equigranular, gabbroic to quartz-monzodioritic dykes and sills (herein referred to as “mafic dykes”), typically from 3 to 30 cm in thickness and rarely exceeding 1m. Porphyritic intrusions in the Malartic area cross cut both the Piché Group as well as the metasedimentary Pontiac Group, and have been dated to syn-Timiskaming ages of 2677 and 2679 Ma (Helt et al. 2014; De Souza et al. 2015). These intrusions are deformed by D_2 and are commonly altered and mineralized along contacts with the Pontiac metasedimentary rocks (Issigonis 1980; Desrochers and Hubert 1996; Helt et al. 2014; De Souza et al. 2015).

2.2.3 Gold Mineralization

Gold mineralization at the Canadian Malartic deposit overwhelmingly occurs south of the CLLTZ (De Souza et al. 2015). The Sladen fault is a splay of the CLLTZ that extends into the Pontiac subprovince and much of the gold mineralization forms proximal to this fault. The Canadian Malartic mine incorporates the low grade disseminated gold peripheral to the higher grade historic underground workings of the original Canadian Malartic, Sladen, Barnet, and East Malartic mines, all of which were situated along the trace of the Sladen fault. The mineralization follows two principal orientations: 1) a dominant east-west orientation that is generally subparallel to the Sladen fault, and 2) a subordinate northwest-southeast orientation that is parallel to S_2 , the principal foliation attributed to D_2 (De Souza et al. 2015; Perrouty et al. 2017).

Typically, gold mineralization at the Canadian Malartic deposit occurs as microscopic grains of native gold and gold tellurides associated with minor amounts of pyrite (<5% by volume) disseminated throughout the hydrothermally altered host rocks and in quartz-carbonate veins parallel to S_2 (Helt et al. 2014; Perrouty et al. 2017). Mineralization also includes subordinate pyrrhotite, sphalerite, and chalcopyrite within veins and disseminated preferentially throughout altered greywackes and mudstones, whereas, galena and molybdenite occurs preferentially in veins and disseminations throughout the monzodiorite and granodiorite porphyries (De Souza et al. 2015).

Gold mineralization is mostly hosted by altered Pontiac greywackes. Proximal alteration of greywackes is characterized by a pervasive beige to brown colour imparted by a very fine-grained albite, microcline, dolomite, calcite, quartz, and biotite assemblage. Distal alteration of greywackes is typified by a biotite, white mica, and plagioclase mineral assemblage with minor amounts of carbonate and pyrite that increase towards mineralization (De Souza et al. 2015). In these altered metasedimentary rocks, overall mass gains are reported in most alkali and alkali earth metals (K, Na, Ca, Ba) select transition metals and metalloids (Au, Ag, Mo, W, Cd, Pb, Sb, Bi, Te) as well as S. Mass losses were reported mostly for a limited number of divalent cations including Fe, Mg, and Cu (Helt et al. 2014).

2.3 Methodology

2.3.1 Sampling methods

A total of 120 samples were collected over a 4 by 5 km area south of the Canadian Malartic deposit and along three sections labeled P1, P2 and P3. Sections P1 and P2 begin in the Canadian Malartic open pit and extend approximately 3 km due south. Section P3 starts northwest of the Canadian Malartic deposit,

cuts obliquely through the deposit, extending for a length of approximately 9 km from the weakly mineralized Cartier zone in the northwest to the Bravo zone in the southeast of the study area. Of the 120 samples, 95 samples are from drill cores and 25 are from outcrops to provide a regional distribution (Fig. 2.1). Samples consist of Pontiac greywackes and mafic dykes and were selected to be homogenous and free of veins for geochemical and isotopic analysis. Vein fill and near-surface oxidation were removed prior to analysis. Typically, one representative sample of Pontiac greywacke and mafic dyke was taken from each drill core on the sections. However, P2 was more extensively sampled with 1 to 5 samples of greywackes taken from each drill core.

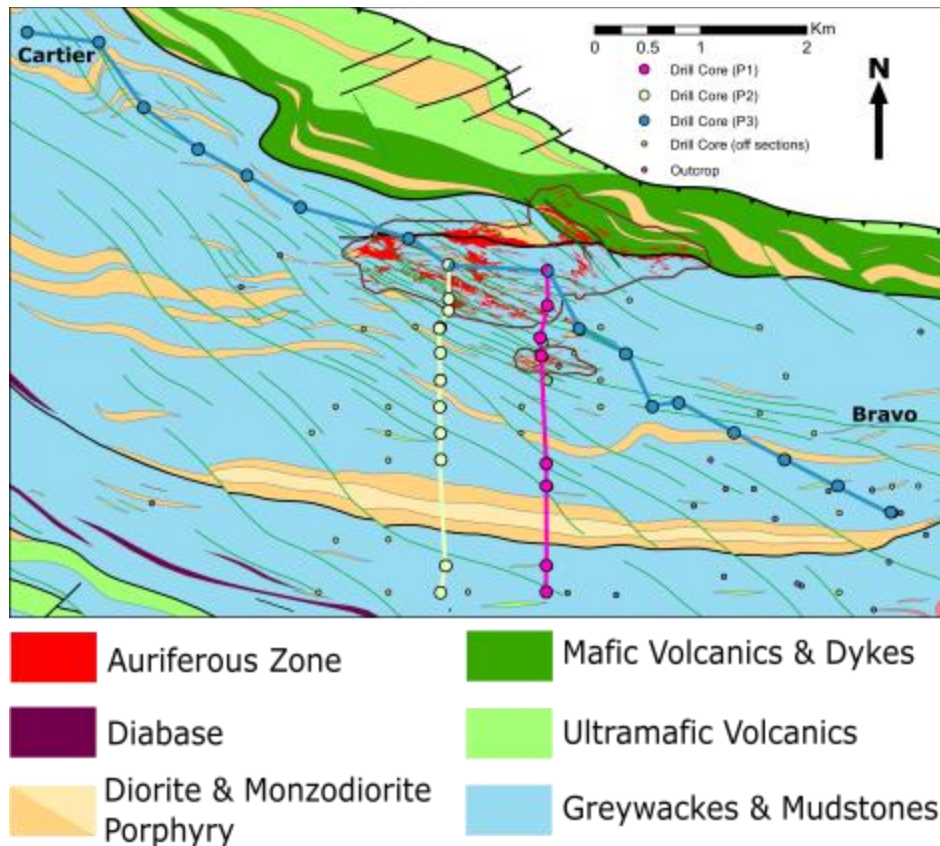


Figure 2.1: Geological Map of the Malartic area with sample locations and trace of sections P1, P2 and P3. The mineralized domain is shown in red delineating areas greater than 300 ppb Au within the confines of the 2013 open pit design. Geological map modified after Perrouty et al. (2017).

2.3.2 Analytical Methods

Samples were crushed, pulverized and sieved to less than 106 microns at ActLabs or ALS laboratories. The Au values were measured by ALS laboratories (Vancouver, British Columbia) by digestion in aqua

regia followed by analysis using inductively coupled plasma mass spectrometry (ICP-MS). Major elements were analyzed at SGS laboratories (Vancouver, British Columbia) by wavelength-dispersive X-ray fluorescence spectrometry (WD-XRFS) while Zr, Y, and Nb were analyzed by ICP-AES after fusion with a sodium peroxide flux. C and S were determined using Leco® inductive combustion and infrared detection. Results below the lower limits of detection make up less than 2% of the data for any given analyte and have been replaced by the lower detection limit divided by the square root of two (Croghan and Egeghy 2003).

Oxygen and hydrogen isotopic analyses of whole-rock powders were carried out at the Queen's Facility for Isotopic Research (QFIR) in Kingston, Ontario. All isotopic data are reported using the δ -notation, whereby isotopic ratios are reported as values relative to Vienna Standard Mean Ocean Water (V-SMOW). The $\delta^{18}\text{O}$ values were determined by reacting the samples with BrF_5 overnight in Ni tubes heated to 550°C . The oxygen gas released was then converted to CO_2 by reaction with graphite (Clayton and Mayeda, 1963) and oxygen isotope ratios were measured using a Finnigan MAT 252 Isotope Ratio Mass Spectrometer. The $\delta^2\text{H}$ values were measured using a method adapted from Sharp et al. (2001) after degassing in silver capsules for 1 hour and then reduced in a graphite tube at 1450°C to convert the released H_2O into H_2 . The isotopic composition of the $\text{H}_{2(\text{g})}$ was measured using a DELTAplusXP IRMS, and the volume of $\text{H}_{2(\text{g})}$ was used to determine wt.% H_2O . Accuracy and precision of isotope data were determined by repeat analyses of internal standards and duplicate samples. Reproducibility was determined to be better than 0.2‰ and 2‰ (1σ) for oxygen and hydrogen, respectively.

2.3.3 Data Transformation and Principal Component Analysis

Geochemical data are normally presented as parts of a whole (% , ppm, or ppb) therefore closure of geochemical data to 100% can lead to problems when interpreting correlations (e.g. Chayes 1960; Pawlowsky-Glahn and Egozcue 2006). In a closed data set, correlations of compositional data may not necessarily represent geological processes and therefore potentially lead to erroneous interpretations. The use of log-ratio data transformations for statistical analysis involves the comparison of relative magnitudes of variables as opposed to absolute magnitudes (Aitchison 1986; Rollinson 1993). Three common types of log-ratio data transformations are: (1) isometric log-ratio (ilr), (2) additive log-ratio (alr), and (3) centered log-ratio (clr) (Aitchison 1986; Egozcue et al. 2003). With ilr transformations, the raw data matrix is transformed using a chosen orthonormal basis of reference with one less dimension than the raw data. With alr, data are transformed by taking the logarithm of each sample's components divided by another component. With clr, transformations are made using the logarithm of each component divided by the geometric mean of all components for each sample. (Aitchison 1986; Egozcue et al. 2003; Filzmoser

et al. 2009). For the application of transformed geochemical compositional data to multivariate statistical techniques, clr transformation has been used (Egozcue et al. 2003; Filzmoser et al. 2009; Makvandi et al. 2016). In contrast, isotopic values reported in the δ -notation are not considered to be affected by closure as isotopic values are based on atomic ratios of isotopes for one element and are independent of the absolute concentration of that element (Dodson 1982). Therefore, the $\delta^2\text{H}$ and $\delta^{18}\text{O}$ values are not clr-transformed.

Using the clr-transformed data and whole-rock isotopic values, principal component analysis (PCA) was conducted using the ioGAS® geochemical data processing software to detect correlations within the multivariate data set. PCA is a method by which a complex, multivariate data set can be simplified to a smaller set of orthogonal and uncorrelated principal components that capture the main sources of variance within the data set (Le Maitre 1982; Rollinson 1993). With this technique, the extracted principal components of the original data set are ranked in the order of decreasing variance.

2.3.4 Geostatistical Models and Kriging

Geostatistical analysis of oxygen and hydrogen isotopic values enables modeling of the spatial variation of these data (Clark and Harper 2000). Geostatistical analysis was conducted using ArcGIS® software on the isotopic data excluding three outlying mafic dyke samples determined to have abnormal mineralogy and are discussed later. Semivariograms of whole-rock isotopic data have been constructed using $\delta^{18}\text{O}$ and $\delta^2\text{H}$ data for mafic dikes and $\delta^{18}\text{O}$ data for greywackes. The $\delta^2\text{H}$ data for greywackes have been converted to positive values so they can be log transformed before construction of the semivariogram. This data transformation was used as it extracted strong spatial continuity in the $\delta^2\text{H}$ data. The greywacke data were converted back to negative values for mapping. All semivariograms have been fitted with functions corresponding to orthogonal major and minor ranges that model the spatial variation of the data between observation points. The major and minor ranges define to the long and short axes of the search ellipse used to model the isotopic variation throughout the study area.

The $\delta^{18}\text{O}$ and $\delta^2\text{H}$ values of greywackes and mafic dykes throughout the study area can be estimated using simple kriging methods. Simple kriging estimates the $\delta^{18}\text{O}$ and $\delta^2\text{H}$ values of greywackes and mafic dykes at any point within the study area using neighbouring points within the confines of the search ellipse based on the functions determined from the semivariograms. Simple kriging assumes the average value of each dataset remains constant over the entire study area (Davis 1973).

2.4 Results

2.4.1 Whole-rock lithochemistry

Major element geochemical data are given in Table 2.1. Greywacke samples ($n = 87$) range from 62 - 80 mol% SiO_2 ($\bar{x} \pm 1\sigma = 72.8 \pm 2.7\%$), 9 -15 mol% Al_2O_3 ($\bar{x} \pm 1\sigma = 10.6 \pm 1.1\%$), 1.3 - 7.6 mol% Na_2O ($\bar{x} \pm 1\sigma = 3.7 \pm 0.9\%$), and 0.6 - 4.0 mol% K_2O ($\bar{x} \pm 1\sigma = 1.9 \pm 0.7\%$). The geochemical classification of sedimentary rocks of Herron (1988) based on $\log(\text{SiO}_2/\text{Al}_2\text{O}_3)$ versus $\log(\text{Na}_2\text{O}/\text{K}_2\text{O})$ in wt% oxides confirms the field description of these rocks and although these rocks are altered, the majority of samples plot within the field of greywackes (Fig. 2.2). Au values in greywackes range from below detection limits (0.0002 ppm) to 1.5 ppm ($\bar{x} \pm 1\sigma = 0.04 \pm 0.22$ ppm), wt% H_2O ranges from 0.49% to 3.9% ($\bar{x} \pm 1\sigma = 1.9 \pm 0.76\%$), wt% S ranges from 0.013% to 1.7% ($\bar{x} \pm 1\sigma = 0.26 \pm 0.22\%$), and wt% C ranges from 0.006% to 0.6% ($\bar{x} \pm 1\sigma = 0.07 \pm 0.1\%$; Table 2.1).

Mafic dyke ($n = 33$) major element geochemistry is consistent with typical gabbros. SiO_2 ranges 49 - 64 Mol% ($\bar{x} \pm 1\sigma = 57.2 \pm 2.9\%$), Na_2O ranges 0.5 - 4.7 mol% ($\bar{x} \pm 1\sigma = 2.0 \pm 1.0\%$), K_2O ranges 0.3 - 4.2 mol% ($\bar{x} \pm 1\sigma = 1.5 \pm 1.0\%$; Table 2.2). Despite the fact that these rocks are hydrothermally altered, major element classification of these rocks based on SiO_2 , Na_2O , and K_2O content confirm field descriptions of these rocks being gabbros. Moreover, the immobile element classification of Floyd and Winchester (1977) place most of these samples within the field of sub-alkaline gabbros (Fig. 2.4). Au contents in mafic dykes range from below detection limits (0.0002 ppm) to 0.9 ppm ($\bar{x} \pm 1\sigma = 0.04 \pm 0.17$ ppm), wt% H_2O ranges from 0.45% to 4.1% ($\bar{x} \pm 1\sigma = 2.0 \pm 0.95\%$), S ranges from 0.009% to 0.48% ($\bar{x} \pm 1\sigma = 0.10 \pm 0.13\%$), and wt% C ranges from 0.01% to 2.4% ($\bar{x} \pm 1\sigma = 0.47 \pm 0.6\%$; Table 2.2).

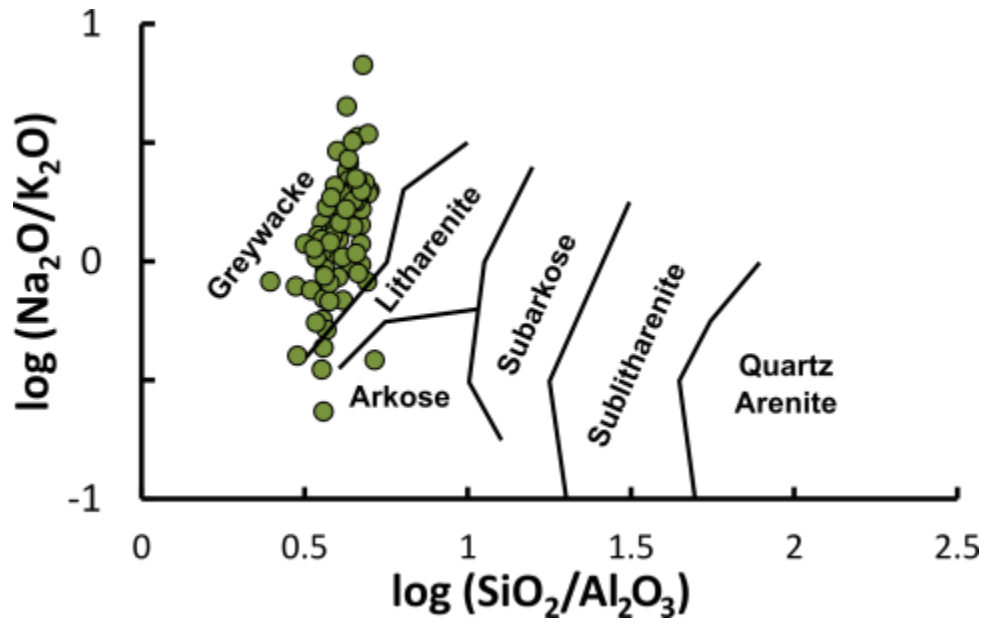


Figure 2.2: Geochemical classification of sedimentary rocks after Herron (1988) using weight percent oxides places the bulk of the sedimentary rock samples within the field for greywackes.

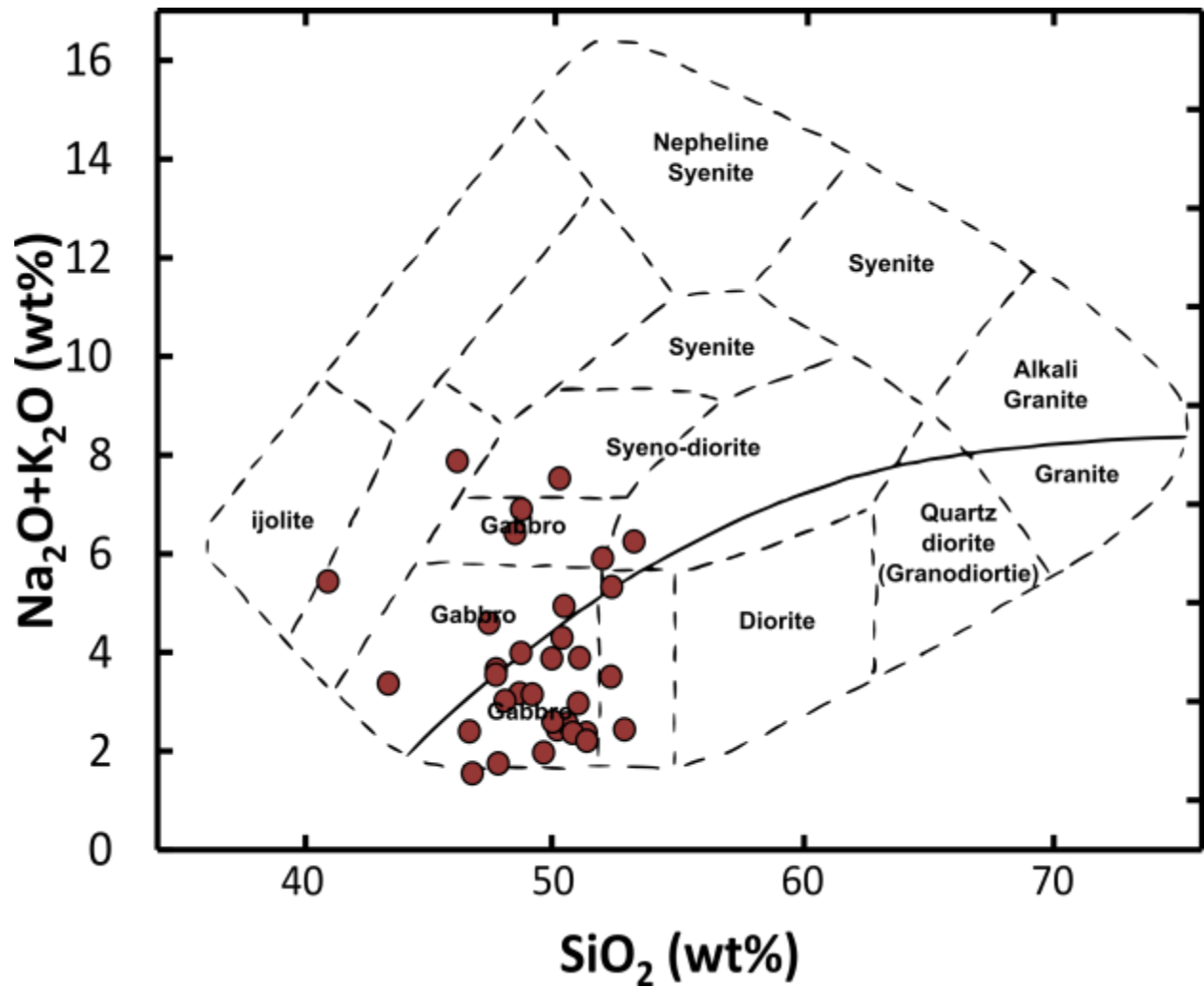


Figure 2.3: Geochemical classification for plutonic rocks after Wilson (2007) places the bulk of mafic dyke samples within the fields for gabbros. The solid black line separates calc-alkaline series (above) and tholeiitic series (below).

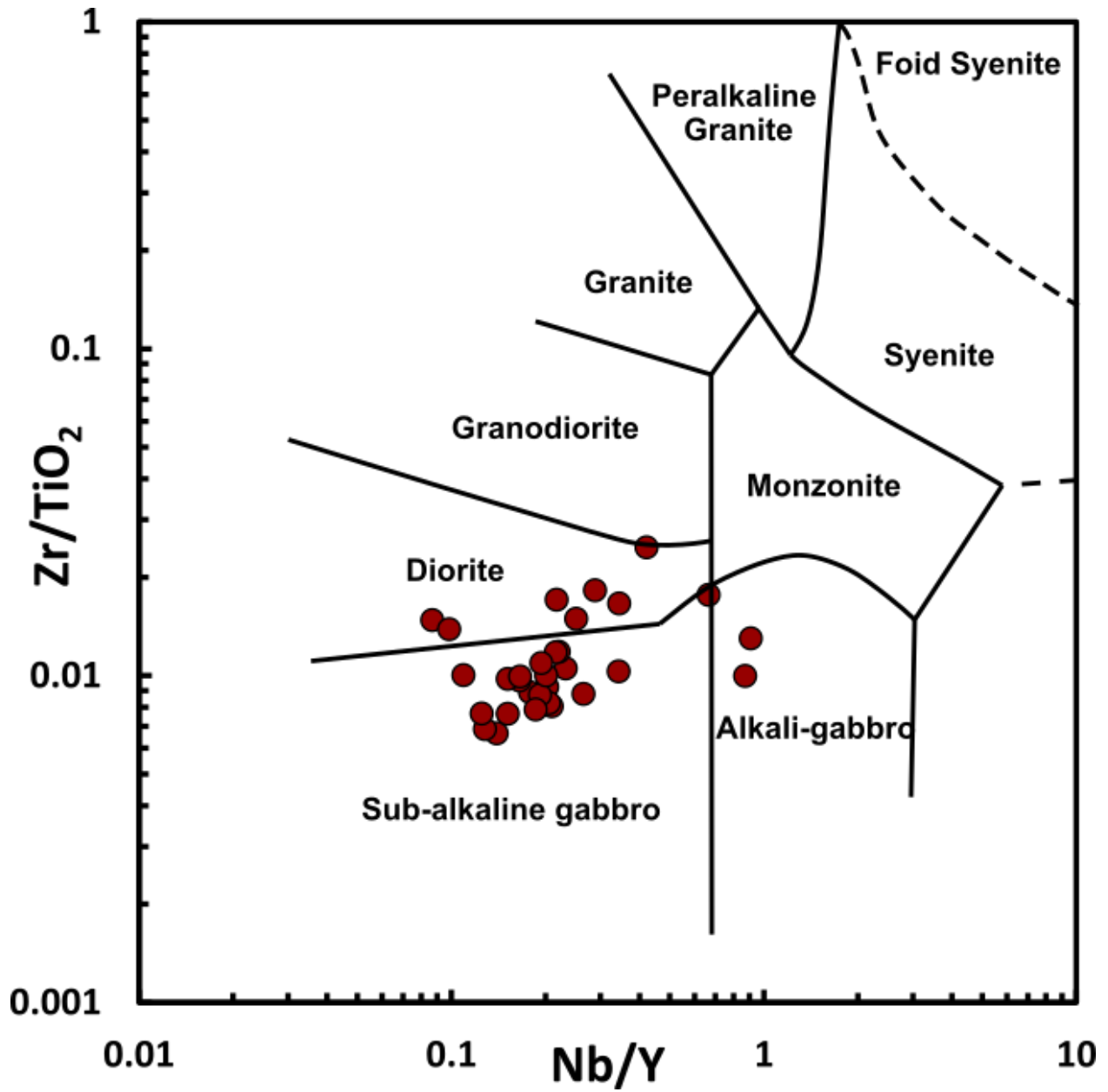


Figure 2.4. Geochemical classification for plutonic rocks after Floyd and Winchester (1977) places the bulk of mafic dyke samples within the fields for sub-alkaline gabbros.

2.4.2 Whole-rock stable isotopes

Histograms of oxygen and hydrogen isotopic compositions for the set of 87 greywacke samples and 33 mafic dyke samples are presented in Figure 2.5. The $\delta^{18}\text{O}$ values of greywackes range from 7.8‰ to 11.9‰ and are normally distributed ($\bar{x} \pm 1\sigma = 9.9 \pm 0.7\%$; Fig. 2.5 A; Table 2.3). The $\delta^2\text{H}$ values of greywackes are also normally distributed (Fig. 2.5 B; Table 2.3) and exhibit values from -91‰ to -41‰ ($\bar{x} \pm 1\sigma = -59 \pm 8\%$). Mineralized greywackes that contain >0.1 ppm Au have $\delta^2\text{H}$ values less than -70‰ whereas, $\delta^{18}\text{O}$ values are near the average of 9.9‰ (Figs. 2.5 A and B). Modal mineralogy correlations with isotopic values in greywackes are shown in Figures 2.6 A, B, and C (Tables 2.4 and 2.3).

The $\delta^{18}\text{O}$ values of mafic dykes are also normally distributed with the exception of two outlying samples with high values of 11.6‰ and 12.2‰. With these outliers removed, the $\delta^{18}\text{O}$ values of mafic dykes range from 6.8‰ to 9.8‰ ($\bar{x} \pm 1\sigma = 8.2 \pm 1.3\%$; Fig. 2.5 C; Table 2.6). The $\delta^2\text{H}$ values of mafic dykes contain one outlying value of -105‰. Excluding this sample, the range of $\delta^2\text{H}$ is between -84‰ and -55‰ ($\bar{x} \pm 1\sigma = -71 \pm 7\%$; Fig. 2.5 D).

Biotite and amphibole in the mafic dykes make up the dominant proportion of the rock volume in the mafic dykes. However, there is no apparent correlation of whole-rock isotopic values with modal mineralogy. Petrographic analysis of the mafic dyke outliers indicates that the two samples with high $\delta^{18}\text{O}$ values contain abnormal amounts of quartz and feldspar; sample K38934 contains approximately 40 vol. % plagioclase (Figs. 2.9 A and B; Table 2.7) and K388105 is composed of approximately 60 vol.% quartz (Figs. 2.9 C and D; Table 2.7). While the sample with the lowest $\delta^2\text{H}$ value (K388338) contained relict feldspars that have been altered to fine-grained phyllosilicates (Figs. 2.9 E and F; Table 2.7). These samples have been excluded from subsequent geostatistical analysis.

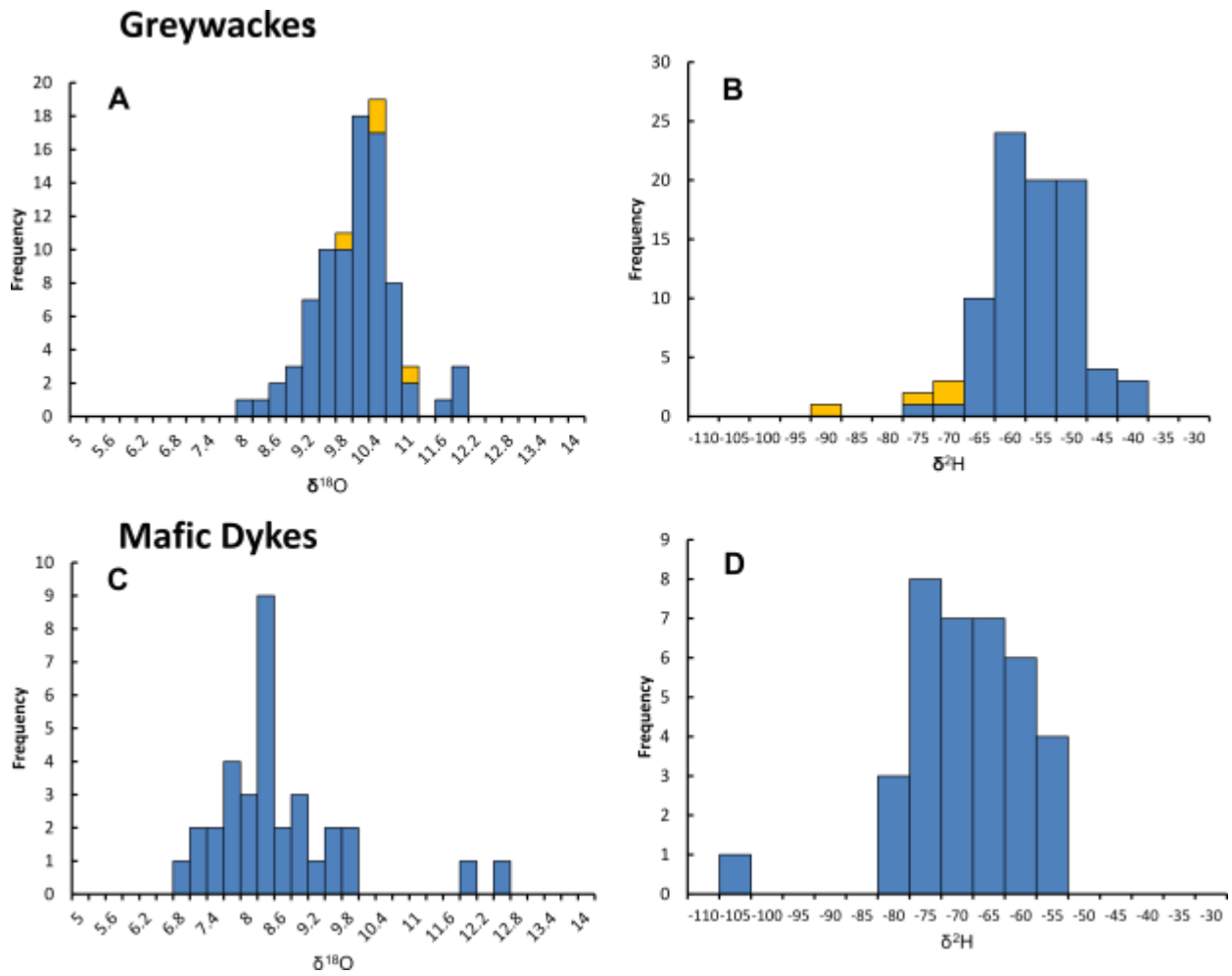


Figure 2.5: Histograms of oxygen and hydrogen isotopic data. Top: Greywackes from the Pontiac Group ($n=87$). Mineralized greywackes with $>0.1\text{ ppm Au}$ are shown in yellow. Bottom: Mafic dykes that intrude the Pontiac Group ($n=33$).

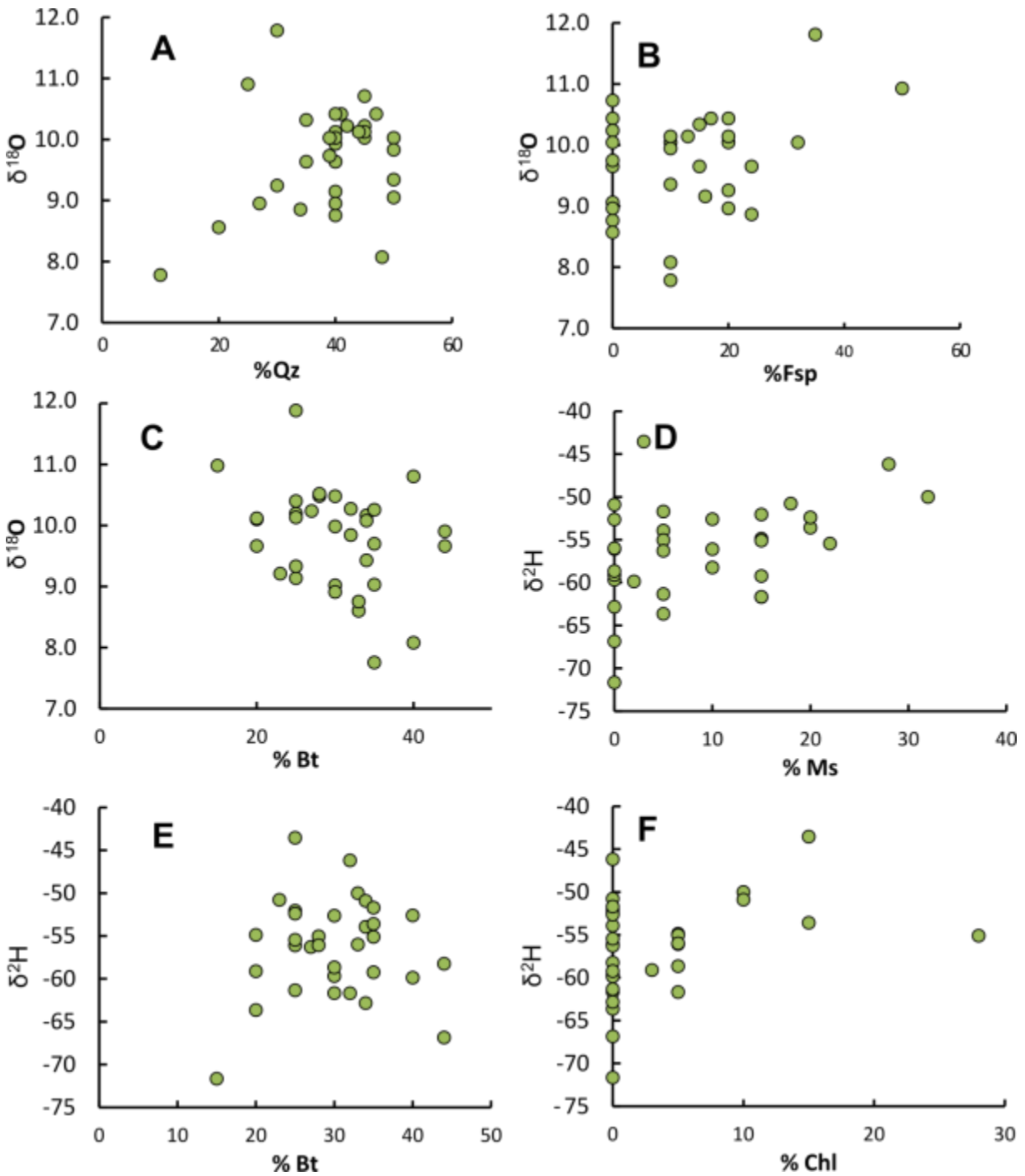


Figure 2.6: Bivariate plots of whole-rock oxygen and hydrogen stable isotopic values versus visual estimates of mineral abundances within Pontiac metasedimentary greywackes show weak relationships between modal mineralogy and isotopic values. A and B show siliceous minerals such as Qz and Fsp tend to increase the whole rock $\delta^{18}\text{O}$ values whereas C displays a negative relationship between $\delta^{18}\text{O}$ values and biotite. D, E and F indicate the differing effects of mica species on whole-rock $\delta^2\text{H}$ values wherein Ms and Chl tend to increase $\delta^2\text{H}$, while modal proportion of Bt has little effect on the $\delta^2\text{H}$. For the purposes of these diagrams, hydrothermal and metamorphic generations of biotite are not distinguished.

2.4.3 Petrography

Petrography of a subset of greywacke samples ($n = 33$; Table 2.4) provides evidence for mineralogical control on whole-rock lithochemistry and isotopic composition. These 33 samples are distributed throughout the study area and include both mineralized (>0.1 ppm Au) and non-mineralized (<0.1 ppm Au) samples. The typical mineral assemblage of greywackes is composed of quartz, orthoclase, plagioclase, biotite, chlorite, and muscovite. Accessory phases include pyrite, pyrrhotite, and carbonate with lesser amounts of chalcopyrite and rutile.

Near the southwestern extent of the study area, the mineral assemblage changes to higher metamorphic grade characterized by overprinting garnet and staurolite. The grain size of quartz in greywackes ranges from <0.1 mm to about 1 mm and forms subrounded grains or lenticular patches elongated parallel to the dominant foliation (Figs. 2.7 A and B). Quartz patches may contain equant polygonal subgrains. Quartz constitutes a large modal proportion of the volume of these rocks, typically on the order of 30 to 40% (Table 2.4). Biotite occurs throughout the greywackes, normally as porphyroblastic crystals ranging in grain size from about 0.2 to 1 mm. Biotite commonly defines the dominant foliation (Figs. 2.7 A and B). In mineralized samples, biotite may appear as fine, feathery grains, sometimes along sutured fissures with pyrite and carbonate minerals (Figs. 2.7 E and F). Biotite occurs in similar abundances as quartz, making up approximately 30 to 40% of the rock volume (Table 2.4). When present, orthoclase makes up 10 to 20% of the rock volume and appears texturally similar to quartz grains. Larger, orthoclase grains are distinguished by irregular grain boundaries and are partially altered to fine-grained white mica. The modal proportion of albite increases from background values near 15% to approximately 50% in mineralized samples. In these samples, albite is the dominant feldspar, displaying angular to subangular crystals and polysynthetic twinning (Figs. 2.7 E and F). Muscovite is found in approximately two thirds of all samples where it makes up about 10 to 20% of the rock volume. Muscovite is finely disseminated throughout the groundmass (Figs. 2.7 A and B) or as an alteration of orthoclase. Chlorite is found in less than one quarter of all samples. Chlorite is a texturally late phase typically overprinting biotite (Figs. 2.7 C and D). Major element lithochemistry is consistent with the estimated modal mineralogy. The best correlations are between modal mineralogy and molar % K_2O , Na_2O , MgO and SiO_2 (Fig. 2.8, Tables 2.1 and 2.2).

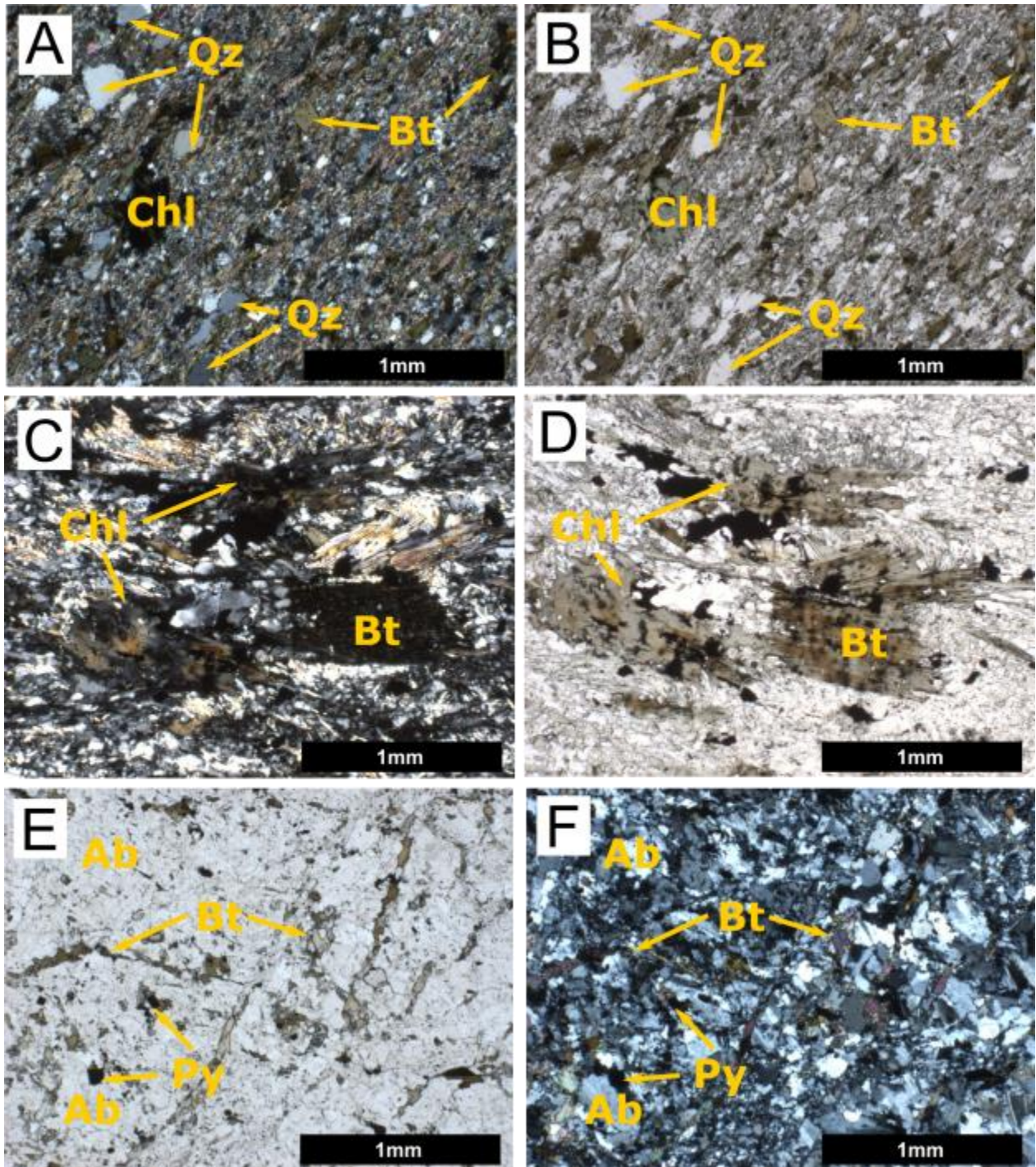


Figure 2.7: Photomicrographs of Pontiac metasedimentary greywackes. (A) and (B) Sample K389961 displays very fine grained Ms throughout the groundmass of the slide with coarser grained Bt and Chl as well as quartz grains. ($\delta^2\text{H} = -50\text{‰}$, $\delta^{18}\text{O} = 8.6\text{‰}$) (C) and (D) sample K389951 shows Chl and Ms overgrowing and replacing Bt ($\delta^2\text{H} = -44\text{‰}$, $\delta^{18}\text{O} = 9.1\text{‰}$). (E) and (F) show sample K389002 a mineralized sample (431ppb Au) dominantly made up of Qz and Fsp with fissure filled Bt ($\delta^2\text{H} = -72\text{‰}$, $\delta^{18}\text{O} = 11.0\text{‰}$).

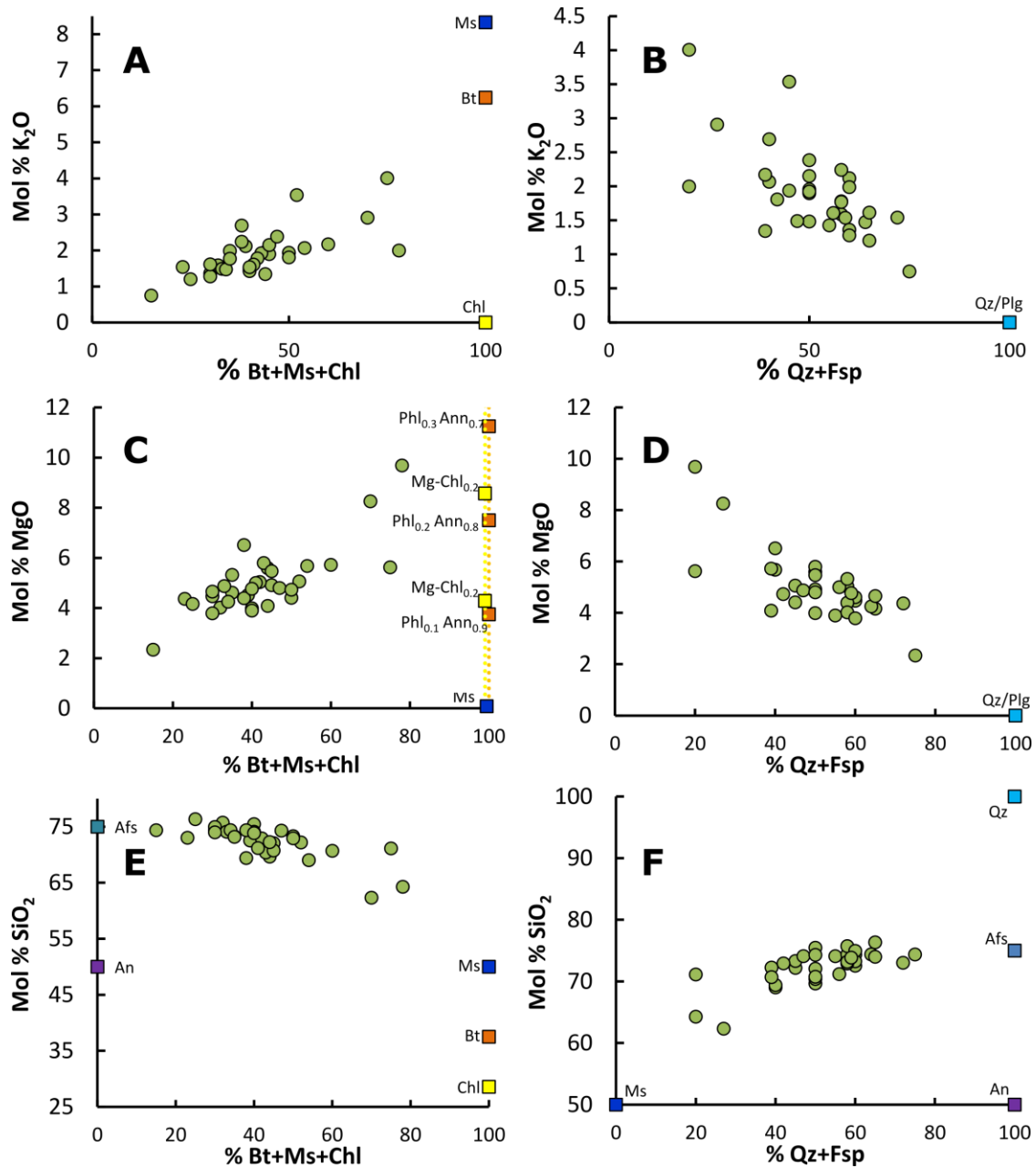


Figure 2.8: Bivariate plots of whole-rock lithochemistry versus visual estimation of mineral abundances within Pontiac metasedimentary greywackes. Molecular compositions of minerals have been plotted and are labeled according to Whitney and Evans (2010): Ms – muscovite, Bt – biotite, Chl – chlorite, Qz – quartz, Plg – plagioclase, Phl – phlogopite, Ann – annite, Afs – alkali feldspar, and An – anorthite. A and B indicate micaceous minerals in the rock exhibit a positive control on K₂O content while siliceous minerals exhibit a negative control. C and D show similar patterns whereby total mica content is positively correlated with MgO content and Qz and Fsp is negatively correlated. Conversely, E and F indicate that SiO₂ is negatively correlated with the total mica content of greywackes and positively correlated with Qz and Fsp.

Petrography of mafic dyke samples (n = 20) shows the typical mineral assemblage is dominated by amphibole, plagioclase, quartz, biotite, chlorite, and carbonate. Fine-grained white mica and pyrite are accessory minerals. Amphibole typically constitutes 30 to 50% of the volume of the rock and displays subhedral to euhedral, 0.5 to 1 mm laths in interstitial fine grained groundmass (Figs. 2.9A, B, C and D, Table 2.7). Biotite is less common than amphibole, typically making up approximately 30 to 40% of the rock volume. Biotite forms feathery laths about 0.1 to 0.5 mm in length. Biotite may form lenticular patches defining the dominant foliation (Figs. 2.9 A and B). Plagioclase is distinguished by polysynthetic twinning and forms interstitially to both biotite and amphibole. Plagioclase grains range in size from <0.1 mm to about 0.5 mm and display sutured grain boundaries localizing the finer grained (<1.0 mm) crystals (Figs. 2.9 A and B). The modal proportion of plagioclase is approximately 10 to 20% of the rock volume. When present, quartz in mafic dykes is typically very fine grained (<0.1 mm) constituting an aphanitic texture. Quartz forms interstitially to biotite and amphiboles. Locally, quartz is partially annealed forming polygonal grains and has similar modal proportions to biotite and amphibole (Figs. 2.9 C and D). Chlorite is found in approximately three quarters of all samples where it replaces biotite. Carbonate, fine grained white mica, and pyrite tend to have modal proportions ranging from 0 to 10% of the rock volume. Carbonate and pyrite are more commonly found in samples yielding trace amounts of gold. In these rocks, carbonate forms ragged and irregular patches throughout the rock, while pyrite grains are intergrown with ferromagnesian minerals such as pyrite and amphibole (Figs. 2.9 A, B, C and D). The fine grained white mica typically forms within the interstitial groundmass in association with quartz and plagioclase feldspar (Figs. 2.9 C, D, E and F). Geochemical data collected from mafic dykes, when combined with modal mineralogy suggest alkali content and MgO contents of these rocks are linked to a trade-off between the modal proportion of biotite versus amphibole (Figs. 2.10, Tables 2.4 and 2.6). Other major element oxides such as SiO₂ and Al₂O₃ did not show significant correlation with observable changes in mineralogy.

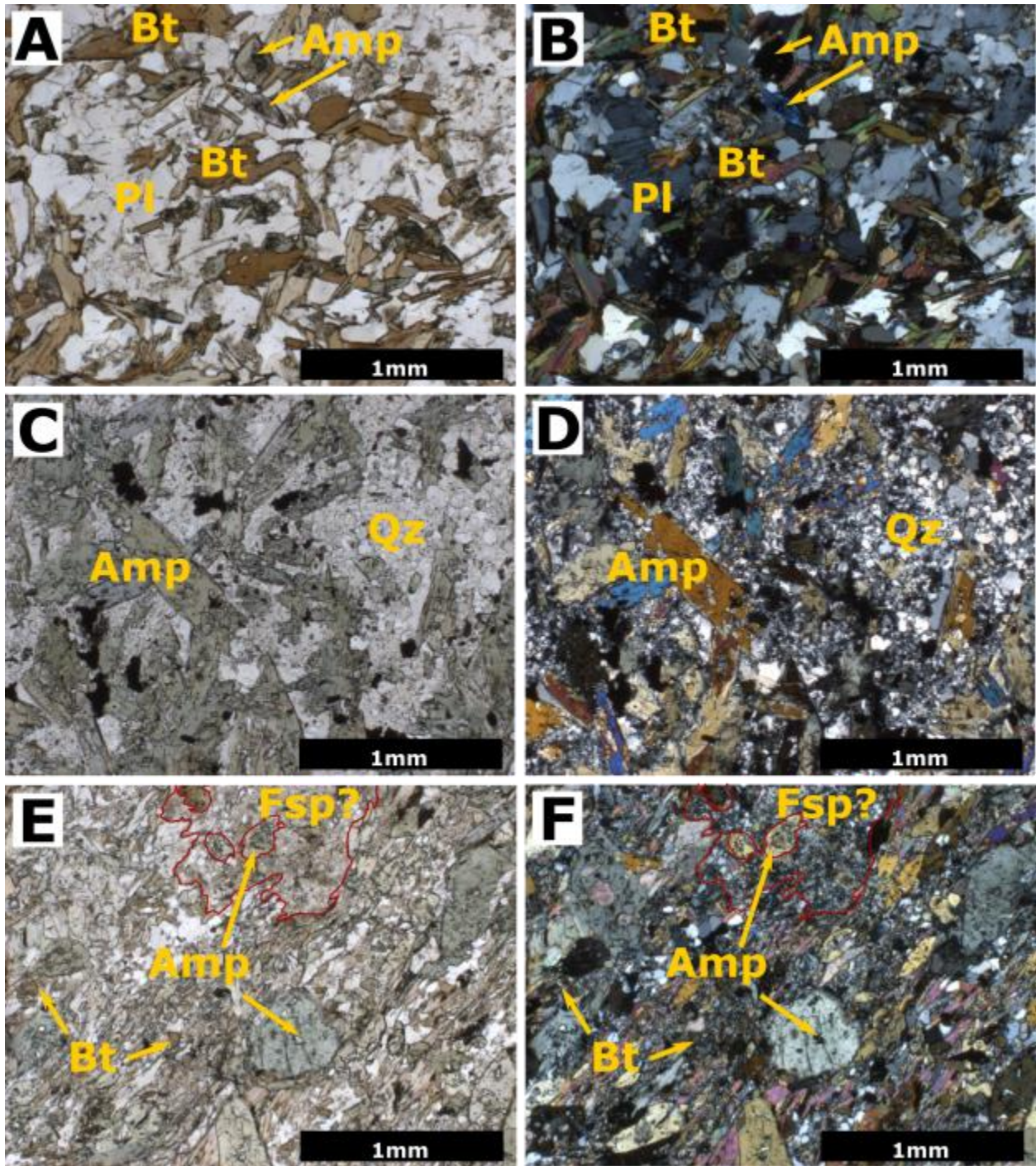


Figure 2.9: Photomicrographs of isotopically anomalous mafic dykes. (A) and (B) Sample K389349 displays Bt and Amp that is suspended by interstitial Pl ($\delta^2\text{H} = -63\text{‰}$, $\delta^{18}\text{O} = 12.2\text{‰}$). (C) and (D) Sample K388105 displays hypidiomorphic Amp suspended within a groundmass almost entirely made up of fine grained ($<0.1\text{mm}$) Qz ($\delta^2\text{H} = -70\text{‰}$, $\delta^{18}\text{O} = 11.6\text{‰}$). (E) and (F) Sample K388338 displaying Amp significantly more decomposed, and suspended between interstitial groundmass of fine grained Bt (0.1 to 0.5mm) and fine grained Qz ($<0.1\text{mm}$) and local, ragged cryptocrystalline patches (relict Fsp?) (outlined in red) ($\delta^2\text{H} = -105\text{‰}$, $\delta^{18}\text{O} = 9.8\text{‰}$).

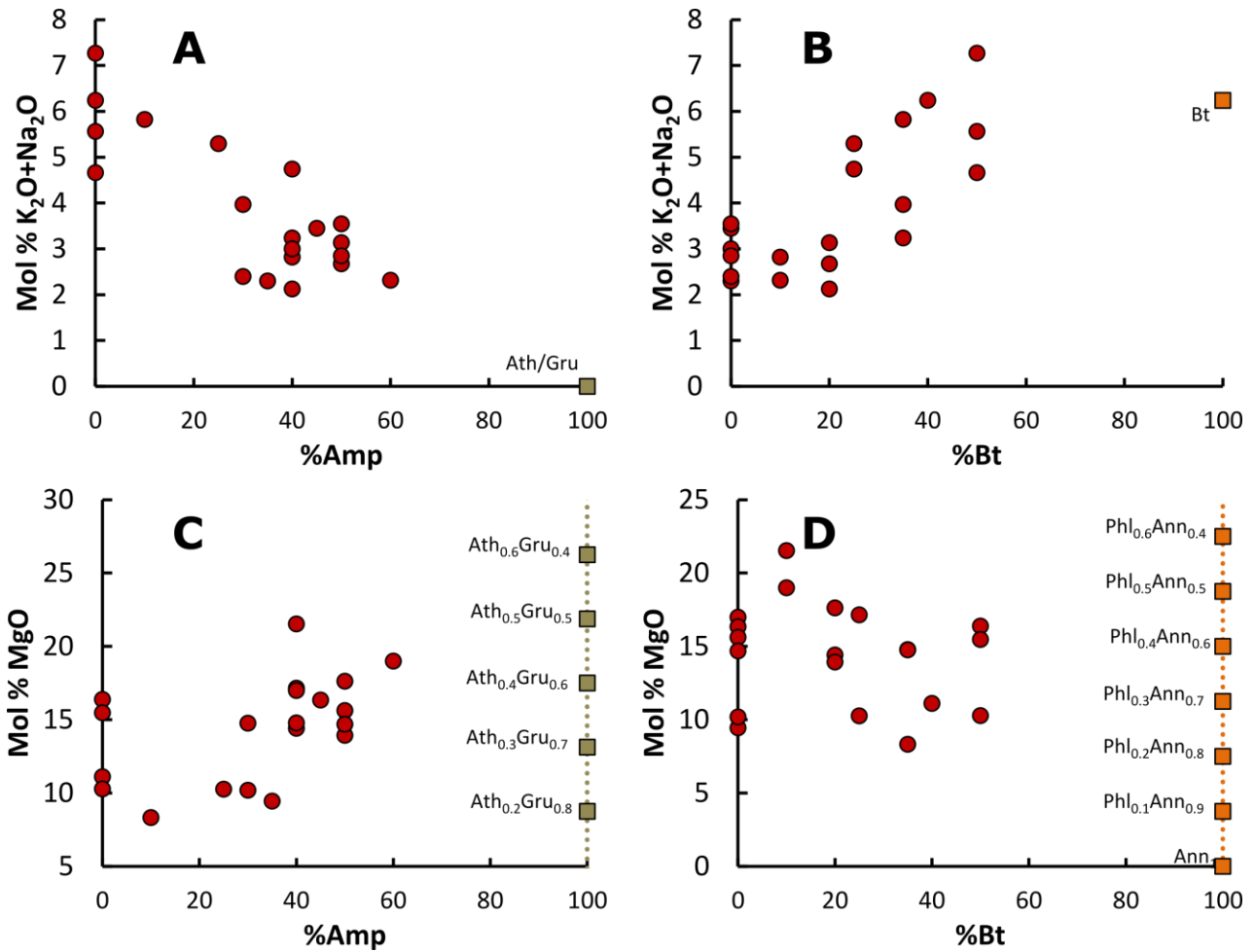


Figure 2.10: Bivariate plots of whole-rock lithochemistry versus visual estimation of mineral abundances within mafic dykes. Molecular compositions of minerals have been plotted and are labeled according to Whitney and Evans (2010): Ath – anthrophyllite, Gru – grunerite and Bt – biotite. A and B show alkaline elements are positively correlated with Bt while Amp exhibits a negative control on these elements. Conversely, C and D indicate that MgO content in mafic dykes is positively affected by Amp and negatively affected by Bt. Other major element oxides such as SiO_2 and Al_2O_3 did not show significant correlation with observable changes in mineralogy and were not included in this figure.

2.4.4 Principal Component Analysis (PCA)

The PCA was performed using whole-rock oxygen and hydrogen isotopic values, major element oxides, as well as Au, C, H₂O, and S (Tables 2.2, 2.3, 2.6, and 2.7). Principal components 1 and 2 (PC1 and PC2) account for 54.05% and 13.15% respectively, of the variance exhibited by the greywacke data (Fig. 2.11). The other principal components make up less than 10% of the total variance each, and are not discussed further. The loading plot from the PCA of greywackes cluster components that directly co-vary (Fig. 2.11 A), whereas components that are inversely co-vary plot on opposite sides of the diagram. PC1 indicates Au, C, and S are correlated and form an association that is inversely co-varies to a second association comprised of $\delta^2\text{H}$, MgO, Fe₂O₃, TiO₂, Al₂O₃, and MnO (Figs 2.11 A and B). PC2 discriminates between a coupled K₂O and H₂O association that inversely co-varies with a Na₂O and CaO association whereas $\delta^2\text{H}$, $\delta^{18}\text{O}$ and other major elements associated with mineralization are not well discriminated by PC2 (Figs. 2.11 A and C).

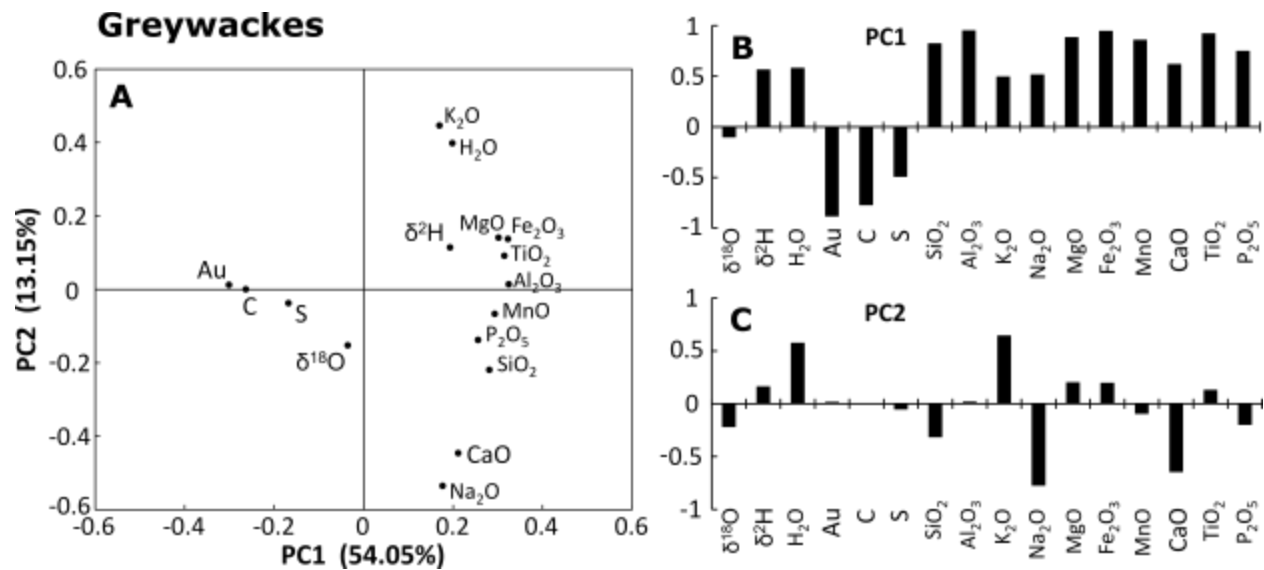


Figure 2.11: (A) PC1 and PC2 accounting for 67.2% of the variance in the greywacke data. (B) eigenvalues or the weightings of each component incorporated into PC1 which defines the line maximum variance through a data set with n -number of components in n -dimensional space. (C) eigenvalues or the weightings of each component incorporated into PC2 which defines a line of maximum variance orthogonal to PC1 in n -dimensional space.

The mafic dyke samples contain three outlier samples with respect to the isotopic data; two samples with high $\delta^{18}\text{O}$ values (K389349 and K388105) and one sample with a low $\delta^2\text{H}$ value (K389338; Fig. 2.4).

Outlying data points from these samples will skew PCA results and may cause erroneous interpretations

(Filzmoser et al. 2009), these samples are therefore not considered for PCA. The first two principal components extracted from the mafic dyke dataset capture 53.75% (PC1) of the 11.41% (PC2) of the total variance (Fig. 2.12). Other principal components capture less than 10% each, and are not discussed. PC1 indicates that components associated with mineralization (Au, C, S, and $\delta^{18}\text{O}$) are again inversely correlated with the rock forming elements (MgO Fe₂O₃, MnO, CaO, TiO₂, SiO₂, Al₂O₃) and $\delta^2\text{H}$ (Figs 2.12 A and B). PC2 distinguishes mostly between an alkaline association (K₂O, Na₂O and P₂O₅) versus a calcium-hydrous association (CaO and H₂O) and to a lesser extent discriminates S from other components associated with mineralization ($\delta^{18}\text{O}$, C, and Au). Major elements and $\delta^2\text{H}$ are not well discriminated by PC2 (Figs 2.12 A and C).

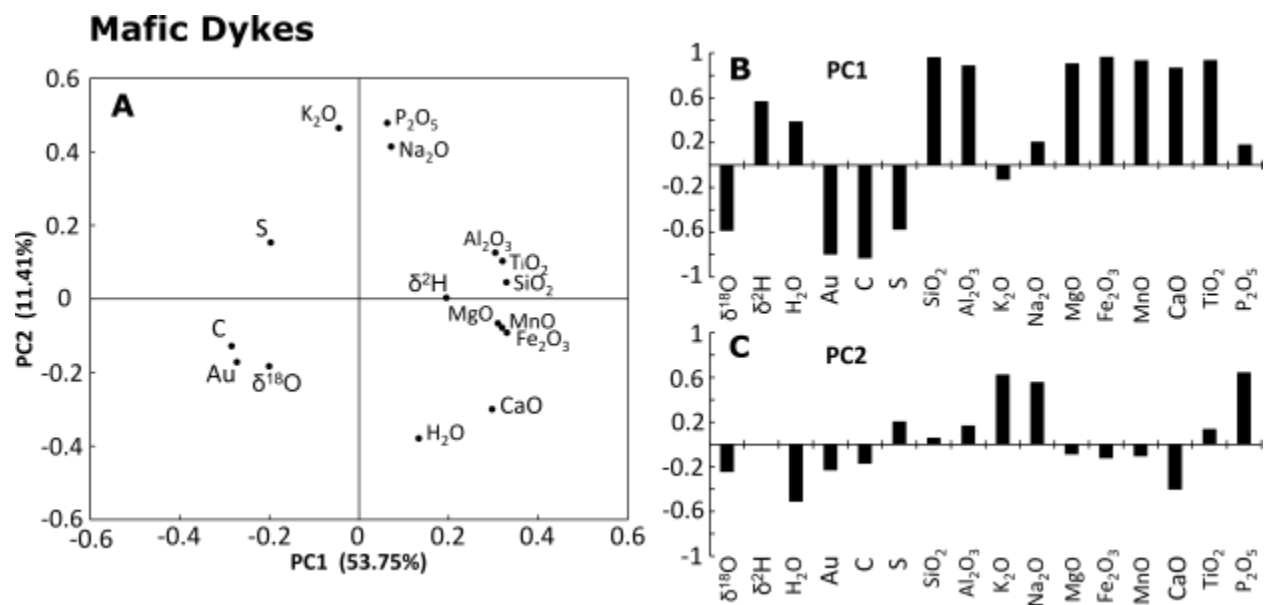


Figure 2.12: PCA results integrating whole-rock stable isotopic data with geochemical data of mafic dykes. (A) shows PC1 and PC2 are plotted against each other accounting for 65.16% of the variance in the mafic dyke data. (B) displays the eigenvalues or the weightings of each component incorporated into PC1 which defines the line maximum variance through the data set. (C) displays the eigenvalues or the weightings of each component incorporated into PC2 which defines a line of maximum variance orthogonal to PC1 in n-dimensional space.

2.4.5 Isotopic variation along sections P1, P2, and P3

Whole-rock $\delta^{18}\text{O}$ and $\delta^2\text{H}$ values of both greywackes and mafic dykes are plotted in Figures 2.13, 2.14, and 2.15. The $\delta^2\text{H}$ values of greywacke samples from within the pit and close to the mineralized domain tend to be less than ca. -60‰ (Figs 2.13 A, 2.14 A, and 2.15 A). Section P1 shows greywacke samples

with $\delta^2\text{H}$ values below -60‰ within the Canadian Malartic pit and up to 2 km south, with the exception of one sample from the Gouldie Zone with a $\delta^2\text{H}$ value of -57‰ after which, $\delta^2\text{H}$ values of greywackes increase to a maximum of -53‰ towards the south (Fig. 2.13 A). The $\delta^2\text{H}$ values of greywackes along P2 increase progressively from -91‰ near the centre of the mineralized domain to approximately -60‰ near the edge of the pit. Values continue to increase slightly towards the south for approximately 500 m where the overall trend begins to again decrease, reaching a local minimum of -76‰ approximately 2 km south of the Canadian Malartic pit. The southernmost greywacke sample along P2 yields a $\delta^2\text{H}$ value of -47‰ (Fig. 2.14 A). Greywacke $\delta^2\text{H}$ values along section P3 are characterized by a single low value (-91‰) near the core of the mineralized domain and increase reaching values between -60‰ to -50‰ towards the northwest and southeast. To the southeast, $\delta^2\text{H}$ values of greywackes are constant near -60‰ for up to 2 km beyond the Canadian Malartic pit, before increasing to values of -55‰ to -40‰ . To the northwest, values are more variable, but all range from -50‰ to -65‰ with the lower values tending to occur closer to the Canadian Malartic pit (Fig. 2.15 A). In all three sections the lowest $\delta^2\text{H}$ values of greywackes are found within the Canadian Malartic pit (-67 in P1, and -91‰ in P2 and P3) and the footprint is recorded as values increase away from the Canadian Malartic pit to between ca. -60‰ to -50‰ .

The $\delta^{18}\text{O}$ values of greywackes do not show the same spatial relationship with mineralization. Section P1 shows the $\delta^{18}\text{O}$ values of all samples are between 9.3‰ to 10.3‰ and the two samples from within the Canadian Malartic pit yield values of 10.1‰ and 10.0‰ which is within analytical uncertainty of the of the 9.9‰ average. One sample has a $\delta^{18}\text{O}$ value of 9.3‰ and is sourced from the Gouldie Zone (Fig. 2.13 B). Section P2 displays $\delta^{18}\text{O}$ minimum of 8.3‰ and maximum of 11.7‰ from the two most proximal drill cores outside of the Canadian Malartic pit. However, the rest of the samples remain near the 9.9‰ average and do not show a spatial relationship to mineralization (Fig. 2.14 B). The $\delta^{18}\text{O}$ values of greywacke samples along section P3 range from 8.9‰ to 11.4‰ with the maximum and minimum values found southeast of the Canadian Malartic pit; all other values are near the average of 9.9‰ . Section P3 exhibits a greater variance in $\delta^{18}\text{O}$ values towards the southeast than the northwest, but does not show systematic change with respect to the Canadian Malartic pit (Fig. 2.15 B). Examination of the three sections indicates that the $\delta^{18}\text{O}$ values of greywackes remain relatively constant at about 9.9‰ irrespective of their distance to the mineralized domain (Figs. 2.13 B, 2.14 B, and 2.15 B).

Mafic dykes display similar spatial variations in their $\delta^2\text{H}$ along the three sections. In section P1, $\delta^2\text{H}$ of greywackes within the pit begin at -64‰ and decrease southward towards a minimum value of -83‰ ca. 2 km south of the Canadian Malartic pit. After this local minimum, $\delta^2\text{H}$ values along P1 begin to increase towards the south with the southernmost value reaching -65‰ (Fig. 2.13 A). Along section P2, the $\delta^2\text{H}$

values of greywackes increase from a low of -79‰ within the Canadian Malartic pit to -69‰ towards the south. With respect to section P3, the $\delta^2\text{H}$ values of mafic dykes gradually increase from -79‰ near the core of the mineralized domain and within the Canadian Malartic pit to -59‰ approximately 2 km southeast of the Canadian Malartic pit, whereas, the northwest extension of P3 remains unsampled with respect to mafic dykes (Fig. 2.15).

Mafic dykes within the Canadian Malartic pit typically yield the highest $\delta^{18}\text{O}$ values. Along section P1 and excluding the outlying $\delta^{18}\text{O}$ value of 11.6‰, the highest $\delta^{18}\text{O}$ value of 9.2‰ is found within the Canadian Malartic pit and is followed by a decrease in $\delta^{18}\text{O}$ values southward for approximately 500 m where $\delta^{18}\text{O}$ values of mafic dykes reach ca. 8‰. (Fig. 2.13 B) Section P2 shows the $\delta^{18}\text{O}$ values of mafic dykes are highest from within the Canadian Malartic pit reaching values of 8.7‰ and tend to decrease southward to 6.8‰ just outside of the pit margin. Further southward along P2, there is a slight increase in $\delta^{18}\text{O}$ observed with the southernmost sample having a $\delta^{18}\text{O}$ value of 8.2‰ (Fig. 2.14 B). Section P3 shows $\delta^{18}\text{O}$ values near the Canadian Malartic pit tend to be higher (8.7‰ to 9.5‰) whereas, more distal samples (>300 m from the Canadian Malartic pit) have lower $\delta^{18}\text{O}$ values of 7.3‰ to 8.3‰ (Fig. 2.15 B).

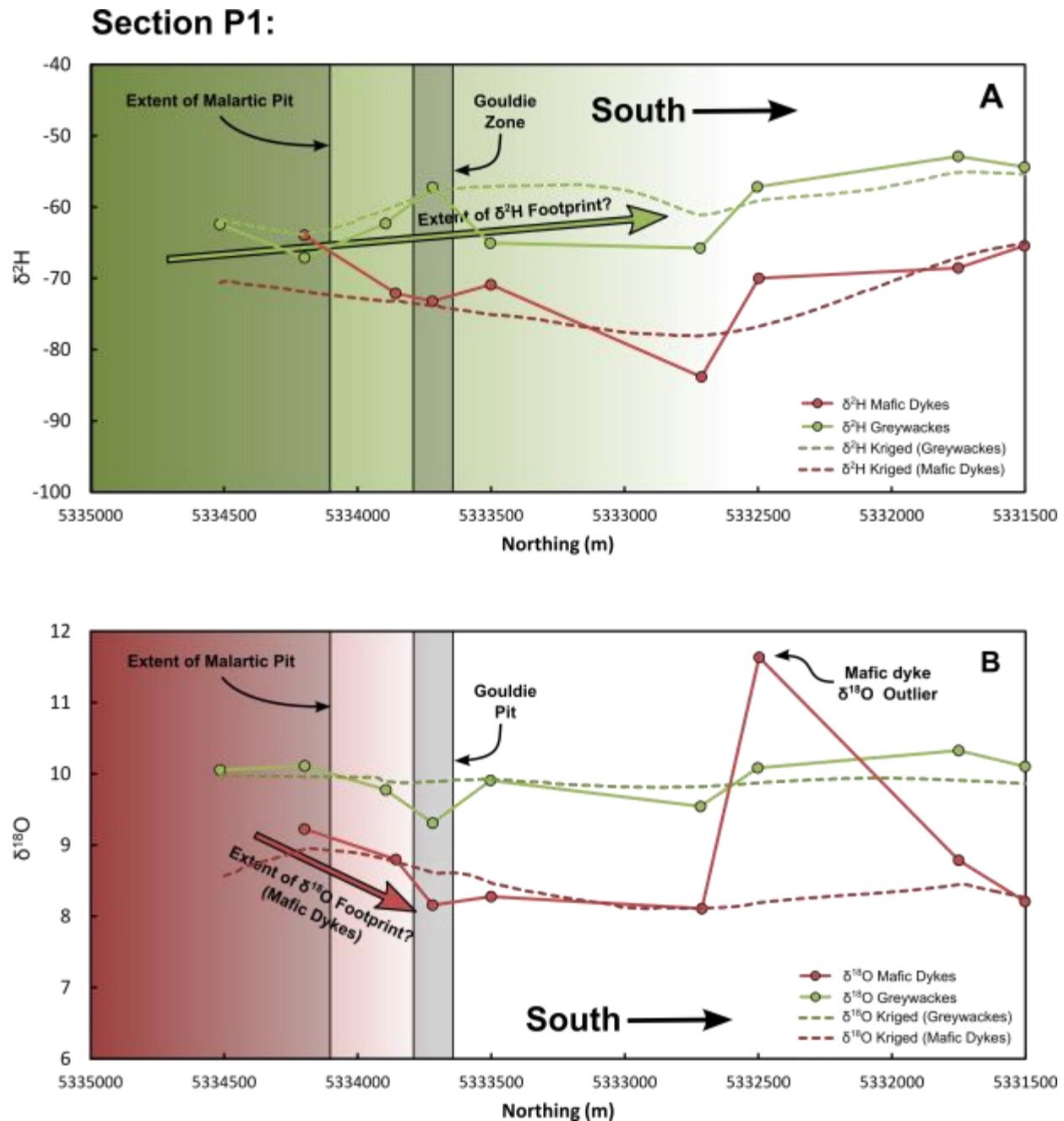


Figure 2.13: Section P1 extending south from the 2013 pit of the Canadian Malartic deposit. (A) $\delta^2\text{H}$ values of greywackes sourced from within and proximal to the pit tend to be lower than the more distal samples. The interpreted extent of the $\delta^2\text{H}$ footprint along P1 is marked by the green gradation extending towards the south. $\delta^2\text{H}$ data from mafic dykes do not systematically vary with distance from the pit. (B) $\delta^{18}\text{O}$ values of greywackes do not indicate the presence of a footprint along section P1. The $\delta^{18}\text{O}$ values of mafic dykes are higher inside and proximal to the Malartic pit. The $\delta^{18}\text{O}$ footprint in mafic dykes is marked by the red gradation.

Section P2:

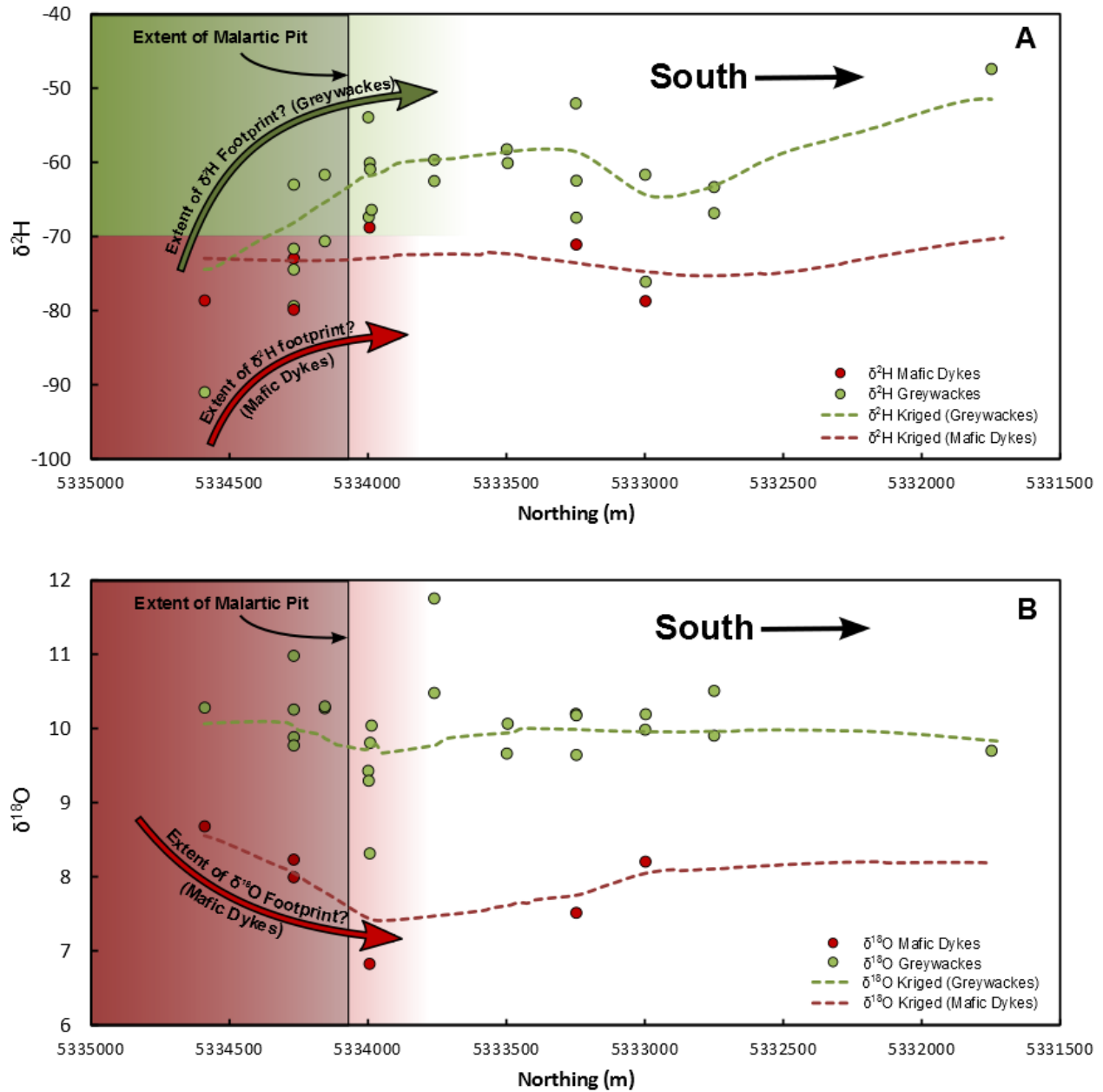


Figure 2.14: Section P2 extending south from the 2013 pit of the Canadian Malartic deposit. (A) $\delta^2\text{H}$ of both lithologies tend to increase with distance away from the pit. The extent of the $\delta^2\text{H}$ footprint in greywackes and mafic dykes is marked by the green and red gradation respectively. (B) $\delta^{18}\text{O}$ of greywackes does not systematically vary with distance from the pit. $\delta^{18}\text{O}$ of mafic dykes appears to decrease with distance south along P2. The extent of the $\delta^{18}\text{O}$ footprint in mafic dykes is marked by the red gradation.

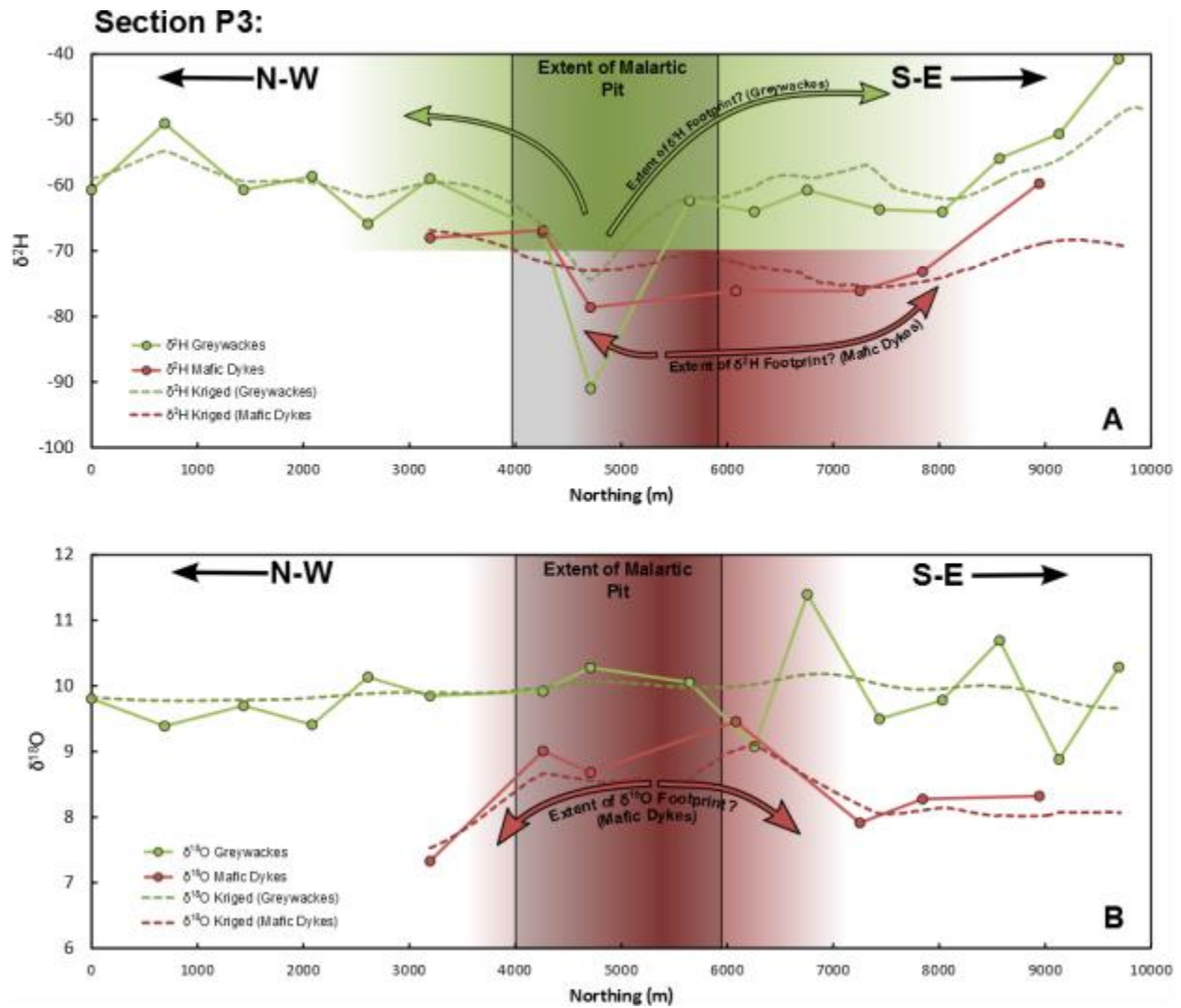


Figure 2.15: Section P3 originating northwest of the Canadian Malartic Deposit and extending southeast of the deposit is shown in relation to the extent of the 2013 pit design. (A) $\delta^2\text{H}$ values in greywackes record lower values proximal and inside the pit. The extent of the $\delta^2\text{H}$ footprint in greywackes has been marked by the green gradation. Mafic dykes also record low values within the pit and higher values outside. The interpreted extent of the $\delta^2\text{H}$ footprint in mafic dykes along P3 is marked by the red gradation. (B) Greywacke $\delta^{18}\text{O}$ do not systematically vary with respect to the pit. $\delta^{18}\text{O}$ of mafic dykes tend to be higher from in-pit and proximal samples. The extent of the interpreted $\delta^{18}\text{O}$ footprint in mafic dykes is marked by the red gradation.

2.4.6 Regional mapping of whole-rock O-H isotopic composition

Semi-variograms describe continuity of (in this case) isotopic values between samples at given distances from each other. By plotting the isotopic data as semi-variograms, best-fit models can be used to extrapolate values over the entire study area. These models may be anisotropic indicating that values are more continuous in the direction of the major range and less continuous in the direction of the orthogonal minor range. Moreover, these models integrate values with the spatial distribution of where they were sampled. The models illustrate the increase in variance of samples taken at the same location (nugget effect) to the point at which variance becomes independent of the distance between samples (sill; Clark and Harper, 2000). Geostatistical analysis has fitted $\delta^2\text{H}$ data from greywackes with an anisotropic stable model oriented 110° , with a nugget effect of 0.0076, a sill of 0.0155, a major range of 1400 m and a minor range of 700 m (Fig. 2.16 A). The spatial variation of $\delta^{18}\text{O}$ values of greywackes was fitted with an anisotropic gaussian model oriented 100° , with a nugget effect of 0.62, a sill of 1.14, a major range of 750 m and a minor range of 300 m (Fig. 2.16 B). The semi-variograms of $\delta^2\text{H}$ values of mafic dykes is fitted with an anisotropic gaussian model oriented towards 112.5° , a nugget effect of 0.54, a sill of 1.15, a major range of 2000 m and a minor range of 1500 m (Fig. 2.16 C). The $\delta^{18}\text{O}$ spatial variation in mafic dykes is fitted with an anisotropic spherical model oriented towards 100° , a nugget effect of 0.42, a sill of 1.17, a major range of 1600 m and a minor range of 1100 m (Fig. 2.16 D).

The kriged models of the $\delta^{18}\text{O}$ and $\delta^2\text{H}$ values of both rock types are contoured over the study area (Figs 2.17 and 2.18). Regional distribution of $\delta^{18}\text{O}$ values in greywackes show subtle variations throughout the study area, giving insights into the isotopic footprint that are not apparent along the sections. Figure 2.17 shows the 9.9‰ isopleth wrapping around most of the Canadian Malartic pit and extends toward the east and southeast subparallel to the CLLTZ in the eastern half of the study area. The 9.9‰ isopleth also encircles most of the southwest corner of the study area (Fig. 2.15 A). The -59‰ $\delta^2\text{H}$ isopleth encloses nearly the entire Canadian Malartic deposit, and extends about 1.5 km northwest of the pit, the -59‰ isopleth also encloses another area 1 to 2 km southwest of the pit. The $\delta^2\text{H}$ values in greywackes from the rest of the study area tend to have values greater than -58‰ (Fig. 2.15 B).

The spatial variation of $\delta^{18}\text{O}$ values of mafic dykes shows a good association of the 8.3‰ isopleth with the outline of the Canadian Malartic pit and the area extending between 500 m to 1 km southeast of the Canadian Malartic pit centered on an area near the Gouldie Zone. The 8.3‰ isopleth also delineates a small area towards the southern extent of the map (Fig. 2.16 A). Typically, mafic dykes with lower $\delta^{18}\text{O}$ values between 8.0‰ and 7.5‰ characterize the rest of the study area. The $\delta^2\text{H}$ data of mafic dykes indicates there is a large area of low $\delta^2\text{H}$ centered south and southeast of the Canadian Malartic pit as

delineated by the -72‰ isopleth. This area has a protuberance that extends towards the north near the centre of the Canadian Malartic deposit (2.17 B).

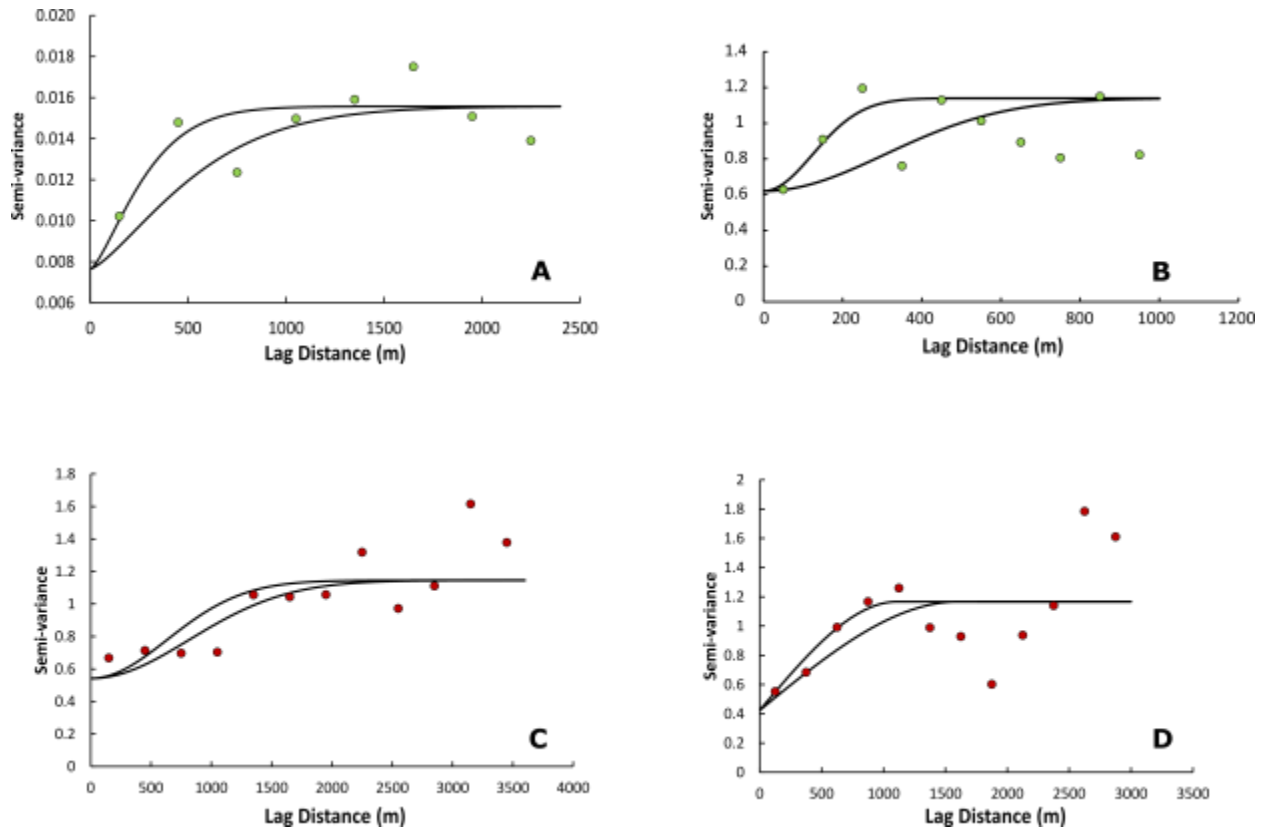


Figure 2.16: Semivariograms and fitted models of δ^2H and $\delta^{18}O$ data from greywackes (green points) and mafic dykes (red points). (A) Spatial variation of δ^2H values in greywackes is fitted by an anisotropic gaussian model. Minimum number of sample pairs represented for each point = 156. (B) Spatial variation of $\delta^{18}O$ values in greywackes is fitted by an anisotropic gaussian model. Minimum number of sample pairs represented for each point = 42. (C) δ^2H values of mafic dykes have been fitted with an anisotropic gaussian model. Minimum number of sample pairs represented for each point = 24. (D) Spatial variation of $\delta^{18}O$ values in mafic dykes have been fitted with an anisotropic spherical model. Minimum number of sample pairs represented for each point = 18. The multiple curves in each semivariograms illustrate the differences between the major and minor ranges.

Greywackes

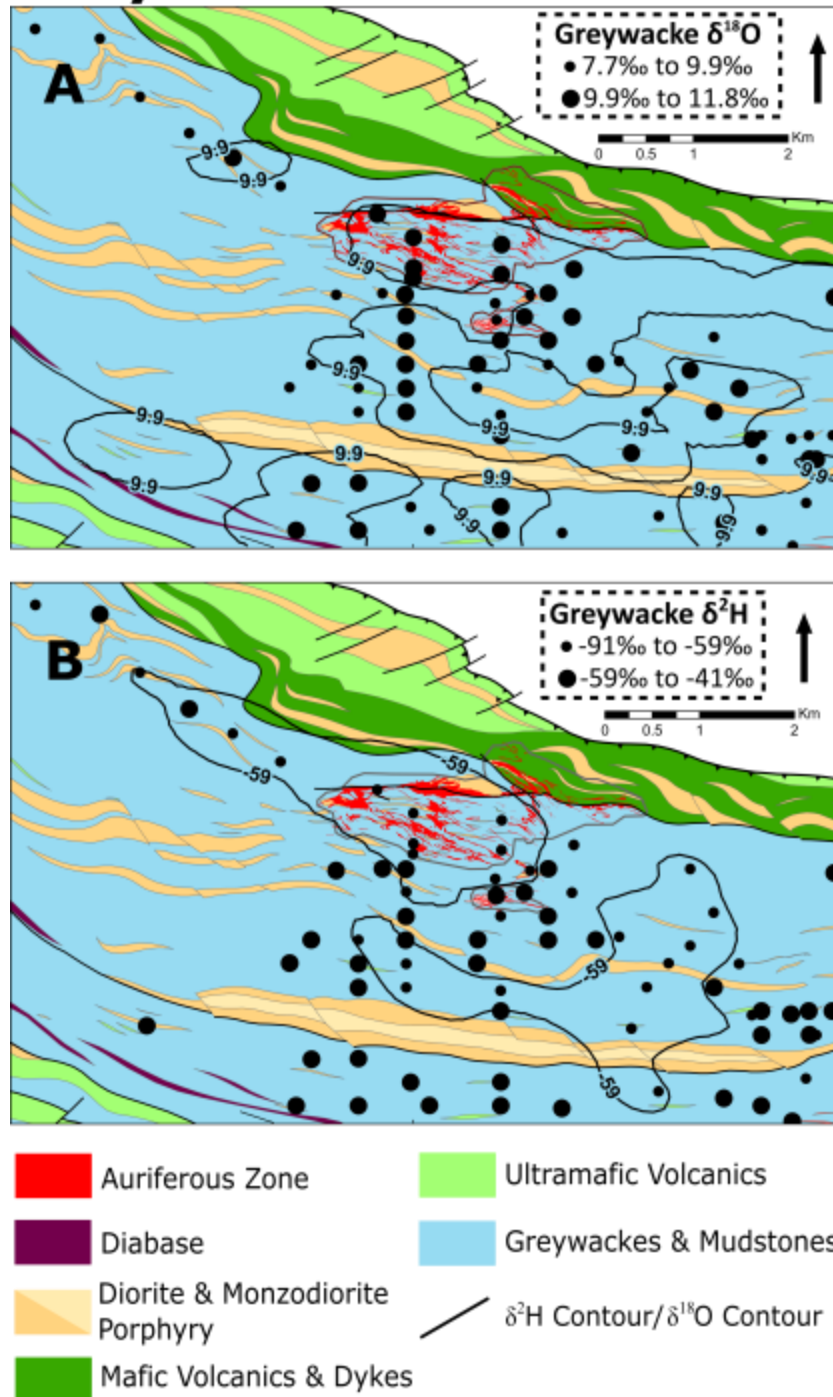


Figure 2.17: Geostatistical models of whole-rock $\delta^{18}\text{O}$ and $\delta^2\text{H}$ values in greywackes throughout the study area in relation to the mineralized domain (red) and 2013 pit outline. (A) $\delta^{18}\text{O}$ values of greywackes are modeled and the 9.9‰ isopleth is shown. (B) $\delta^2\text{H}$ values of greywackes modeled and the -59‰ isopleth is shown. Anisotropic gaussian models are predict spatial variation in both instances. Geological map modified after Perrouty et al. (2017)

Mafic Dykes

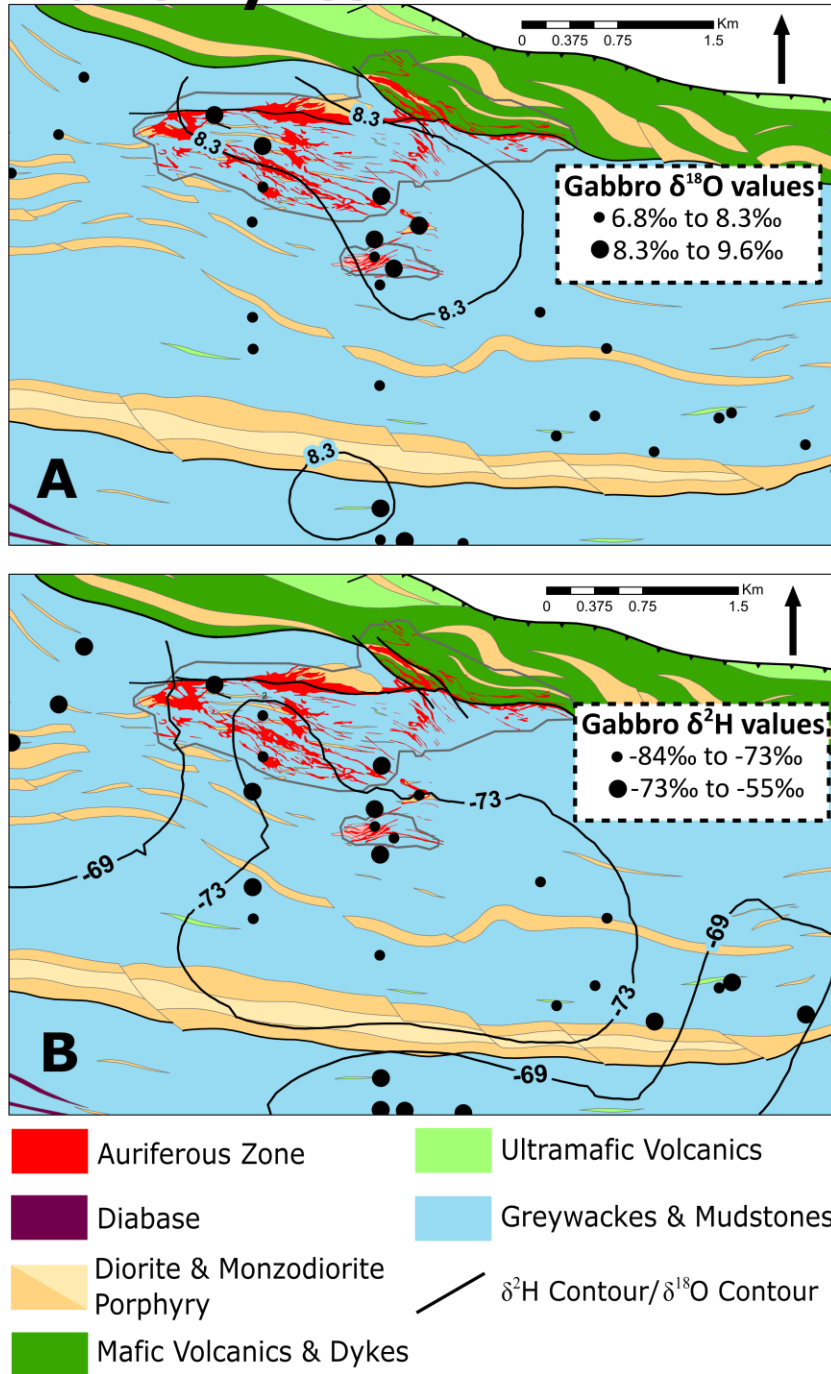


Figure 2.18: Geostatistical models of whole-rock $\delta^{18}\text{O}$ and $\delta^2\text{H}$ of mafic dykes throughout the study area in relation to the mineralized domain (red) and 2013 pit outline. (A) shows the $\delta^{18}\text{O}$ values of mafic dykes and the 8.3‰ isopleth is shown. Spatial variation is estimated using an anisotropic spherical model. (B) shows mafic dyke $\delta^2\text{H}$ values the -73‰ and -69‰ isopleths are depicted. Spatial variation is estimated using an anisotropic gaussian model. Geological map modified after Perrouy et al. (2017)

2.5 Discussion

The purpose of this study is to understand and define the isotopic footprint of the Canadian Malartic deposit. This insight can be found by mapping and modeling the isotopic composition of the host rocks surrounding the Canadian Malartic deposit and investigating how these isotopic variations correlate with geochemical and mineralogical changes in these rocks. The results of this study are compared and discussed within the framework of knowledge gained from other large gold deposits similar to the Canadian Malartic deposit.

The Canadian Malartic deposit represents the remnants of a large auriferous hydrothermal system. Globally, these systems are associated with crustal scale fault zones such as the CLLTZ and Porcupine-Destor tectonic zone (PDTZ) in the Abitibi. Mineralization however, does not occur directly within these major structures, but along secondary and tertiary splays (Groves 1993; Robert and Poulsen 1997; Goldfarb et al. 2001; Goldfarb et al. 2005). These crustal scale fault zones have been interpreted to be the main conduit of gold bearing fluids driven up through the crust and down gradients of pressure and temperature (Ridley and Diamond 2000) or, as local breaches in an impermeable crustal boundary that allow for the draining of deep-seated, over pressured fluids. Isotopically, the gold bearing fluids typically range in $\delta^{18}\text{O}$ from 6‰ to 13‰ and $\delta^2\text{H}$ from -80‰ to -20‰ (Goldfarb et al. 2005). There are, however, orogenic gold deposits with fluid compositions outside this range in isotopic values; select Archean gold deposits from Australia's Yilgarn craton yield $\delta^2\text{H}_{\text{fluid}}$ values up to -4‰. High values such as these have been interpreted to be the result of the influence of mixing between deep-seated fluids and surficial waters (Hagemann et al. 1994; Beaudoin and Pitre 2005; Beaudoin and Chiaradia 2016). Isotopic fractionation between vein minerals give a wide range of mineralization temperatures from ca. 200°C to greater than ca. 450°C (Kerrick and Fryer 1979; Groves 1993; Goldfarb et al. 2005). Also, the gold bearing fluids consist mostly of H_2O and CO_2 , with aqueous gold complexed with H_2S (Kerrick and Fyfe 1981; Phillips and Groves 1983). The reactivity of the CO_2 and H_2S bearing gold fluids with ferromagnesian minerals of the host rocks aids in the precipitation of mineralization. The reaction between the gold fluid and the host rock typically forms Mg and Fe bearing carbonates and Fe sulfides in the alteration mineral assemblages (Kerrick and Fyfe 1981; Böhlke 1988). Moreover, if the host rocks contain sufficient Al, minerals with K and Na such as biotite and albite are precipitated during alteration (Goldfarb et al. 2005).

2.5.1 Geochemical and isotopic relationships

Mineralization at the Canadian Malartic deposit has been associated with pervasive potassic, carbonatization, and sulfidation alterations (Helt et al. 2014). The PCA's of both greywackes and mafic

dykes provide more insight into correlations between alteration and mineralization. The first components (PC1) indicate Au, C, S and $\delta^{18}\text{O}$ co-vary, and are inversely related to major rock forming elements (SiO_2 , Al_2O_3 , MgO , and Fe_2O_3) and $\delta^2\text{H}$. This is interpreted to reflect the mineralizing process whereby the auriferous fluids reacted with these host rocks by replacing primary minerals with a Au-, C-, and S-bearing mineralization assemblage accompanied by increasing whole-rock $\delta^{18}\text{O}$ and decreasing whole-rock $\delta^2\text{H}$. The second component (PC2) for both greywackes and mafic dykes reflects the changes in alkali-bearing minerals that are attributed to potassic alteration (Fig. 2.11 and 2.12). In greywackes, alkali-covariation captured by PC2 is related to hydrothermal biotite infilling micro-fissures (Figs. 2.7 E and F). In mafic dykes, PC2 may be ascribed to overgrowths of biotite on amphibole (Figs. 2.9 A and B; 2.10 A and B).

2.5.2 Oxygen and hydrogen isotopic footprint

Mapping of the whole-rock isotopic values of the host rocks to the Canadian Malartic deposit has revealed an isotopic footprint that can be attributed to mineralization (Figs 2.17 and 2.18). This footprint is best identified by an increase in $\delta^2\text{H}$ away from mineralization in greywackes from values below -80‰ within the Canadian Malartic pit to background values greater than ca. -59‰ 1 to 2 km outside of the pit. In mafic dykes, the footprint is best described as a decrease in $\delta^{18}\text{O}$ from values greater than 9.0‰ within and proximal to the Canadian Malartic pit, to background values near 8.3‰ up to 1 km outside of the pit (Fig. 2.19).

In greywackes, the oxygen isotopic footprint is not apparent along sections P1, P2, and P3 (Figs. 2.13, 2.14, and 2.15). However, geostatistical analysis and kriging of the greywacke $\delta^{18}\text{O}$ values may indicate a subtle footprint as the 9.9‰ isopleth wraps around the Canadian Malartic pit, extends eastward along the CLLTZ, and delineates an area southeast of the Canadian Malartic deposit similar to the area outlined by the -59‰ $\delta^2\text{H}$ greywacke isopleth (Fig. 2.17). The footprint attributed to mineralization cannot be unequivocally defined using $\delta^{18}\text{O}$ values of greywackes alone, due to the low amplitude of $\delta^{18}\text{O}$ values which makes distinguishing mineralization from background values difficult (Fig. 2.17 A). However, the $\delta^2\text{H}$ values of greywackes surrounding the Canadian Malartic deposit form a distinct footprint. Figure 2.17 B shows the -59‰ isopleth encircling two areas of low $\delta^2\text{H}$. The first area includes the lowest $\delta^2\text{H}$ values and is centered on the core of Canadian Malartic deposit. The second area outlines a more diffuse region towards the southeast and south of the Canadian Malartic deposit. These areas of low $\delta^2\text{H}$ extend towards, but do not encompass, the weakly mineralized Cartier zone towards the northwest, and the Bravo zone to the southeast of the study area. However, the northwest region of the map is sparsely sampled (Fig. 2.17). Furthermore, the Gouldie Zone immediately southeast of the Canadian Malartic pit is not

enclosed by either the 9.9‰ $\delta^{18}\text{O}$ isopleth or the -59‰ $\delta^2\text{H}$ isopleth. The overall northwest-southeast geometry of both $\delta^{18}\text{O}$ and $\delta^2\text{H}$ isotopic footprints is sub-parallel with the orientation of the CLLTZ and other structural features in the area such as the Sladen fault and dominant foliation throughout the area. Therefore, these structural features can be interpreted to have acted as conduits focusing fluid/rock interaction throughout the area.

In mafic dykes, the 8.3‰ $\delta^{18}\text{O}$ isopleth covers an area centered on the Canadian Malartic pit and up to 1 km southeast of the pit as well as a small area near the southern margin of the mapped region. The highest $\delta^{18}\text{O}$ values are found within the mineralized domain (Figs. 2.13 B, 2.14 B, and 2.15 B). Overall, the general orientation of the 8.3‰ isopleth is northwest-southeast suggesting that it has been influenced by the CLLTZ (Fig. 2.18 A). The $\delta^2\text{H}$ values of mafic dykes show less of a spatial association with the mineralization as compared to greywackes. The spatial association between $\delta^2\text{H}$ values of mafic dykes and mineralization may have not been discerned with the wide sample spacing of this rock type (Fig. 2.18 B).

Mapping of the isotopic footprint using oxygen and hydrogen isotopes from both rock types has revealed that the general trends defined in both lithologies are the same. In both cases, the isotopic footprint can be attributed to a decrease in $\delta^2\text{H}$ and an increase in $\delta^{18}\text{O}$ (Figs. 2.13, 2.14, and 2.15). and this is also supported by the results of the PCAs (Figs. 2.11 and 2.12). However, the spatial identification of the isotopic footprint is best identified in the $\delta^2\text{H}$ values of greywackes, which enlarge the footprint up to 1.5 km south and 2 km southeast of the Canadian Malartic pit (Fig. 2.17), and the $\delta^{18}\text{O}$ values of mafic dykes, which enlarge the footprint up to 1 km southeast of the Canadian Malartic pit (Figs 2.18, 2.19). Also, the general northwest-southeast orientation of the isotopic footprint is subparallel to the dominant structural features throughout the study area, further suggesting these features have focused fluid flow throughout these host rocks and acted as loci of fluid/rock interaction.

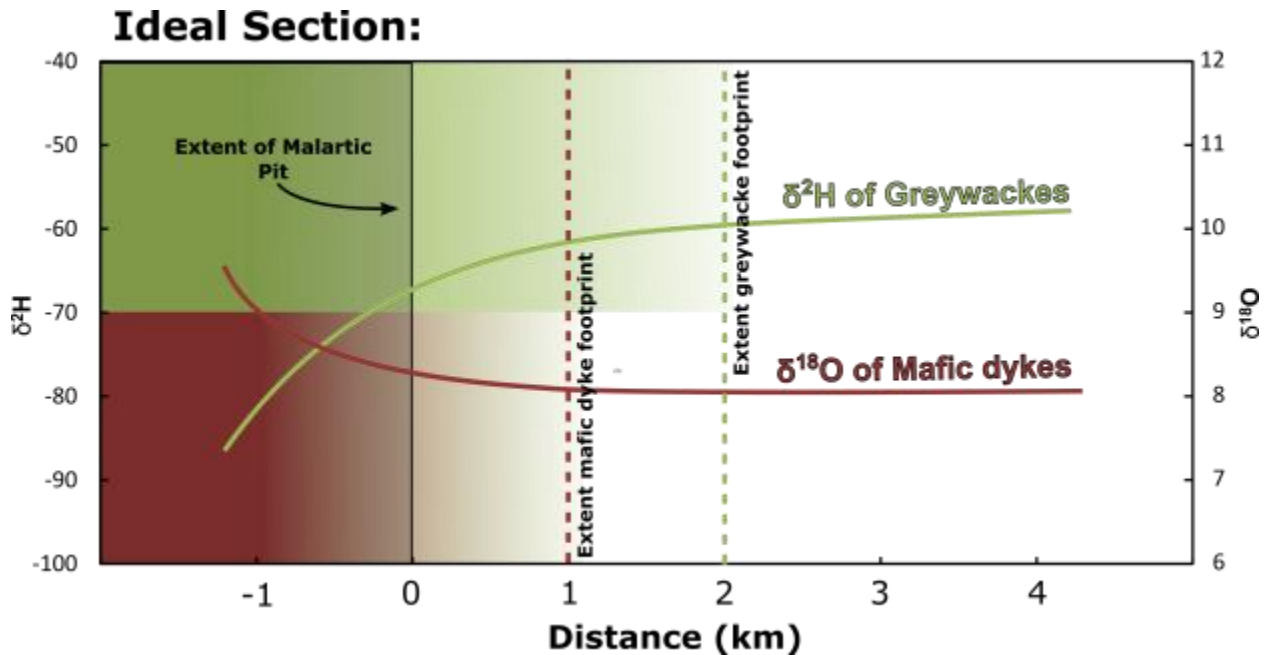


Figure 2.19: Schematic section of changes in $\delta^2\text{H}$ in greywackes and $\delta^{18}\text{O}$ of mafic dykes with distance from the Canadian Malartic pit.

2.5.3 Fluid oxygen and hydrogen isotopic composition

In order to facilitate the computation of the isotopic composition of fluids interacting with the host rocks to the Canadian Malartic deposit, an idealized mineralogy of the greywacke corresponding to 50 vol.% quartz and 50 vol.% biotite has been used in isotopic fractionation equations. Other minerals identified in thin sections such as feldspar, chlorite, and white micas have been left out of the modeling calculations. Due to the typically lower modal abundances (Table 2.4) of these minerals in the rocks and similar fractionation factors to either quartz or biotite, the elimination of these minerals results in much simpler calculations with little effects on the resulting models. Similarly, the average oxygen and hydrogen isotopic composition of greywacke samples from outside of the hydrothermal footprint (defined herein to be the -59‰ $\delta^2\text{H}$ isopleth; Fig. 2.17 B), is 9.8‰ and -53‰ respectively ($n = 32$). These values come from the least altered rocks in the studied area and have been used as an initial rock composition in the equations (δ_{Rock}^i). The composition of the metamorphic water in equilibrium with the least altered greywacke can be calculated using the fractionation equations of Bottinga and Javoy (1975) and Matsuhisa et al. (1979). At a temperature close to that of the greenschist-amphibolite transition of 475°C , the fluid in equilibrium with the least altered greywacke is calculated to have a $\delta^{18}\text{O}$ value of 7.6‰ and $\delta^2\text{H}$ value of -12‰ (Fig. 2.20). These values are very similar to the isotopic composition computed from vein biotite mineral separates of $\delta^{18}\text{O}_{\text{Fluid}} = 6.3\text{‰}$ to 9.4‰ and $\delta^2\text{H}_{\text{Fluid}} = -11\text{‰}$ to -4‰ from the Canadian Malartic deposit (Helt et al. 2014; Beaudoin and Raskevicius, 2014) and also the calculated composition

of mineralizing fluids of nearby metamorphic gold deposits (Beaudoin and Pitre 2005; Beaudoin and Chiaradia 2016). Using this evidence, the metamorphic fluid in equilibrium with least altered greywackes has been used as the initial fluid composition for the subsequent fluid/rock isotopic exchange models.

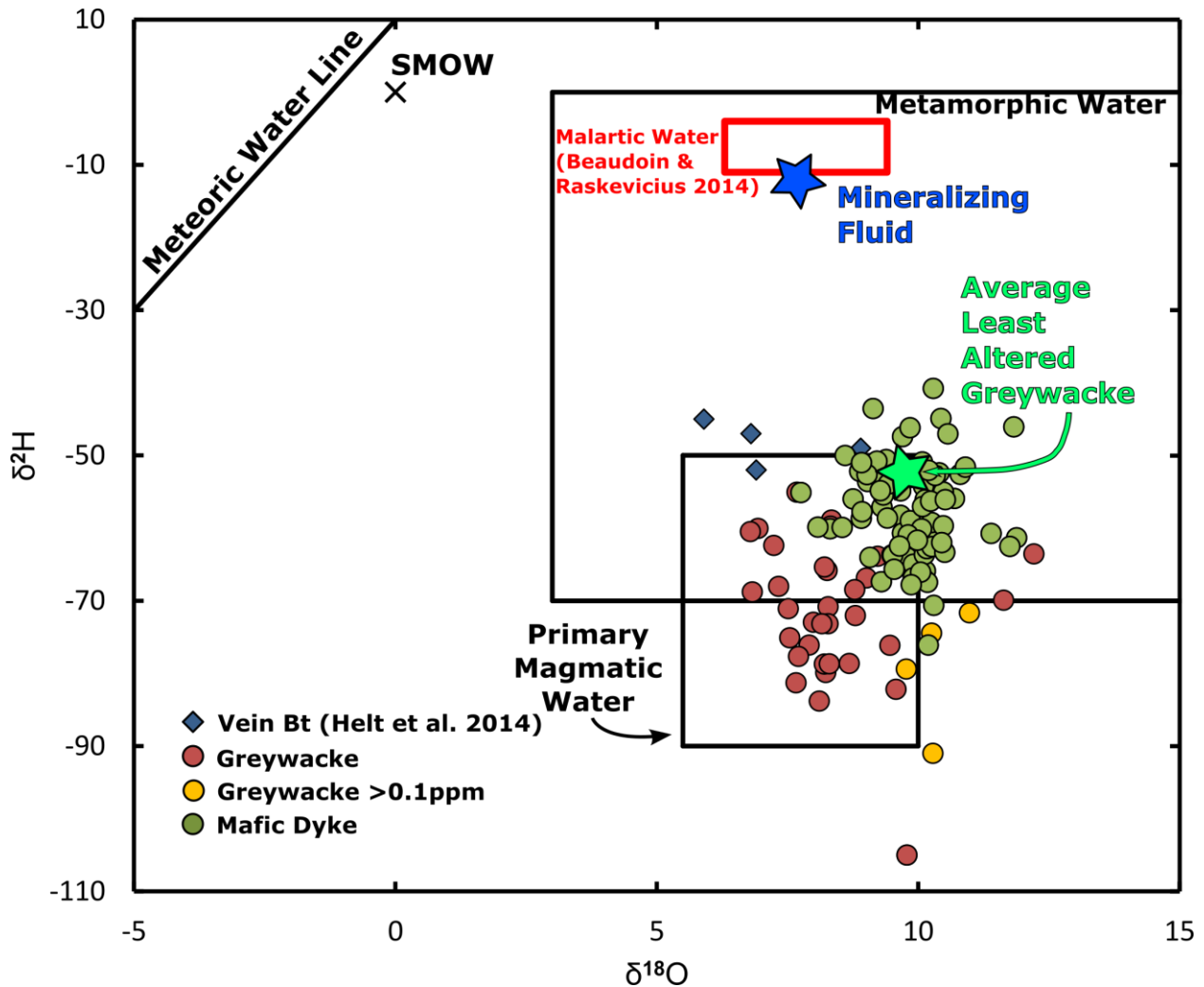


Figure 2.20: Plot of $\delta^{18}\text{O}$ and $\delta^2\text{H}$ values of whole-rock greywackes and mafic dykes from the Canadian Malartic deposit, vein biotite from the deposit and fields of various natural waters from Sheppard (1986). Composition of the average unmineralized greywacke is indicated with the green star and the water in equilibrium with this rock at upper greenschist to amphibolite conditions is shown by the blue star. The values for this fluid coincides with the fluid composition calculated from biotite in veins from the Canadian Malartic deposit (Beaudoin and Raskevicius 2014; Helt et al. 2014).

2.5.4 Modeling of fluid/rock reactions

With the composition of the metamorphic fluid constrained to that in equilibrium with average least altered greywacke, which is similar to the isotopic composition of the mineralizing fluid, the processes involved in generating the isotopic footprint can be modeled. The final isotopic composition of the host rocks observed throughout the footprint (Figs 2.17 and 2.18) is determined by (1) the mineralogy of these rocks (2) the initial isotopic composition of the rock (3) the fluid/rock ratio, and (4) the temperature of reaction (Taylor 1978). To compute these models, several simplifications are required: (1) Idealized mineralogy for both rock types have been used as including accessory mineral phases results in complicated computations and has a negligible effect on the resulting models. These idealized mineralogies correspond to the aforementioned assemblage for greywackes and 45 vol. % hornblende, 45 vol. % biotite and 10 vol. % anorthite for mafic dykes. (2) The initial isotopic composition of greywackes is approximated using the average least altered greywacke samples as described above ($\delta^{18}\text{O} = 9.7\text{‰}$, $\delta^2\text{H} = -53\text{‰}$). Similarly, the initial isotopic composition of mafic dykes is approximated by the average of the least altered and most distal samples outside of the -69‰ $\delta^2\text{H}$ isopleth (Fig. 2.18 A; $n = 11$, $\delta^2\text{H} = -63\text{‰}$ and $\delta^{18}\text{O} = 7.3\text{‰}$). Using these assumptions, we compute the final rock composition for both rock types using equations outlined by Taylor (1978) for fluid/rock ratios of 0 to 8 assuming open system conditions at temperatures of 350°C, 300°C and 250°C to span the geologically relevant temperatures of greenschist facies metamorphism and orogenic gold deposits.

Fluid/rock reaction paths indicate that the trend towards higher $\delta^2\text{H}$ values observed in rocks away from mineralization may be explained by fluid/rock isotopic exchange with a deep-seated metamorphic fluid derived from dewatering of the Pontiac Group metasediments near 475°C (Fig. 2.21). The isotopic values of mineralized greywackes (>0.1 ppm) have $\delta^2\text{H}$ values of -91‰ to -72‰ and $\delta^{18}\text{O}$ values of 9.8‰ to 11.0‰ . These values are best approximated by the fluid/rock reaction path at ca. 300°C. This model suggests that rocks in the footprint to Canadian Malartic deposit have reacted at a temperature of ca. 300°C with the mineralizing fluid at molecular fluid/rock ratios up to a maximum of 0.5, indicating that the system was rock dominated and fluid/rock ratios throughout the footprint remained low. Due to the relative differences in atomic ratios of oxygen and hydrogen that make up a rock and fluid respectively, during fluid/rock isotopic exchange in any hydrothermal system, the final rock composition will at first exhibit more change in $\delta^2\text{H}$ values up to a point. After this threshold, the shift in $\delta^2\text{H}$ of the rock has approached its asymptote, and the $\delta^{18}\text{O}$ values will exhibit greater change. The data collected from greywackes indicates fluid/rock reaction has more extensively altered the $\delta^2\text{H}$ values of the rocks, with the $\delta^{18}\text{O}$ values mostly unchanged (Fig. 2.21).

At the time of mineralization, the mineralizing fluid would have been sourced from a deeper and hotter structural level in the crust than the location of gold deposition. Thus, the isotopic composition of this fluid would have reflected a temperature of equilibration corresponding to this deeper level in the crust near the greenschist-amphibolite transition (ca. 475°C), but, after rising through the crust to a level of thermochemical disequilibrium coinciding to gold mineralization, the fluid/rock exchange and alteration in the footprint of the deposit would reflect a lower temperature closer to ca. 300°C (Fig. 2.21). This explanation of the whole-rock isotopic data is consistent with the timing of mineralization being pre- to syn- metamorphic and occurring prior to or during burial of the now -mineralized Pontiac metasediments as proposed by Piette-Lauzière (2017).

The isotopic footprint of mafic dykes is better observed as an increase in $\delta^{18}\text{O}$ values proximal to mineralization rather than a shift in $\delta^2\text{H}$ values (Fig. 2.18 A). The observed $\delta^{18}\text{O}$ footprint exhibited by mafic dykes from background values near 8.3‰ to values greater than 9‰ proximal to mineralization cannot be well explained by fluid/rock reaction paths (Fig. 2.21). Alternatively, the incorporation of epigenetic carbonates as an alteration from the mineralizing process may be the cause of the increase in $\delta^{18}\text{O}$ proximal to mineralization in the footprint attributed to mafic dykes. Principal component analysis has shown carbon to correlate well with gold (Fig. 2.12). Moreover, due to the magnesium and iron in the mafic dykes, carbonate alteration has a greater chemical affinity to form in this rock type than the greywackes. Carbonates also contain a high atomic proportion of oxygen than other rock forming minerals in the dykes, and tend to have high $\delta^{18}\text{O}$ values when precipitated from hydrothermal fluids. As a result, even a small addition of carbonate material has the potential to have a large effect on whole-rock $\delta^{18}\text{O}$ values. Therefore, the increase in $\delta^{18}\text{O}$ of the footprint may be attributed to increasing carbonatization proximal to mineralization rather than isotopic exchange with the mineralizing fluid.

The PCAs of both greywackes and mafic dykes throughout the study area show a strong association between gold mineralization, sulfidation, and carbonatization (Figs. 2.11 and 2.12). The altered rocks throughout the footprint also show a subtle increase in $\delta^{18}\text{O}$ values proximal to mineralization and a marked decrease in $\delta^2\text{H}$ values proximal to mineralization (Figs. 2.13, 2.14, and 2.15). These changes throughout the footprint of the deposit are consistent with a mineralizing fluid formed by dehydration of the Pontiac metasediments near the greenschist-amphibolite transition at ca. 475°C. This metamorphic fluid would have subsequently ascended along structural conduits to a higher level in the crust to precipitate gold, carbonates and sulphides at ca. 300°C.

Isotopic values of biotite mineral separates sourced from veins from the Canadian Malartic deposit have been shown to have equilibrated at 475°C (Helt et al. 2014; Beaudoin and Raskevicius, 2014). In order to reconcile these results with a fluid/rock exchange at 300°C in the footprint to the deposit we must consider the entire geologic history of these rocks. Although the biotite in auriferous veins may be in equilibrium with quartz, the ca. 475°C calculated temperature of equilibration may not represent a temperature of precipitation, but rather, likely reflects a temperature close to the post-mineralizing peak metamorphic conditions after burial of the mineralized system. Burial of the Canadian Malartic deposit would have subjected the host rocks in the footprint and constituent biotite veins to increasing temperatures and prograde metamorphism. During this process, oxygen and hydrogen isotopic exchange between individual mineral grains would re-equilibrate to reflect increasing temperatures. However, during isochemical metamorphism the net-transfer of oxygen and hydrogen isotopes between minerals in the rocks and veins is a zero-sum game (Chamberlain et al. 1990; Young 1993). Therefore, the bulk isotopic values of whole-rock samples that have been used to identify the hydrothermal footprint to the Canadian Malartic deposit preserve the effects of an infiltrating fluid, whereas, mineral separates may represent a thermal re-equilibration to higher temperatures during prograde metamorphism. This exchange of O and H isotopes between the mineralizing fluid and host rocks throughout the footprint appears to be preserved only in whole-rock data and illustrates the effectiveness of these methods to exploration programs.

Alternative hypotheses for a fluid that may have caused the decrease in $\delta^2\text{H}$ observed in the footprint to could invoke either (1) a magmatic source or (2) a high latitude meteoric source. Although a magmatic fluid would have a sufficiently low $\delta^2\text{H}$ composition to decrease the $\delta^2\text{H}$ values of greywackes and mafic dykes near the Canadian Malartic deposit (Sheppard 1986), correlations captured by the PCAs indicate that the potassic alteration commonly associated with a magmatic fluids has little co-variance with whole-rock $\delta^2\text{H}$ and $\delta^{18}\text{O}$ values, Au, C, or S (Figs 2.11 and 2.12). Second, a high latitude meteoric fluid is also unlikely to have been the source of isotopic variation in these rocks because at the time of mineralization during the Archean, the planet lacked much of the continental landforms and cold polar regions needed to produce a fractionated, low $\delta^2\text{H}$ meteoric water. However, interaction between a geologically recent meteoric fluid with low $\delta^2\text{H}$ values may be the cause of retrograde chloritization of biotites observed in select greywacke samples (Figs 2.7 C and D) and the decomposition of feldspars to hydrous minerals is seen some mafic dykes (Figs 2.9 E and F). This type of late alteration appears to be very localized and not spatially associated with the mineralized domain. Therefore, it is unlikely that the entire isotopic footprint to the Canadian Malartic deposit can be attributed to a late meteoric fluid.

2.5.5 Canadian Malartic and disseminated gold deposits

The Canadian Malartic gold deposit shares many features with other large gold deposits from around the globe. The isotopic footprint surrounding this deposit shows a clear association with carbonatization and sulfidation of the Pontiac greywackes and mafic dykes, which are ubiquitous alteration styles of orogenic gold deposits. The temperature inferred for fluid/rock exchange (ca. 300°C) is also typical of this type of mineralization (Kerrick and Fyfe 1981; Phillips and Groves 1983; Groves 1993; Robert and Poulsen 1997; Goldfarb et al. 2005). The isotopic composition of the mineralizing fluid ($\delta^{18}\text{O} = 7.6\text{‰}$ and $\delta^2\text{H} = -12\text{‰}$) have $\delta^2\text{H}$ values higher than those of the “typical” range determined by Goldfarb et al. (2005) of $\delta^{18}\text{O}$ from 6‰ to 13‰ and $\delta^2\text{H}$ from -80‰ to -20‰. The isotopic composition of the mineralizing fluid at the Canadian Malartic deposit is also outside of the range of magmatic fluids exsolved from fractionating silicate melts (Sheppard 1986).

In previous studies, gold deposits that exhibit mineralizing fluid compositions with anomalously high $\delta^2\text{H}$ values have been interpreted to be a result of fluid mixing between a deep seated metamorphic fluid and a supracrustal fluid (Hagemann et al. 1994; Beaudoin and Pitre 2005; Beaudoin and Chiaradia 2016). Moreover, Beaudoin and Chiaradia (2016) indicate a temperature gradient from ca. 500°C to ca. 250°C coupled with fluid mixing with a supracrustal-derived fluid caused the range in isotopic values observed in quartz-tourmaline veins from the Val-d’Or vein field. In contrast, the high $\delta^2\text{H}$ values of the mineralizing fluid at the Canadian Malartic deposit could be in isotopic equilibrium with the metamorphic fluid sourced from dehydration of the voluminous Pontiac metasedimentary host rocks.

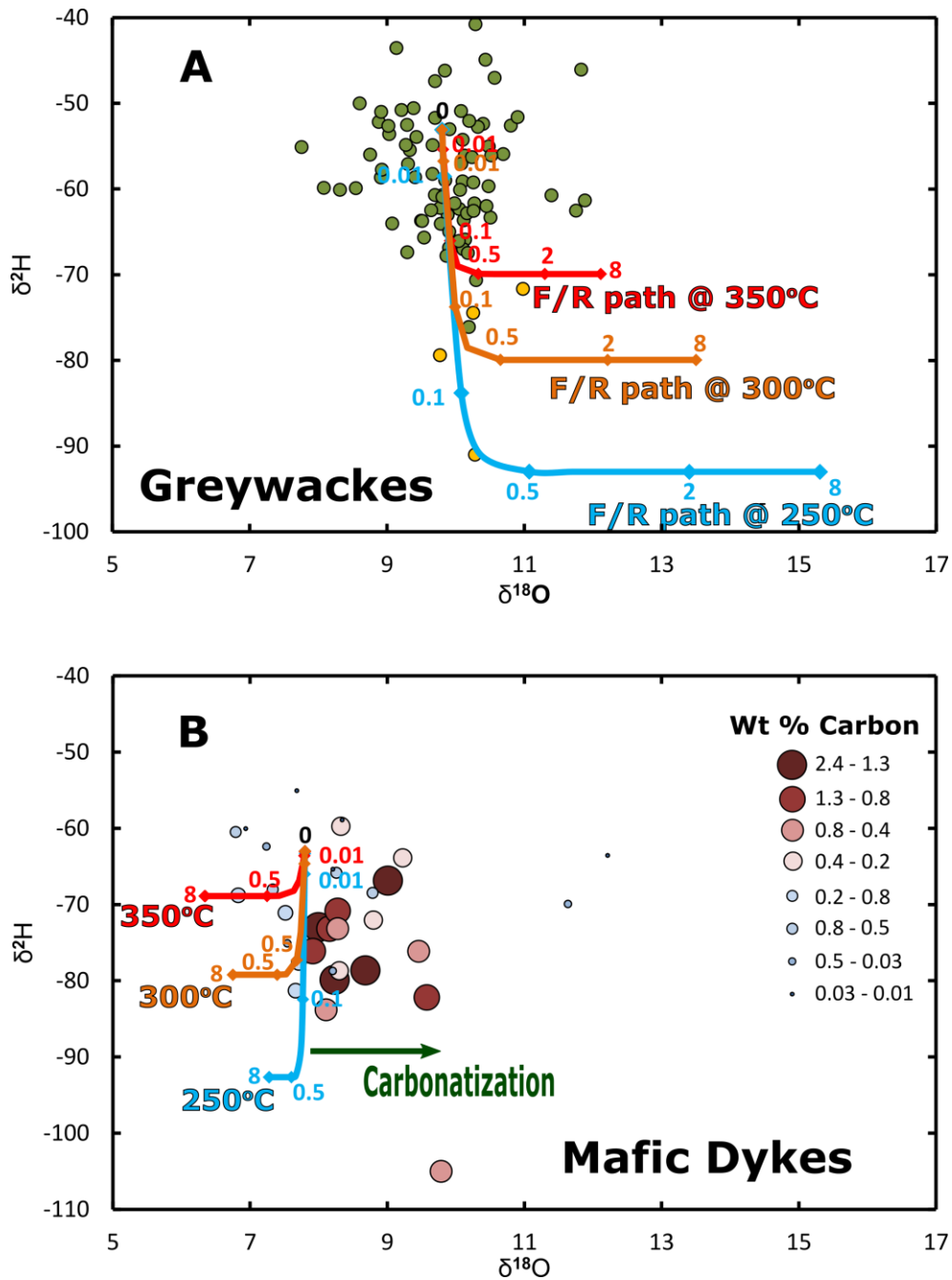


Figure 2.21: Plot of $\delta^{18}\text{O}$ and $\delta^{2}\text{H}$ values of (A) greywackes and (B) mafic dykes from the study area. Models for open system fluid/rock isotopic exchange between the rocks and the mineralizing fluid are presented for temperatures of equilibration at 350°C (red), 300°C (orange) and 250°C (blue). Greywackes with >0.1 ppm Au are shown as yellow points. Ticks along fluid/rock reaction paths indicate molecular fluid/rock ratios.

2.5.4 Applications to Exploration

Whole-rock stable isotopic data are currently underused in the application to exploration of ore deposits. This study has shown that the isotopic footprint attributed to the Canadian Malartic deposit can be identified up to 2.5 km outside of the actual mineralized domain. This footprint is best identified by a decrease in $\delta^2\text{H}$ in Pontiac metasedimentary greywackes surrounding the deposit and by an increase in the $\delta^{18}\text{O}$ of mafic dykes throughout the same area. The $\delta^2\text{H}$ of greywackes decreases from background values of ca. -59‰ to values less than -90‰ near the core of the mineralized domain. This $\delta^2\text{H}$ footprint extends approximately from 0.5 to 2 km south of the Canadian Malartic pit, up to 1 km to the northwest and up to 2.5 km to the southwest. The smaller isotopic footprint of the $\delta^{18}\text{O}$ composition of mafic dykes is marked by an increase in whole-rock $\delta^{18}\text{O}$ values from background values ca. 8.3‰ to values greater than 9‰ within the mineralized domain. This $\delta^{18}\text{O}$ footprint extends approximately, 1 km to the southeast beyond the open pit.

Despite obvious benefits to exploration programs, stable isotopic data remains underused normally because of the high analytical cost, long processing times, and number of samples needed to determine statistically useful exploration vectors (Barker et al. 2013). These reasons remain true with respect to the application of oxygen isotopes. In silicate minerals, oxygen atoms are tightly bound in crystal structures and require overnight reaction with BrF_5 in order for the $\text{O}_{2(\text{g})}$ to be liberated and analyzed by IRMS (Clayton and Mayeda 1963). This method is extremely laborious and results in the high analytical costs associated with stable isotopic analysis. Alternatively, hydrogen (as well as carbon and sulfur) have been shown have a strong association with Au content as shown by the PCAs (Figs. 2.11 and 2.12). These elements are more easily volatilized from a rock, thus, making measurements of their isotopic ratios easier and less expensive. This study exemplifies the benefits of the application of whole-rock hydrogen isotopic ratios to the exploration of mineral deposits. Moreover, due to the relatively low analytical cost, potential bulk sampling methods, and the sensitivity of hydrogen isotopes to record subtle fluid/rock interactions even in rock dominated systems, whole-rock hydrogen isotopes are shown to have great potential in the application to exploration for new hydrothermal ore deposits.

2.6 Conclusions

The oxygen and hydrogen isotopic footprint to the Canadian Malartic deposit is observed in both the Pontiac metasedimentary greywackes and the less voluminous mafic dykes up to 2.5 km outside the open pit of the Canadian Malartic deposit. The majority of the variance in the geochemical and isotopic data for these rocks can be ascribed to the mineralizing process that resulted in carbonatization, sulfidation, and

mineralization. This process also records subtle increases in $\delta^{18}\text{O}$ and moderate decreases in $\delta^2\text{H}$ values in these rocks.

The isotopic footprint to the Canadian Malartic deposit is best expressed in greywackes by an increase in $\delta^2\text{H}$ values from less than -90‰ within the Canadian Malartic pit to background values of ca. -59‰, and in mafic dykes by a decrease in $\delta^{18}\text{O}$ from values greater than 9‰ to background values of ca. 8.3‰. In greywackes, the $\delta^2\text{H}$ footprint extends approximately from 0.5 to 2 km south of the Canadian Malartic pit, up to 2 km to the northwest and up to 2 km to the southwest, whereas, the $\delta^{18}\text{O}$ footprint in greywackes is subtler and may only be apparent after geostatistical analysis by the wrapping of the 9.9‰ isopleth around the Canadian Malartic deposit and the CLLTZ. In mafic dykes, the $\delta^2\text{H}$ footprint may be represented by the -72‰ isopleth, which encircles much of the area south and southeast of the Canadian Malartic deposit, whereas the $\delta^{18}\text{O}$ footprint is centered on the deposit and extends beyond the open pit approximately 0.5 km towards the south and up to 1 km to the southeast.

The nature of the isotopic footprint and alteration in the footprint to the Canadian Malartic deposit is hypothesized to be the result of exchange between rocks throughout the footprint with a metamorphic fluid formed by the breakdown of hydrous mineral phases in the Pontiac metasediments near the greenschist-amphibolite transition at ca. 475°C that subsequently ascended along structural conduits to a the location of gold deposition and alteration coinciding with a temperature of ca. 300°C. Mineralization appears to be early to syn-metamorphism (Piette-Lauzière, 2017) therefore, regional deformation and peak metamorphic conditions may overprint evidence of original mineralizing conditions (De Souza et al. 2015; Perrouy et al. 2017). But, the isotopic exchange between the mineralizing fluid and the rocks throughout the footprint is preserved in whole-rock isotopic data.

Notwithstanding the processes that have resulted in the isotopic footprint to the Canadian Malartic deposit, the $\delta^{18}\text{O}$ and $\delta^2\text{H}$ data of these host rocks has proven useful in highlighting domains prospective for mineralization. Particularly due to the lower analytical costs, logistically simpler laboratory methods, and sensitivity to low fluid/rock ratios, the use of whole-rock $\delta^2\text{H}$ data lends itself to be particularly useful to future exploration programs for hydrothermal ore deposits.

Acknowledgements

This study is part of the NSERC-CMIC Footprints network. Support has also been provided by the Society of Economic foundation (SEGF). We also would like to acknowledge the logistic support given by Canadian Malartic as well as other sponsors of the NSERC-CMIC footprints project. Special thanks are given to the supervisors of this work (Georges Beaudoin and Kurt Kyser), Colleagues who are part of the NSERC-CMIC gold team (Nicolas Gaillard, and Stephane Perrouty). NSERC-CMIC Mineral Exploration Footprint Project Contribution #157.

2.7 Tables

Table 2.1: Whole-rock geochemical data for Pontiac metasedimentary greywackes. Locations are listed in Table 2.3.

Sample Number	Au (ppm)	C (Wt%)	S (Wt%)	SiO ₂ (Mol%)	Al ₂ O ₃ (Mol%)	Fe ₂ O ₃ (Mol%)	MnO (Mol%)	MgO (Mol%)	CaO (Mol%)	Na ₂ O (Mol%)	K ₂ O (Mol%)	TiO ₂ (Mol%)	P ₂ O ₅ (Mol%)
K388003	0.008	0.102	0.29	74.53	9.34	2.25	0.06	4.8	3.08	3.74	1.73	0.43	0.03
K388026	0.003	0.022	0.21	73.28	10.29	2.16	0.06	4.81	2.93	4.41	1.59	0.43	0.04
K388035	0.003	0.02	0.23	73.88	10.22	2.14	0.06	4.8	3.02	4.23	1.16	0.43	0.04
K388065	0.016	0.067	0.31	72.68	10.68	2.54	0.06	4.88	2.43	3.49	2.67	0.52	0.05
K388070	0.002	0.013	0.26	75.41	9.63	2.04	0.06	4.28	3	4.28	0.84	0.43	0.03
K388084	0.001	0.199	0.43	73.24	9.58	2.38	0.06	5.09	2.9	5.15	1.04	0.5	0.05
K388095	0.001	0.021	0.2	74.3	9.94	2.31	0.07	4.59	3.13	3.88	1.28	0.48	0.03
K388106	0.000	0.096	0.2	72.37	11.75	2.75	0.06	5.7	2.17	2.41	2.28	0.47	0.04
K388117	0.007	0.032	0.28	74.79	9.71	2.18	0.06	4.22	3.19	3.93	1.45	0.44	0.03
K388202	0.022	0.387	0.45	73.41	9.94	2.41	0.07	4.49	3.15	3.56	2.4	0.52	0.04
K388235	0.002	0.093	0.28	74.7	9.77	2.32	0.07	4.07	3.28	3.9	1.42	0.43	0.03
K388243	0.003	0.023	0.14	72.31	10.7	2.55	0.08	4.93	3.08	4.75	1.07	0.47	0.04
K388254	0.002	0.067	0.26	76.4	9.08	1.93	0.06	4.07	2.75	3.94	1.34	0.4	0.03
K388268	0.001	0.047	0.18	76.93	9.15	1.85	0.05	3.67	2.5	4.55	0.87	0.37	0.04
K388277	0.002	0.027	0.32	74.03	9.81	2.29	0.06	4.72	3.01	4.08	1.5	0.47	0.03
K388292	0.003	0.029	0.05	80.32	9.13	1.49	0.04	3.34	1.87	1.31	2.24	0.25	0.01
K388303	0.002	0.021	0.2	73.89	9.41	2.74	0.07	5.15	2.56	4.15	1.45	0.53	0.04
K388333	0.002	0.017	0.53	70.72	9.79	2.89	0.07	8.31	2.87	4.22	0.62	0.47	0.04
K388360	0.013	0.119	0.38	76.58	9.17	2.11	0.05	4.22	2.13	2.93	2.35	0.44	0.03
K388386	0.001	0.048	0.39	72.37	9.55	2.56	0.07	6.03	3.59	3.61	1.7	0.48	0.04
K388397	0.003	0.014	0.3	74.86	9.8	2.11	0.05	4.55	2.13	4.29	1.75	0.43	0.04
K388418	0.001	0.358	0.14	69.35	8.98	2.67	0.09	9.46	4.69	2.65	1.62	0.45	0.05
K388433	0.005	0.018	0.27	74.3	9.44	2.31	0.06	4.67	3.01	4.12	1.58	0.47	0.04
K389002	0.431	0.564	1.65	74.37	9.18	1.44	0.04	2.34	3.7	7.64	0.75	0.47	0.08
K389017	1.52	0.487	1.07	71.52	9.75	2.17	0.06	4.63	3.46	6.34	1.61	0.44	0.02

K389022	0.138	0.238	0.73	74.34	9.3	2.41	0.06	4.75	2.74	3.47	2.35	0.55	0.04
K389027	0.007	0.113	0.62	71.75	11.84	2.7	0.05	6.1	1.99	1.7	3.19	0.64	0.03
K389030	0.004	0.039	0.2	69.02	11.39	3.17	0.12	5.68	4.42	3.45	2.07	0.64	0.04
K389036	0.001	0.027	0.3	71.76	11.45	2.88	0.08	5.66	1.98	2.44	3.12	0.6	0.04
K389049	0.021	0.048	0.29	72.19	11.77	2.62	0.06	5.06	1.81	2.33	3.54	0.58	0.04
K389053	0.022	0.471	0.48	74.84	9.37	1.98	0.09	3.37	4.4	3.53	1.96	0.43	0.03
K389069	0.001	0.027	0.1	72.54	11.05	2.32	0.06	4.51	2.75	4.13	2.12	0.49	0.03
K389073	0.06	0.07	0.34	66.17	13.11	3.13	0.07	6.53	3.35	3.81	3.19	0.61	0.03
K389078	0.004	0.016	0.12	72.62	10.4	2.65	0.07	5.26	3.1	4.05	1.33	0.48	0.03
K389080	0.001	0.024	0.14	72.59	11.35	2.51	0.06	4.82	2.69	3.09	2.33	0.53	0.03
K389086	0.036	0.025	0.08	69.06	11.74	2.74	0.06	5.77	3.48	4.32	2.22	0.56	0.04
K389089	0.000	0.017	0.23	75.46	9.41	2.1	0.06	3.99	2.58	4.46	1.48	0.41	0.03
K389105	0.001	0.015	0.27	68.73	13.48	3.48	0.08	6.25	1.94	2.02	3.32	0.66	0.04
K389106	0.000	0.01	0.08	71.31	11.68	2.71	0.06	5.81	1.99	2.72	3.15	0.52	0.04
K389110	0.001	0.02	0.3	74.34	9.46	2.5	0.09	4.47	3.67	3.6	1.36	0.48	0.04
K389115	0.002	0.02	0.22	70.14	11.19	2.72	0.07	5.32	3.33	4.76	1.85	0.56	0.05
K389127	0.001	0.019	0.06	69.66	11.5	2.75	0.07	5.59	3.57	4.29	1.95	0.59	0.04
K389128	0.001	0.013	0.29	71.31	11.81	2.81	0.07	6.03	2.48	2.97	1.87	0.61	0.03
K389148	0.001	0.067	0.31	72.06	11.22	2.63	0.07	4.91	2.82	3.79	1.9	0.56	0.04
K389154	0.001	0.029	0.23	72.59	11.21	2.6	0.07	5.24	2.51	3.37	1.83	0.56	0.04
K389213	0.977	0.459	0.73	71.44	10.15	2.57	0.08	5.2	4.06	3.03	2.9	0.52	0.05
K389232	0.001	0.079	0.19	71.94	11.66	2.59	0.07	5.33	2.64	2.96	2.24	0.54	0.04
K389326	0.001	0.009	0.01	73	11.41	1.95	0.05	5.93	2.08	2.66	2.58	0.3	0.02
K389328	0.002	0.014	0.17	72.15	11.28	2.83	0.07	5.69	2.26	2.82	2.3	0.56	0.04
K389333	0.000	0.016	0.02	74.29	10.16	1.92	0.04	3.9	2.92	5.1	1.25	0.38	0.04
K389334	0.002	0.006	0.11	74.79	10.13	2.01	0.07	4.05	3	4.07	1.41	0.43	0.03
K389335	0.001	0.009	0.22	70.63	12.14	3.04	0.06	5.79	2.48	2.37	2.82	0.62	0.05
K389336	0.000	0.011	0.05	72.32	10.89	2.2	0.06	4.69	3.18	4.48	1.71	0.44	0.04
K389339	0.000	0.011	0.19	75.34	9.69	2.11	0.06	4.37	2.75	3.99	1.2	0.47	0.03
K389342	0.000	0.024	0.16	73.93	9.83	2.29	0.07	4.92	3.16	4.41	0.91	0.46	0.03
K389345	0.001	0.021	0.07	71.93	11.28	2.61	0.07	5.01	3.07	3.36	2.07	0.56	0.04

K389347	0.001	0.012	0.14	69.91	11.68	2.76	0.06	5.62	3.01	4.1	2.29	0.54	0.04
K389348	0.001	0.041	0.18	75.27	9.76	1.78	0.05	4.41	4.04	3.3	0.97	0.37	0.03
K389350	0.001	0.012	0.24	76.74	9.04	2.05	0.06	4.04	2.69	3.7	1.23	0.42	0.03
K389951	0.005	0.016	0.33	70.4	12.27	2.94	0.1	5.8	2.64	3.31	1.92	0.59	0.04
K389953	0.004	0.01	0.15	73.26	10.73	2.3	0.06	4.61	2.8	3.73	1.99	0.49	0.04
K389954	0.003	0.117	0.18	74.09	10.1	2.07	0.07	3.9	3.08	4.77	1.43	0.47	0.04
K389955	0.002	0.009	0.27	73.31	10.65	2.37	0.06	4.41	2.46	4.27	1.94	0.5	0.04
K389956	0.003	0.012	0.37	62.33	14.8	4.3	0.11	8.26	2.86	3.63	2.91	0.76	0.04
K389957	0.001	0.012	0.52	64.27	11.96	4.24	0.1	9.69	3.28	3.59	2	0.8	0.08
K389959	0.009	0.034	0.16	73.02	10.48	2.18	0.07	4.37	3.04	4.8	1.54	0.46	0.03
K389961	0.012	0.237	0.3	71.12	11.6	2.95	0.07	5.62	2.57	1.42	4.01	0.6	0.04
K389962	0.001	0.01	0.23	72.91	10.22	2.72	0.08	5.04	2.98	3.81	1.78	0.44	0.03
K389963	0.003	0.012	0.13	70.75	11.68	2.7	0.07	5.47	2.55	4.04	2.15	0.55	0.04
K389964	0.002	0.024	0.14	76.34	9.29	2.06	0.05	4.16	2.53	3.93	1.2	0.4	0.03
K389965	0.001	0.02	0.09	74.37	10.61	2.02	0.05	4.39	2.3	3.55	2.24	0.43	0.03
K389966	0.001	0.034	0.14	75.73	9.43	2.11	0.06	4.02	2.65	3.99	1.59	0.4	0.03
K389967	0.001	0.009	0.21	74.1	11.1	2.52	0.07	4.88	2.18	3.12	1.49	0.52	0.04
K389968	0.001	0.012	0.22	72.65	10.36	2.38	0.07	4.62	3.13	4.66	1.6	0.5	0.04
K389969	0.000	0.013	0.19	74.95	9.75	2.03	0.07	3.79	3.44	4.2	1.28	0.45	0.03
K389971	0.002	0.008	0.37	74.39	9.44	2.42	0.07	4.25	3.41	4.02	1.47	0.49	0.04
K389973	0.001	0.008	0.31	71.18	10.99	2.78	0.07	5	3.25	4.54	1.61	0.56	0.03
K389975	0.002	0.188	0.32	74.3	9.49	2.42	0.06	4.8	2.8	3.23	2.38	0.48	0.04
K389976	0.003	0.057	0.18	72.92	10.93	2.6	0.07	4.73	2.75	3.64	1.81	0.51	0.04
K389977	0.002	0.033	0.28	69.4	12.36	3.16	0.05	6.51	2.12	3.1	2.69	0.56	0.04
K389978	0.001	0.011	0.28	72.25	10.88	2.4	0.08	4.09	4.19	4.24	1.34	0.5	0.04
K389979	0.017	0.019	0.25	73.99	9.76	2.37	0.07	4.66	2.6	4.42	1.61	0.49	0.03
K389981	0.001	0.03	0.18	73.19	9.71	2.36	0.07	5.32	2.78	4.31	1.77	0.47	0.04
K389982	0.001	0.023	0.17	72.44	11.25	2.43	0.07	5	3.1	3.32	1.82	0.54	0.04
K389984	0.002	0.01	0.04	72.12	11.65	2.79	0.08	5.57	2.37	2.83	2	0.55	0.04
K389985	0.001	0.007	0.22	70.69	12.12	2.79	0.08	5.72	2.36	3.42	2.17	0.6	0.04
K389986	0.001	0.013	0.17	73.86	10.27	2.4	0.06	4.77	2.68	3.88	1.54	0.52	0.03

Table 2.2: Whole-rock geochemical data for mafic dykes. Locations are listed in Table 2.5.

Sample Number	Au (ppm)	C (Wt%)	S (Wt%)	SiO ₂ (Mol%)	Al ₂ O ₃ (Mol%)	Fe ₂ O ₃ (Mol%)	MnO (Mol%)	MgO (Mol%)	CaO (Mol%)	Na ₂ O (Mol%)	K ₂ O (Mol%)	TiO ₂ (Mol%)	P ₂ O ₅ (Mol%)	Zr (ppm)	Nb (ppm)	Y (ppm)
K388025	0.058	0.39	0.03	59.95	10.09	4.1	0.15	9.45	13.29	1.71	0.59	0.65	0.04	70.2	3	14.8
K388039	0.004	0.28	0.07	58.5	7.99	2.84	0.09	17.15	8.15	3.1	1.64	0.46	0.07	104	3	10.4
K388064	0.002	1.14	0.04	57.99	7.75	4.01	0.14	16.38	7.4	1.35	4.22	0.62	0.13	106	5	19.9
K388077	0.009	0.92	0.01	49.41	7.28	4.7	0.18	21.53	13.41	1.21	1.61	0.61	0.05	72.8	17	19.5
K388088	0.018	0.62	0.37	57.66	10.55	4.54	0.12	11.11	8.92	4.37	1.87	0.79	0.06	73.3	3	14.3
K388105	0.002	0.04	0.21	61.03	10.49	4.36	0.14	10.19	10.58	1.92	0.48	0.75	0.05	79.1	3	16.8
K388108	0.002	0.05	0.01	57.53	8.9	4.2	0.19	15.37	11.06	0.96	1.03	0.72	0.04	71.7	3	14.6
K388120	0.001	0.03	0.02	54.89	6.6	4.34	0.17	19	12.21	1.93	0.39	0.46	0.03	49.7	2	10.4
K388220	0.009	0.45	0.21	63.95	11.21	3.51	0.13	8.32	6.37	3.47	2.35	0.62	0.07	118	6	17.4
K388244	0.003	1.27	0.02	55.19	7.62	4.47	0.19	17.55	13.03	0.5	0.81	0.55	0.08	66.3	3	12.9
K388262	0.005	0.65	0.19	54.36	8.83	5.07	0.19	14.41	14.3	1.12	1.01	0.68	0.03	52.6	2	14.3
K388284	0.001	0.34	0.2	58.9	11.01	4.19	0.13	10.51	10.35	3.2	1.02	0.66	0.03	60.6	3	16.1
K388309	0.015	1.74	0.13	58.59	9.41	4.06	0.14	11.96	11.92	1.58	1.76	0.55	0.03	58.9	2	12.1
K388334	0.002	0.06	0.06	56.97	9.01	4.25	0.16	14.78	10.89	1.44	1.8	0.62	0.09	87.5	4	18.1
K389006	0.162	1.36	0.48	60.94	9.17	3.52	0.15	10.28	8.02	4.71	2.56	0.6	0.06	127	2	23
K389010	0.061	2.37	0.09	51.27	7.79	5.07	0.22	15.47	14.69	1.1	3.56	0.73	0.09	122	2	20.3
K389077	0.002	0.18	0.06	56.2	6.96	4.69	0.2	15.53	13.24	2.25	0.33	0.57	0.03	143	11	12.1
K389103	0	0.09	0.02	57.99	9.28	3.9	0.13	16.66	7.19	2.1	2.14	0.56	0.04	116	4	18.4
K389150	0.005	0.05	0.03	58.65	10.06	4.21	0.15	11.96	12.12	1.79	0.38	0.62	0.06	80.2	-	15.7
K389174	0.056	0.85	0.02	55.93	8.09	4.48	0.18	15.31	12.25	1.16	1.82	0.67	0.1	78.2	2	18.3
K389183	0.001	0.03	0.02	55.34	8.46	4.29	0.17	16.99	11.17	2.34	0.66	0.55	0.03	37.7	-	12.6
K389218	0.946	1.53	0.43	56.1	9.52	3.21	0.14	13.27	9.64	4.27	3.16	0.57	0.11	158	7	16.6
K389329	0.003	0.01	0.03	55.54	8.5	4.56	0.17	17.99	11.07	0.72	0.9	0.52	0.03	48.1	2	13.2
K389332	0.001	0.02	0.03	52.92	6.12	5.98	0.21	19.06	13.57	0.81	0.68	0.65	0	70.3	4	15.1
K389337	0	0.08	0.02	57.58	7.72	3.22	0.14	17.62	9.83	2.18	0.95	0.68	0.06	150	9	13.5
K389338	0.001	0.5	0.3	56.15	9.55	4.92	0.16	14.76	9.59	1.69	2.28	0.81	0.1	93.1	4	19.9
K389340	0	0.16	0.03	56.51	8.54	4.94	0.18	16.34	9.24	1.68	1.77	0.71	0.1	81	3	19.8

K389344	0.002	0.24	0.03	55.3	9.31	5.02	0.22	15.65	10.95	2	0.84	0.68	0.04	54.9	2	15.6
K389349	0.001	0.01	0.2	62.64	11.25	4.68	0.13	10.26	4.78	2.61	2.69	0.86	0.09	101	7	20.4
K389353	0.002	0.03	0.02	58.65	9.15	4.64	0.19	13.93	9.89	1.63	1.04	0.77	0.1	91.4	4	24.1
K389423	0	0.06	0.03	58.87	8.37	4.64	0.2	15.62	8	2.25	1.3	0.67	0.09	93.1	4	18.5
K389514	0.002	0.08	0.03	58.58	9.38	5.1	0.26	13.42	9.96	1.37	0.93	0.89	0.1	80.4	4	32
K389525	0	0.01	0.01	56.76	9.32	4.97	0.22	14.69	10.16	1.61	1.24	0.92	0.12	118	6	30.9

Table 2.3: $\delta^{18}\text{O}$ and $\delta^2\text{H}$ whole-rock values of Pontiac metasedimentary greywackes. Eastings and northings apply to UTM NAD 83 Zone 17

Sample Number	Easting	Northing	Depth	Source Category	$\delta^{18}\text{O}$	$\delta^2\text{H}$
K388003	715059	5334515	38.2	Section (P1)/(P3)	10.1	-62
K388026	715057	5334199	110.2	Section (P1)	10.1	-67
K388035	714992	5333895	9.5	Section (P1)	9.8	-62
K388065	715004	5333719	196.7	Section (P1)	9.3	-57
K388070	715049	5333503	11.8	Section (P1)	9.9	-65
K388084	715049	5332717	8.5	Section (P1)	9.5	-66
K388095	715051	5332503	10.6	Section (P1)	10.1	-57
K388106	715051	5331750	12.5	Section (P1)	10.3	-53
K388117	715050	5331502	6.5	Section (P1)	10.1	-54
K388202	715360	5333984	14	Section (P3)	9.1	-64
K388235	715801	5333750	24	Section (P3)	11.4	-61
K388243	716301	5333286	12.7	Section (P3)	9.5	-64
K388254	716822	5333003	25.2	Section (P3)	9.8	-64
K388268	717300	5332751	10.1	Section (P3)	10.7	-56
K388277	717803	5332502	9.5	Section (P3)	8.9	-52
K388292	718308	5332252	13.4	Section (P3)	10.3	-41
K388303	713749	5334836	17.8	Section (P3)	9.9	-67
K388333	712726	5335131	40	Section (P3)	9.8	-59
K388360	712223	5335430	59	Section (P3)	10.1	-66
K388386	711764	5335688	15	Section (P3)	9.4	-59
K388397	711243	5336073	7.8	Section (P3)	9.7	-61
K388418	710821	5336686	10.8	Section (P3)	9.4	-51
K388433	710137	5336787	297	Section (P3)	9.8	-61
K389002	714130	5334268	5.6	Section (P2)	11	-72
K389017	714129	5334268	52.2	Section (P2)	9.8	-79
K389022	714128	5334268	62.5	Section (P2)	10.3	-74
K389027	714128	5334268	87.6	Section (P2)	9.9	-63
K389030	714050	5333498	14.2	Section (P2)	9.7	-58
K389036	714049	5333495	63.15	Section (P2)	10.1	-60
K389049	714125	5334156	13.3	Section (P2)	10.3	-62
K389053	714124	5334156	29.2	Section (P2)	10.3	-71
K389069	714049	5333999	13.25	Section (P2)	9.4	-54
K389073	714048	5333997	29.2	Section (P2)	9.3	-67
K389078	714045	5333994	71.5	Section (P2)	8.3	-60
K389080	714044	5333992	90.55	Section (P2)	9.8	-61
K389086	714040	5333987	141.95	Section (P2)	10	-66
K389089	714047	5333247	15.2	Section (P2)	10.2	-52

K389105	714047	5333247	127.6	Section (P2)	10.2	-67
K389106	714047	5333247	142.45	Section (P2)	9.6	-62
K389110	714051	5333761	9.5	Section (P2)	10.5	-60
K389115	714051	5333761	37.05	Section (P2)	11.8	-63
K389127	714052	5332750	4.45	Section (P2)	9.9	-67
K389128	714052	5332750	9.1	Section (P2)	10.5	-63
K389148	714051	5332999	8.4	Section (P2)	10	-62
K389154	714051	5332997	66.15	Section (P2)	10.2	-76
K389213	714127	5334590	266.6	Section (P2)/(P3)	10.3	-91
K389232	714099	5331748	21.3	Section (P2)	9.7	-47
K389326	711315	5332344	0	Outcrop	11.8	-46
K389328	718127	5331336	0	Outcrop	9.3	-53
K389333	715697	5331475	0	Outcrop	8.9	-58
K389334	716716	5331651	0	Outcrop	9.5	-64
K389335	718571	5333957	0	Outcrop	10.9	-52
K389336	716590	5332750	0	Outcrop	9.9	-68
K389339	717701	5332458	0	Outcrop	10.4	-62
K389342	718113	5332467	0	Outcrop	8.9	-51
K389345	716428	5332318	0	Outcrop	10.3	-63
K389347	718273	5331789	0	Outcrop	8.5	-60
K389348	717406	5331582	0	Outcrop	10.6	-47
K389350	718381	5332249	0	Outcrop	10	-66
K389951	718301	5332500	0.2	Drill Core	9.1	-44
K389953	714807	5333252	2.6	Drill Core	10.1	-56
K389954	715550	5333249	10.1	Drill Core	9.7	-55
K389955	716052	5333250	22	Drill Core	10.8	-53
K389956	714799	5333003	15.6	Drill Core	9	-54
K389957	717801	5331502	8.4	Drill Core	<u>7.8</u>	-55
K389959	715821	5334254	15.8	Drill Core	10.1	-59
K389961	713801	5334002	38.3	Drill Core	8.6	-50
K389962	717299	5333539	23.6	Drill Core	8.1	-60
K389963	715551	5334000	16.9	Drill Core	10.4	-52
K389964	717050	5333188	4.5	Drill Core	10.1	-64
K389965	715549	5333502	12	Drill Core	10.5	-55
K389966	715300	5333750	6.2	Drill Core	10.2	-56
K389967	712891	5331500	12	Drill Core	10.5	-56
K389968	713548	5333000	4.4	Drill Core	9.3	-55
K389969	712823	5333007	21.2	Drill Core	9	-53
K389971	713548	5333251	3.4	Drill Core	10.2	-63
K389973	718550	5332502	11.7	Drill Core	9.2	-51
K389975	713315	5333983	10.1	Drill Core	9.3	-55
K389976	717565	5333000	7.8	Drill Core	10.3	-59
K389977	714299	5331505	9	Drill Core	8.8	-56

K389978	713052	5331994	15.1	Drill Core	10.1	-51
K389979	717050	5334001	17.1	Drill Core	11.9	-61
K389981	717804	5332248	10.6	Drill Core	8.9	-59
K389982	713550	5331999	6.9	Drill Core	10.4	-45
K389984	713550	5331501	8.7	Drill Core	9.9	-53
K389985	713050	5333250	9	Drill Core	9.8	-46
K389986	713550	5332747	5	Drill Core	9.7	-52

Table 2.4: Visually estimated modal percentage of mineral phases in Pontiac greywackes

Sample Number	Qz (%)	Fsp (%)	Bt (%)	Chl (%)	Ms (%)	Remainder (%)
K389002	25	50	15	0	0	10
K389030	40	0	44	0	10	6
K389049	45	0	32	5	15	3
K389069	50	10	34	0	5	1
K389089	40	10	25	0	15	10
K389110	40	20	30	0	0	10
K389127	50	0	44	0	0	6
K389148	40	10	30	0	15	5
K389951	50	0	25	15	3	7
K389953	50	10	25	0	10	5
K389954	40	15	20	5	15	5
K389955	45	0	40	0	10	5
K389956	27	0	35	15	20	3
K389957	10	10	35	28	15	2
K389959	40	32	20	3	0	5
K389961	20	0	33	10	32	5
K389962	48	10	40	0	2	0
K389963	35	15	25	0	20	5
K389964	45	20	20	0	5	10
K389965	41	17	28	5	5	4
K389966	45	13	27	0	5	10
K389967	47	0	28	5	0	20
K389969	40	20	30	0	0	10
K389971	44	20	34	0	0	2
K389973	40	16	23	0	18	3
K389975	30	20	25	0	22	3
K389976	42	0	35	0	15	8
K389977	40	0	33	5	0	22
K389978	39	0	34	10	0	17
K389979	30	35	25	0	5	5
K389981	34	24	30	5	0	7
K389985	39	0	32	0	28	1
K389986	35	24	35	0	5	1

Table 2.5: $\delta^{18}O$ and δ^2H values of mafic dykes. Eastings and northings apply to UTM NAD 83 Zone 17

Sample Number	Easting	Northing	Depth	Source Category	$\delta^{18}O$	δ^2H
K388025	715057	5334199	94	Section (P1) (P3)	9.2	-64
K388039	715004	5333857	69.7	Section (P1)	8.8	-72
K388064	715004	5333720	190.2	Section (P1)	8.2	-73
K388077	715046	5333501	66.5	Section (P1)	8.3	-71
K388088	715043	5332712	80.5	Section (P1)	8.1	-84
K388105	715055	5332497	140.5	Section (P1)	11.6	-70
K388108	715051	5331750	31.5	Section (P1)	8.8	-68
K388120	715050	5331502	51	Section (P1)	8.2	-65
K388220	715351	5333968	270	Section (P3)	9.5	-76
K388244	716301	5333286	16.5	Section (P3)	7.9	-76
K388262	716822	5333003	92	Section (P3)	8.3	-73
K388284	717801	5332499	81	Section (P3)	8.3	-60
K388309	713748	5334832	96	Section (P3)	9	-67
K388334	712726	5335131	48	Section (P3)	7.3	-68
K389006	714130	5334268	19	Section (P2)	8.2	-80
K389010	714129	5334268	34	Section (P2)	8	-73
K389077	714046	5333994	62	Section (P2)	6.8	-69
K389103	714047	5333247	117	Section (P2)	7.5	-71
K389150	714051	5332998	33	Section (P2)	8.2	-79
K389174	715155	5333631	0	Outcrop	9.6	-82
K389183	718621	5332042	0	Outcrop	7.5	-75
K389218	714127	5334590	318.5	Section (P2) (P3)	8.7	-79
K389329	715239	5331495	0	Outcrop	8.3	-59
K389332	715697	5331475	0	Outcrop	6.9	-60
K389337	716730	5332474	0	Outcrop	7.7	-81
K389338	716994	5332476	0	Outcrop	9.8	-105
K389340	717701	5332458	0	Outcrop	7.7	-78
K389344	716428	5332318	0	Outcrop	8.3	-79
K389349	717447	5331561	0	Outcrop	12.2	-64
K389353	717195	5332194	0	Outcrop	7.2	-62
K389423	712528	5334678	0	Outcrop	6.8	-60
K389514	718381	5332249	0	Outcrop	8.3	-66
K389525	712158	5334377	0	Outcrop	7.7	-55

Table 2.6 Visually estimated modal percentage of mineral phases in mafic dykes

Sample Number	Amp	Plag	Qz	Bt	Chl	Opagues	Carb	Sericite	Groundmass
K388025	35	0	5	0	20	5	5	30	0
K388039	40	30	0	25	5	0	0	0	0
K388064	0	0	30	50	5	0	15	0	0
K388077	40	5	5	10	25	0	15	0	0
K388088	0	15	5	40	15	5	10	10	0
K388105	30	0	60	0	0	10	0	0	0
K388120	60	15	15	10	0	0	0	0	0
K388220	10	10	20	35	0	5	20	0	0
K388244	40	10	5	20	2	5	10	18	0
K388334	40	10	10	35	5	0	0	0	0
K389006	0	0	23	50	5	2	20	0	0
K389010	0	0	35	50	0	5	10	0	0
K389183	40	30	5	0	20	5	0	0	0
K389337	50	5	20	20	0	5	0	0	0
K389338	30	0	5	35	15	0	10	0	5
K389340	45	10	0	0	25	0	5	15	0
K389349	25	40	0	25	5	5	0	0	0
K389353	50	10	10	20	5	5	0	0	0
K389423	50	25	10	0	10	0	0	5	0
K389525	50	20	5	0	5	0	0	20	0

2.8 References

- Aitchison J (1986) *The Statistical Analysis of Compositional Data*. 44:365–374.
- Barker SLL, Dipple GM, Hickey KA, et al (2013) Applying stable isotopes to mineral exploration: Teaching an old dog new tricks. *Econ ...* 108:1–9.
- Bateman R, Ayer J, Dubé B (2008) The Timmins-Porcupine gold camp, Ontario: Anatomy of an Archean greenstone belt and ontogeny of gold mineralization. *Econ Geol* 1285–1308.
- Beaudoin G, Chiaradia M (2016) Fluid mixing in orogenic gold deposits: Evidence from the H-O-Sr isotope composition of the Val-d'Or vein field (Abitibi, Canada). *Chem Geol* 437:7–18. doi: 10.1016/j.chemgeo.2016.05.009
- Beaudoin G, Pitre D (2005) Stable isotope geochemistry of the Archean Val-d'Or (Canada) orogenic gold vein field. *Miner Depos* 40:59–75. doi: <http://dx.doi.org/10.1007/s00126-005-0474-z>
- Beaudoin G, Raskevicius T (2014) Constraints on the genesis of the archean oxidized, intrusion-related Canadian malartic gold deposit, Quebec, Canada--a discussion. *Econ Geol* 109:2067–2071. doi: 10.2113/econgeo.109.3.713
- Beaudoin G, Therrien R, Savard C (2006) 3D numerical modelling of fluid flow in the Val-d'Or orogenic gold district: major crustal shear zones drain fluids from overpressured vein fields. *Miner Depos* 41:82–98. doi: 10.1007/s00126-005-0043-5
- Böhlke JK (1988) Carbonate-sulfide equilibria and “stratabound” disseminated epigenetic gold mineralization: A proposal based on examples from Alleghany, California, U.S.A. *Appl Geochemistry* 3:499–516. doi: 10.1016/0883-2927(88)90022-4
- Bottinga Y, Javoy M (1975) Oxygen isotope partitioning among the minerals in igneous and metamorphic rocks. *Rev Geophys* 13:401–418. doi: 10.1029/RG015i002p00251
- Cathles LM, Spooner ETC, Barrie CT (1993) Oxygen isotope alteration in the Noranda mining district, Abitibi greenstone belt, Quebec. *Econ Geol* 88:1483–1511. doi: <http://dx.doi.org/10.2113/gsecongeo.88.6.1483>
- Chamberlain CP, Ferry JM, Rumble D (1990) The effect of net-transfer reactions on the isotopic composition of minerals. *Contrib to Mineral Petrol* 105:322–336. doi: 10.1007/BF00306542
- Chayes F (1960) On correlation between variables of constant sum. *J Geophys Res* 65:4185–4193. doi: 10.1029/JZ065i012p04185
- Clark I, Harper WV (2000) *Practical Geostatistics*. doi: 10.1198/tech.2001.s52
- Clayton RN, Mayeda TK (1963) The use of bromine pentafluoride in the extraction of oxygen from oxides and silicates for isotopic analysis. *Geochim Cosmochim Acta* 27:43–52.
- Corfu F, Jackson SL, Sutcliffe RH (1991) U–Pb ages and tectonic significance of late Archean alkalic magmatism and nonmarine sedimentation: Timiskaming Group, southern Abitibi belt, Ontario. *Can J Earth Sci* 28:489–503. doi: 10.1139/e91-043
- Criss R, Singleton M, Champion D (2000) Three-dimensional oxygen isotope imaging of convective fluid flow around the Big Bonanza, Comstock Lode mining district, Nevada. *Econ Geol* 95:131–142.

- Criss RE, Fleck RJ (1990) Oxygen isotope map of the giant metamorphic-hydrothermal system around the northern part of the Idaho batholith, U.S.A. *Appl Geochemistry* 5:641–655. doi: 10.1016/0883-2927(90)90062-A
- Croghan CW, Egeghy PP (2003) *Methods of Dealing With Values Below the Limit of Detection Using Sas*. South SAS User Gr 5.
- Davis DW (2002) U–Pb geochronology of Archean metasedimentary rocks in the Pontiac and Abitibi subprovinces, Quebec, constraints on timing, provenance and regional tectonics. *Precambrian Res* 115:97–117. doi: 10.1016/S0301-9268(02)00007-4
- Davis JC (1973) *Statistics and Data Analysis in Geology*, Third. Wiley, New York
- De Souza S, Dubé B, McNicoll VJ, et al (2015) Geology, hydrothermal alteration, and genesis of the world-class Canadian Malartic stockwork-disseminated Archean gold deposit, Abitibi, Quebec. 113–126. doi: 10.4095/296624
- Desrochers J-P, Hubert C (1996) Structural evolution and early accretion of the Archean Malartic Composite Block, southern Abitibi greenstone belt, Quebec, Canada. *Can J Earth Sci* 33:1556–1569.
- Dodson MH (1982) On “spurious” correlations in Rb-Sr isochron diagrams. *Lithos* 15:215–219. doi: 10.1016/0024-4937(82)90013-5
- Egozcue JJ, Pawlowsky-Glahn V, Mateu-Figueras G, Barceló-Vidal C (2003) Isometric Logratio Transformations for Compositional Data Analysis. *Math Geol* 35:279–300. doi: 10.1023/A:1023818214614
- Feng R, Kerrich R, Maas R (1993) Geochemical, oxygen, and neodymium isotope compositions of metasediments from the Abitibi greenstone belt and Pontiac Subprovince, Canada: Evidence for ancient crust and Archean terrane juxtaposition. *Geochim Cosmochim Acta* 57:641–658. doi: 10.1016/0016-7037(93)90375-7
- Floyd PA, Winchester JA (1977) Magma Type and Tectonic Setting Discrimination Using Immobile Elements. *Earth and Planetary Science Letters* 27:211–218.
- Filzmoser P, Hron K, Reimann C (2009) Principal components analysis for compositional data with outliers. *Environmetrics* 20:621–632.
- Gervaus D, Roy C, Thibault A, Pednault C, Doucet D (2014) Technical Report on the Mineral Reserve Estimates for the Canadian Malartic Property. Mine Caladian Malartic. 460.
- Goldfarb R, Baker T, Dube B, Groves D (2005) Distribution, character and genesis of gold deposits in metamorphic terranes. *Econ Geol* 100:407–450.
- Goldfarb RJ, Groves DI, Gardoll S (2001) Orogenic gold and geologic time: A global synthesis. *Ore Geol Rev* 18:1–75. doi: 10.1016/S0169-1368(01)00016-6
- Groves DI (1993) The crustal continuum model for late-Archaean lode-gold deposits of the Yilgarn Block, Western Australia. *Miner Depos* 28:366–374. doi: 10.1007/BF02431596
- Hagemann SG, Gebre-Mariam M, Groves DI (1994) Surface-water influx in shallow-level Archean lode-gold deposits in western Australia. *Geology* 22:1067–1070. doi: 10.1130/0091-7613(1994)022<1067:SWIISL>2.3.CO;2

- Helt KM, Williams-Jones AE, Clark JR, et al (2014) Constraints on the Genesis of the Archean Oxidized, Intrusion-Related Canadian Malartic Gold Deposit, Quebec, Canada. *Econ Geol* 109:713–735.
- Herron MM (1988) Geochemical classification of terrigenous sands and shales from core or log data. *J Sediment Res* 58:820–829.
- Hyde R (1980) Sedimentary facies in the Archean Timiskaming Group and their tectonic implications, Abitibi greenstone belt, northeastern Ontario, Canada. *Precambrian Res* 12:161–195.
- Issigonis MJ (1980) Occurrence of disseminated gold deposits in porphyries in Archean Abitibi Belt, northwest Quebec, Canada. *Trans Inst Min Metall Sect B-Applied Earth Sci* 89:157–158.
- Kerrich R, Fryer B (1979) Archean precious-metal hydrothermal systems, Dome Mine, Abitibi Greenstone Belt. II. REE and oxygen isotope relations. *Can. J. Earth Sci.* 16:
- Kerrich R, Fyfe WS (1981) The Gold-Carbonate association: Source of CO₂, and CO₂ fixation reactions in Archean lode deposits. *Chem Geol* 33:265–294.
- Le Maitre RW (1982) *Numerical Petrology: statistical interpretation of geochemical data*. Elsevier, Amsterdam
- Makvandi S, Ghasemzadeh-Barvarz M, Beaudoin G, et al (2016) Principal component analysis of magnetite composition from volcanogenic massive sulfide deposits: Case studies from the Izok Lake (Nunavut, Canada) and Halfmile Lake (New Brunswick, Canada) deposits. *Ore Geol Rev* 72:60–85. doi: 10.1016/j.oregeorev.2015.06.023
- Matsuhisa Y, Goldsmith JR, Clayton RN (1979) Oxygen isotopic fractionation in the system quartz-albite-anorthite-water. *Geochim Cosmochim Acta* 43:1131–1140. doi: 10.1016/0016-7037(79)90099-1
- Pawlawsky-Glahn V, Egozcue JJ (2006) Compositional data and their analysis: an introduction. *Geol Soc London, Spec Publ* 264:1–10. doi: 10.1144/GSL.SP.2006.264.01.01
- Perrouty S, Gaillard N, Piette-Lauzière N, et al (2017) Structural setting for Canadian Malartic style of gold mineralization in the Pontiac Subprovince, south of the Cadillac Larder Lake Deformation Zone, Québec, Canada. *Ore Geol Rev* 100. doi: 10.1016/j.oregeorev.2017.01.009
- Phillips GN, Groves DI (1983) The nature of Archean gold bearing fluids as deduced from gold deposits of Western Australia. *J Geol Soc Aust* 30:25–39. doi: 10.1080/00167618308729234
- Piette-Lauzière N (2017) *Métamorphisme régional du nord-est de la Sous-province de Pontiac, Abitibi, Québec (Master's Thesis)*. 260
- Rice C, Harmon R, Boyce A, Fallick A (2001) Assessment of grid-based whole-rock δD surveys in exploration: Boulder County epithermal tungsten deposit, Colorado. *Econ Geol* 96:133–143.
- Ridley J, Diamond L (2000) Fluid chemistry of orogenic lode gold deposits and implications for genetic models. *SEG Rev* 13:141–162.
- Robert F (2001) Syenite-associated disseminated gold deposits in the Abitibi greenstone belt, Canada. *Miner Depos* 36:503–516. doi: 10.1007/s001260100186
- Robert F, Poulsen KH (1997) World-class Archean gold deposits in Canada: An overview. *Aust J Earth Sci* 44:329–351. doi: 10.1080/08120099708728316

- Rollinson H (1993) *Using Geochemical Data: Evaluation, Presentation, Interpretation*. Pearson. doi: 10.1180/minmag.1994.058.392.25
- Sheppard S (1986) *Characterization and Isotopic Variations in Natural Waters*. *Rev. Mineral. Geochemistry*. pp 165–183
- Taylor B, Kemp E de, Grunsky E, et al (2014) Three-Dimensional Visualization of the Archean Horne and Quemont Au-Bearing Volcanogenic Massive Sulfide Hydrothermal Systems, Blake River Group, Quebec. *Econ Geol* 109:183–203.
- Taylor H (1974) The application of oxygen and hydrogen isotope studies to problems of hydrothermal alteration and ore deposition. *Econ Geol* 69:843–883.
- Taylor HP (1978) Oxygen and hydrogen isotope studies of plutonic granitic rocks. *Earth Planet Sci Lett* 38:177–210. doi: 10.1016/0012-821X(78)90131-0
- Thompson JFH, Newberry RJ (2000) Gold deposits related to reduced granitic intrusions. *Rev Econ Geol* 13:377–400.
- Thurston P, Chivers K. (1990) Secular variation in greenstone sequence development emphasizing Superior Province, Canada. *Precambrian Res* 46:21–58. doi: 10.1016/0301-9268(90)90065-X
- Whitney DL, Evans BW (2010) Abbreviations for names of rock-forming minerals. *Am Mineral* 95:185–187. doi: 10.2138/am.2010.3371
- Wilson M (2007) *Igneous Petrogenesis: a global tectonic approach*. Springer, Dordrecht, The Netherlands
- Young ED (1993) On the $^{18}\text{O}/^{16}\text{O}$ record of reaction progress in open and closed metamorphic systems. *Earth Planet Sci Lett* 117:147–167. doi: 10.1016/0012-821X(93)90123-Q
- Zhao Z-F, Zheng Y-F (2003) Calculation of oxygen isotope fractionation in magmatic rocks. *Chem Geol* 193:59–80. doi: 10.1016/S0009-2541(02)00226-7

Chapter 3 – Comparison of company and research samples

3.1 Introduction

Whole-rock $\delta^{18}\text{O}$ and $\delta^2\text{H}$ values of the host rocks to the Canadian Malartic deposit should provide a sensitive record of isotopic exchange with the mineralizing fluid. The mapping of oxygen and hydrogen isotopic variation in both the proximal and distal rocks surrounding the Canadian Malartic deposit has the potential to identify and quantify the cryptic or invisible alteration footprint associated with the mineralizing events at the Canadian Malartic deposit. This research is focused on assessing the potential to use existing sample libraries for this type of mapping. This is done by determining the compositional differences between pulps taken from a condemnation drilling program (circa 2008) at Canadian Malartic and the geochemical samples taken by the CMIC group from the same drill holes. Canadian Malartic pulps are crushed rock samples of about 1.5 meters in length of NQ diamond drill core and their isotopic data represent the bulk average of all the material contained within that interval. Conversely, CMIC samples represent a smaller 30 to 75 cm sample of homogeneous drill core, purposely free of veins, and therefore should provide the more reproducible data for the study.

3.2 Methods

Isotopic data have been collected from rock powders from diamond drill cores along the P2 section along a north-south azimuth out from the Canadian Malartic open pit mine. Comparison of the data collected from these two sample sets will aid in determining the usefulness isotopic ratios from existing sample libraries as vectors towards mineralization. All samples were analyzed at the Queen's facility for isotopic research (QFIR) in Kingston, Ontario. The $\delta^{18}\text{O}$ was determined by reacting the powdered samples with BrF_5 overnight in Ni furnaces in order to liberate free oxygen. The elemental oxygen gas is then converted to CO_2 by reaction with a hot graphite rod (Clayton and Mayeda 1963). The $\delta^{18}\text{O}$ of the CO_2 gas is then determined using a Finnigan MAT 252 Isotope Ratio Mass Spectrometer. The $\delta^2\text{H}$ was determined using a method adapted from Sharp et al. (2001) where the samples were degassed in silver capsules for 1 hour and then reduced in a graphite crucible at 1450°C to convert the released H_2O into H_2 . Isotopic measurements of the elemental hydrogen gas were determined using a DELTAplusXP Stable Isotope Ratio Mass Spectrometer.

3.4 Results

Isotopic ratios of hydrogen and oxygen as well as sample locations of both the CMIC and Canadian Malartic sample sets are presented as per mil deviations from V-SMOW in Table 3.1 and Table 3.2, respectively. The first step in the statistical analysis of the data is a direct comparison between the corresponding $\delta^{18}\text{O}$, $\delta^2\text{H}$, and H_2O values from the two sample sets using a series of bivariate plots. The $\delta^{18}\text{O}$ values of both CMIC and Canadian Malartic samples all plot within a small cluster, along or near the 1:1 line, suggesting little difference between the CMIC and Canadian Malartic samples in terms of $\delta^{18}\text{O}$. In addition, the points are clustered together and are not linearly distributed, suggesting a random and minimal variance of $\delta^{18}\text{O}$ values in these two sample sets. The $\delta^2\text{H}$ values from CMIC and Canadian Malartic samples (Fig. 3.2) co-vary below the 1:1 line, indicating that Canadian Malartic samples are consistently lower than CMIC samples by about 5 to 10‰. The concentration of H_2O from each sample set (Fig. 3.3) indicates that the CMIC samples are enriched in H_2O by up to 2 wt%.

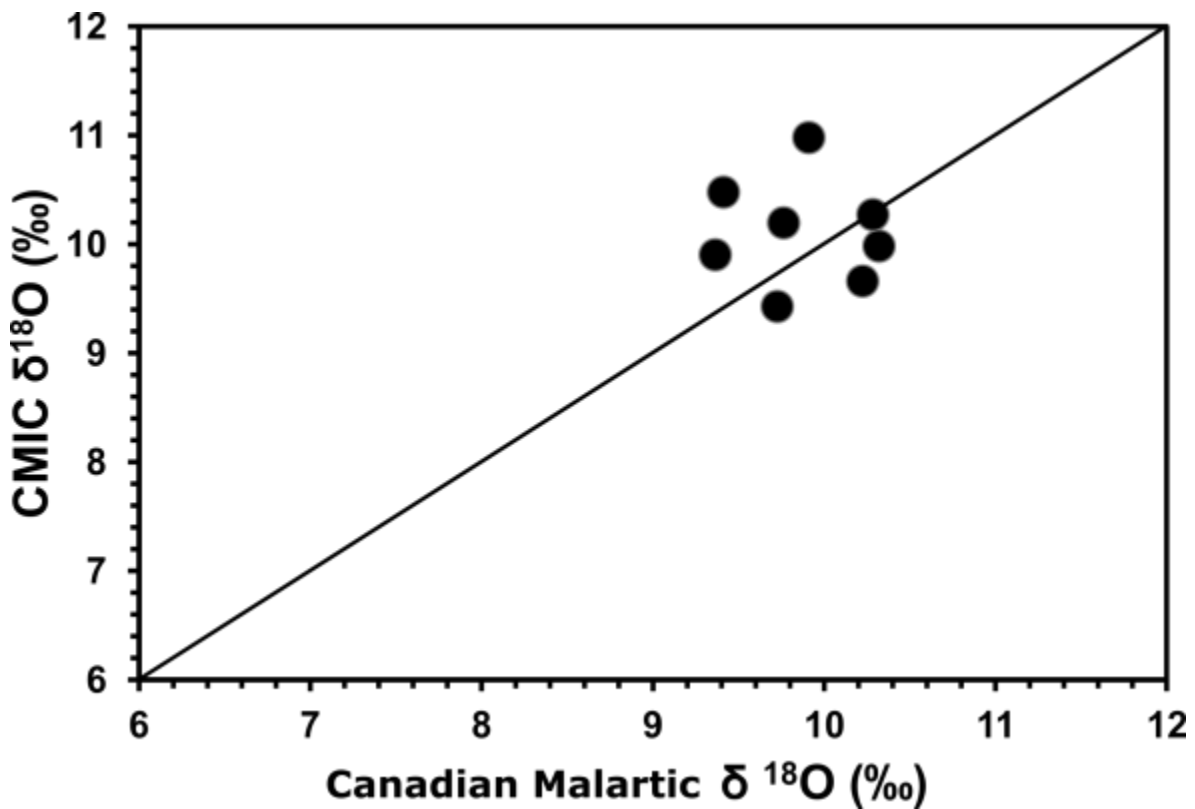


Figure 3.1: Comparison between $\delta^{18}\text{O}$ of Canadian Malartic pulps and CMIC samples from the same drill holes.

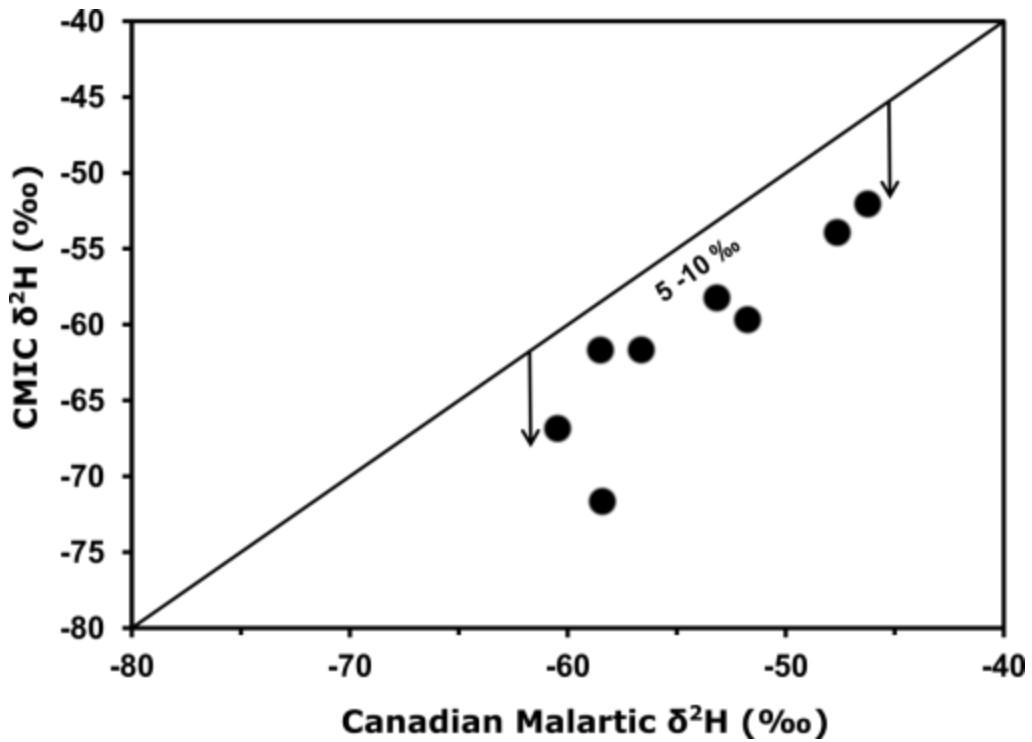


Figure 3.2: Comparison between $\delta^2\text{H}$ from the Canadian Malartic pulps and CMIC samples from the same drill holes.

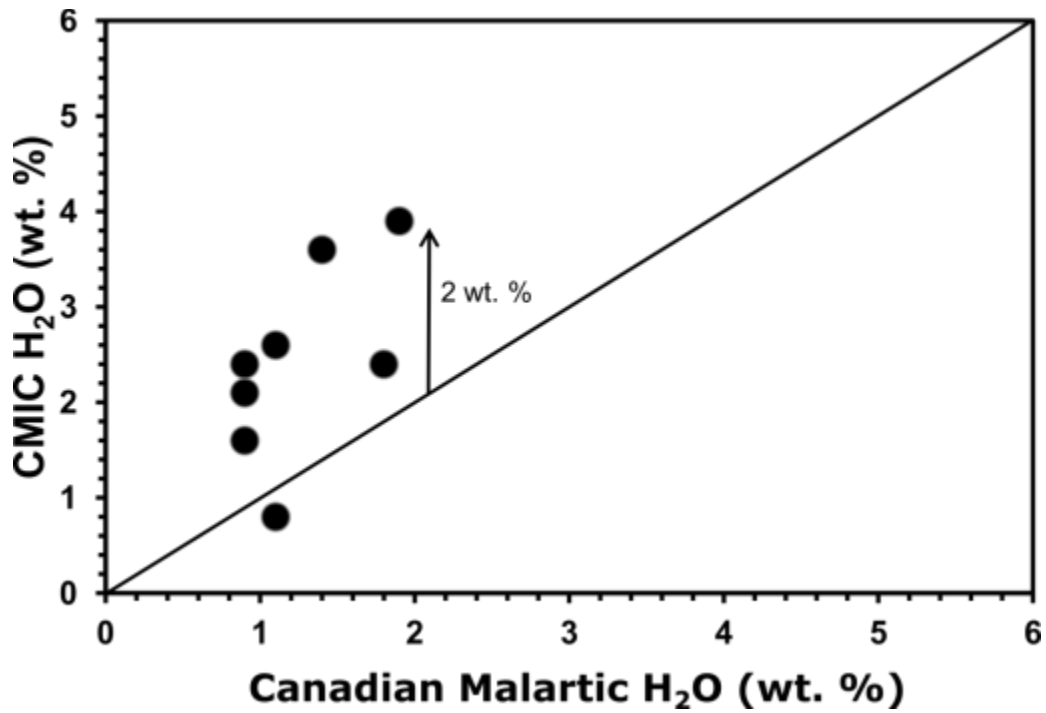


Figure 3.3: Comparison between the water content of Canadian Malartic pulps and CMIC samples from the same drill holes.

3.5 Discussion

The direct bivariate comparison between the isotopic ratios of the CMIC and Canadian Malartic samples show similar trends in all cases. Figure 3.1 indicates that $\delta^{18}\text{O}$ values show a low variance, without systematic trends. Figure 3.2, however, indicates that the Canadian Malartic samples are systematically lower in $\delta^2\text{H}$ by about 5 to 10‰, compared to CMIC samples. One possibility that could account for this difference is the incorporation of hydrothermal biotite from quartz veins in the Canadian Malartic samples that are not present in the CMIC samples. CMIC geochemical samples were taken from homogeneous drill core that was free from significant quartz veins; in contrast to the Canadian Malartic samples, which represent a bulk average of all material contained within a 1.5m interval of drill core. Incorporation of vein biotite with high $\delta^2\text{H}$ values (Helt et al. 2014) could systematically shift the bulk $\delta^2\text{H}$ composition of the Canadian Malartic samples to overall higher $\delta^2\text{H}$ values when compared to vein free CMIC samples. The relationship between wt% H_2O in the CMIC and Canadian Malartic samples indicate that CMIC samples may contain up to 2% more H_2O than the Canadian Malartic samples (Fig. 3), also consistent with the incorporation of varying amounts of quartz vein material in the Canadian Malartic samples. The inclusion of anhydrous quartz in the Canadian Malartic samples will dilute the total H_2O content.

3.5.1 Implications for Exploration Footprint

Comparison of the data from the Canadian Malartic and CMIC samples have two significant implications for the exploration footprint:

(1) Both the CMIC and Canadian Malartic samples record the same patterns, with marginal differences that may be attributed to sampling methods. This observation suggests that isotopic data collected from existing sample libraries may be useful for vectoring into mineralized systems. The use of existing libraries is beneficial to exploration efforts because it circumvents the need to spend time and resources on collecting new samples. However, moving forward, in an effort to corroborate geochemical, mineralogical, and petrophysical data from other CMIC projects, isotopic data should continue using the CMIC rather than the Canadian Malartic sampling protocols.

3.6 Tables

Table 3.1 Isotopic and location data from the CMIC sample set

CMIC Samples						
Sample ID	$\delta^{18}\text{O}$ ‰	$\delta^2\text{H}$ ‰	%H ₂ O	Hole ID	Easting	Northing
1TR 389002C	11.0	-71.7	0.8	CM07-1705	714130	5334268
2TR 389049C	10.3	-61.7	3.9	CM07-1205	714125	5334157
3TR 389069C	9.4	-53.9	2.4	CD08-D1	714049.9	5334000
4TR 389110C	10.5	-59.7	2.1	CD08-D2	714050.5	5333761
5TR 389030C	9.7	-58.2	2.6	CD08-D3	714050.1	5333499
6TR 389089C	10.2	-52.0	1.6	CD08-D4	714044.8	5333250
7TR 389148C	10.0	-61.7	3.6	CD08-D5	714051.1	5332999
8TR 389127C	9.9	-66.8	2.4	CD08-D6	714052.1	5332750

Table 3.2 Isotopic and location data from the Canadian Malartic pulp samples

Canadian Malartic Samples							
Sample ID	ALS ID	$\delta^{18}\text{O}$ ‰	$\delta^2\text{H}$ ‰	%H ₂ O	Hole ID	Easting	Northing
3TR 725292	725292	9.9	-58.4	1.1	CM07-1705	714129.9	5334268
4TR 464766	464766	10.3	-58.5	1.9	CM07-1205	714124.7	5334156
7TR 947839	947839	9.7	-47.6	0.9	CD08-D1	714050	5334000
13TR H963718	963718	9.4	-51.8	0.9	CD08-D2	714050.5	5333761
14TR 840645	840645	10.2	-53.2	1.1	CD08-D3	714050.1	5333499
18TR 770799	770799	9.8	-46.2	0.9	CD08-D4	714049.4	5333249
23TR 878921	878921	10.3	-56.6	1.4	CD08-D5	714051.1	5332999
28TR 768434	768434	9.4	-60.5	1.8	CD08-D6	714052.1	5332750

3.6 References

- Beaudoin G, Raskevicius T (2014) Constraints on the genesis of the archean oxidized, intrusion-related Canadian malartic gold deposit, Quebec, Canada--a discussion. *Econ Geol* 109:2067–2071. doi: 10.2113/econgeo.109.3.713
- Clayton RN, Mayeda TK (1963) The use of bromine pentafluoride in the extraction of oxygen from oxides and silicates for isotopic analysis. *Geochim Cosmochim Acta* 27:43–52.

Helt KM, Williams-Jones AE, Clark JR, et al (2014) Constraints on the Genesis of the Archean Oxidized, Intrusion-Related Canadian Malartic Gold Deposit, Quebec, Canada. *Econ Geol* 109:713–735.

Sharp ZD, Atudorei V, Durakiewicz T (2001) A rapid method for determination of hydrogen and oxygen isotope ratios from water and hydrous minerals, *Chemical Geology*, 178: 197-210

Chapter 4 – Summary and Conclusion

The Canadian Malartic deposit in Northern Quebec is one of Canada's top producing and largest gold mines. The deposit straddles the border between the Superior province's Abitibi and Pontiac subprovinces. Locally, the host rocks to the Canadian Malartic deposit are primarily meta-sedimentary greywackes of the Pontiac Group. Sporadically, throughout the Pontiac metasedimentary rocks, there are discordant mafic dykes and sills, which have also been affected by the mineralizing gold fluid. As part of the research done by the CMIC group, sampling of these rocks has been conducted to identify and define the most distal footprint that can be attributed to the mineralizing event at Malartic. Samples of Pontiac greywackes and mafic dykes were collected and analyzed by ICPMS with digestion in aqua regia for trace elements, XRF for major and select minor elements as well as IRMS to determine the whole-rock $\delta^2\text{H}$ and $\delta^{18}\text{O}$ values.

PCA of geochemical and isotopic data has been carried out on both mafic dykes and greywackes to investigate the geological controls on the variance exhibited by this data set. In both cases, the largest source of variance exhibited by the data set involve an association of co-varying components (C, S, Au, and $\delta^{18}\text{O}$) while $\delta^2\text{H}$ and rock forming elements such as MgO, Fe_2O_3 , Al_2O_3 and SiO_2 form a second co-varying association inversely correlated to the first. These patterns have been ascribed to the mineralizing process. Subordinate sources of variance in the greywacke data and mafic dyke data are attributed to potassic alteration affecting these rocks, which is recorded as white micas and biotite overprinting feldspars in greywackes and biotite overprinting amphiboles in mafic dykes. The variation attributed to potassic alteration does not co-vary with the isotopic composition of these rocks.

Understanding the processes affecting the isotopic and geochemical data also aids in the mapping and delineation of the isotopic footprint associated with fluid/rock interaction at Malartic. The isotopic footprint of the Canadian Malartic deposit has been shown to be best identified by a decrease in whole-rock $\delta^2\text{H}$ values in Pontiac metasedimentary rocks from background values ca. -59‰ to values less than -90‰ near mineralization. Whereas the $\delta^{18}\text{O}$ values of mafic dykes throughout the study area show increase from background values near ca. 8.3‰ to values greater than 9‰ near the core of the Canadian Malartic deposit. The $\delta^2\text{H}$ footprint in Pontiac greywackes extends roughly 500m to 1.5 km south, 2 km northwest, and 2.5 km southeast of the main Malartic pit, while the $\delta^{18}\text{O}$ footprint observed in mafic dykes extends about 500 m south, 250m northwest, and 1 km southeast of the pit. The morphology of this footprint is elongated subparallel to the Cadillac Larder-lake tectonic zone (CLLTZ) which seems to have influenced fluid flow throughout the area.

Computational models of isotopic fluid/rock exchange indicate that the observed isotopic variation may be explained by fluid/rock interaction with a metamorphic fluid formed in equilibrium with the Pontiac meta-sediments near the greenschist-amphibolite transition. This deep-seated fluid would have ascended throughout structural conduits in the crust to the level of gold deposition near ca. 300°C to form the Canadian Malartic gold deposit.

Chapter 3 of this text presents a comparison of the samples collected for CMIC-NSERC research and exploration samples taken by geologists employed by the Canadian Malartic mine. Although, the $\delta^2\text{H}$ values of the Canadian Malartic samples have been systematically shifted, the overall trends remain the same, suggesting that this type of work could be successfully employed for the use of exploration programs searching for deposits analogous to the Canadian Malartic deposit. Moreover, $\delta^2\text{H}$ analysis will be particularly useful in the exploration because of the relatively low analytical cost and potential for laboratory bulk sampling. Moving forward, exploration companies may gain new prospective targets simply by revisiting the libraries of samples already held in their warehouses.

Appendix A

PCA analysis

Eigenvalues of the principal components extracted from the variance in greywacke data:

Analyte	PC1	PC2	PC3
$\delta^{18}\text{O}$	-0.10	-0.22	0.68
$\delta^2\text{H}$	0.57	0.17	0.03
H_2O	0.58	0.58	-0.20
Au	-0.89	0.02	0.19
C	-0.77	0.00	0.08
S	-0.49	-0.05	-0.63
SiO_2	0.83	-0.32	0.23
Al_2O_3	0.95	0.02	0.19
K_2O	0.50	0.65	0.40
Na_2O	0.52	-0.78	-0.04
MgO	0.89	0.20	-0.05
Fe_2O_3	0.95	0.20	-0.10
MnO	0.86	-0.10	-0.13
CaO	0.62	-0.65	-0.02
TiO_2	0.92	0.13	-0.13
P_2O_5	0.75	-0.20	-0.11

Breakdown of total variance explained by select principal components of greywacke data:

	%	Cumulative %
PC1	54.05	54.05
PC2	13.15	67.19
PC3	7.86	75.06

Principal components extracted from greywacke data:

Sample Number	PC1	PC2	PC3
K388003	-2.85	-0.63	0.44
K388026	-0.39	-1.11	0.30
K388035	-0.01	-1.26	-0.51
K388065	-2.79	1.34	-0.19
K388070	0.37	-1.80	-0.88
K388084	-1.48	-1.59	-1.48
K388095	0.86	-1.16	-0.10
K388106	0.56	1.97	0.47
K388117	-1.39	-1.20	0.24
K388202	-5.29	0.62	-0.43

K388235	-1.62	-1.46	1.16
K388243	0.47	-1.18	-0.59
K388254	-1.41	-1.17	-0.10
K388268	0.09	-1.27	0.02
K388277	-0.12	-0.51	-1.20
K388292	0.43	2.28	2.81
K388303	0.26	-0.53	-0.31
K388333	0.01	-0.59	-2.46
K388360	-4.03	0.85	0.69
K388386	0.19	-0.67	-1.12
K388397	-0.17	-0.28	-0.27
K388418	-0.94	0.43	-0.40
K388433	-0.57	-1.03	-0.15
K389002	-10.18	-4.10	-0.27
K389017	-10.82	-0.99	0.11
K389022	-7.27	0.81	0.25
K389027	-3.25	3.65	-0.20
K389030	-0.02	0.43	-0.45
K389036	0.40	2.30	0.02
K389049	-2.85	3.36	0.88
K389053	-5.96	-0.97	0.49
K389069	1.24	0.51	0.42
K389073	-4.03	1.67	0.06
K389078	0.77	-0.01	-1.22
K389080	1.50	0.95	0.31
K389086	-1.35	0.00	1.61
K389089	2.95	-1.03	-0.32
K389105	1.67	3.13	-0.11
K389106	4.01	1.88	0.58
K389110	0.97	-0.92	-0.53
K389115	0.26	-0.54	1.13
K389127	2.42	-0.13	0.73
K389128	1.96	1.14	-0.38
K389148	-0.16	0.82	-0.61
K389154	0.99	0.39	-0.26
K389213	-9.75	0.64	0.64
K389232	0.41	1.14	0.13
K389326	4.38	-0.44	5.28
K389328	1.48	1.50	-0.28
K389333	4.44	-1.96	1.17
K389334	2.29	-1.47	0.08
K389335	2.23	1.77	0.72
K389336	3.77	-1.47	1.04

K389339	2.29	-1.43	-0.04
K389342	2.45	-1.14	-1.53
K389345	2.22	0.03	1.22
K389347	2.46	0.41	-0.86
K389348	1.07	-1.78	0.38
K389350	1.12	-1.10	-0.40
K389951	0.27	1.65	-1.27
K389953	0.91	-0.04	0.70
K389954	-1.34	-1.30	0.15
K389955	1.16	-0.40	0.64
K389956	1.30	2.43	-1.56
K389957	2.65	1.75	-3.93
K389959	-1.23	-1.14	0.75
K389961	-3.21	4.00	-0.26
K389962	1.68	-0.05	-1.73
K389963	1.41	0.56	0.85
K389964	0.33	-1.01	0.39
K389965	1.79	0.20	1.66
K389966	0.86	-1.01	0.81
K389967	2.55	-0.03	0.07
K389968	2.30	-1.12	-0.84
K389969	2.49	-1.76	-1.05
K389971	1.05	-1.58	-0.58
K389973	2.17	-0.35	-1.40
K389975	-1.96	0.81	-0.37
K389976	-0.77	0.31	0.51
K389977	-0.02	2.27	-0.82
K389978	2.10	-2.04	-0.52
K389979	-1.72	-0.94	1.74
K389981	1.13	-0.34	-0.80
K389982	1.57	0.17	0.49
K389984	3.56	0.78	1.37
K389985	2.84	1.27	-0.49
K389986	1.83	-0.19	-0.25

Eigenvalues of the principal components extracted from the variance in mafic dyke data:

Analyte	PC1	PC2	PC3
$\delta^{18}\text{O}$	-0.58	-0.03	0.17
$\delta^2\text{H}$	0.50	-0.27	-0.12
H_2O	0.41	-0.48	0.11
Au	-0.75	-0.36	-0.05
C	-0.84	-0.12	0.27
S	-0.58	0.22	-0.59
SiO_2	0.96	0.08	-0.11
Al_2O_3	0.89	0.21	-0.19
K_2O	-0.16	0.67	0.41
Na_2O	0.22	0.47	-0.74
MgO	0.91	-0.04	0.18
Fe_2O_3	0.96	-0.07	0.04
MnO	0.94	-0.08	0.12
CaO	0.87	-0.37	0.05
TiO_2	0.92	0.21	0.02
P_2O_5	0.16	0.72	0.46

Breakdown of total variance explained by select principal components of mafic dyke data:

	%	Cumulative %
PC1	52.53	52.53
PC2	12.00	64.53
PC3	9.38	73.91

Principal components extracted from mafic dyke data:

Sample Number	PC1	PC2	PC3
K389218	-6.89	0.49	0.02
K389006	-5.93	0.25	-0.97
K389010	-3.74	-1.35	1.98
K388025	-1.29	-1.54	-1.55
K389174	-2.68	-1.32	1.20
K388088	-3.66	0.90	-0.91
K388309	-3.05	-1.13	-0.83
K388077	-0.69	-2.28	1.29
K388220	-3.03	1.78	-0.74
K388262	-1.39	-1.54	-0.93

K389150	1.43	-0.30	-1.09
K388039	-1.64	0.81	-0.03
K389329	2.65	-0.94	-0.42
K388244	-0.45	-2.62	1.35
K389077	1.10	-1.75	-1.54
K389344	0.67	-0.80	-0.43
K389514	1.89	0.47	0.92
K388064	-1.98	0.25	2.41
K388108	2.33	-0.58	0.29
K388334	0.73	0.20	0.77
K389353	2.49	0.77	1.02
K388105	0.75	1.69	-2.64
K388120	3.10	-1.04	-1.18
K389183	3.03	0.24	-0.14
K389349	0.60	4.24	-1.04
K388284	-0.09	0.72	-1.80
K389332	4.39	-2.32	-1.69
K389338	-1.45	2.32	1.19
K389337	1.89	0.43	0.63
K389525	4.36	1.36	1.30
K389103	1.85	0.79	0.83
K389423	2.73	1.05	1.21
K389340	1.95	0.75	1.51

Appendix B

Fluid/rock ratio calculations

The following equation has been taken from Taylor (1978). It has been rearranged to solve for the final isotopic (δ -value) composition of a rock after interacting with a fluid in a closed system:

$$(1) \quad \begin{aligned} F/R &= \frac{\delta_{Rock}^f - \delta_{Rock}^i}{\delta_{fluid}^i - (\delta_{Rock}^f - \Delta_{R-F})} \\ \delta_{Rock}^f &= \frac{\delta_{Rock}^i + W/R (\Delta + \delta_{water}^i)}{W/R + 1} \end{aligned}$$

The resulting equation relates the final δ -value of a rock in a closed system given: (1) the initial δ -value of the fluid (δ_{Fluid}^i), (2) the initial δ -value of the rock with which it interacted (δ_{Rock}^i), (3) the fractionation factor between the rock and fluid (Δ_{R-F}), and (4) the atomic fluid/rock ratio for the element in question (F/R).

With respect to an open system of fluid/rock interaction, the following equation is used and rearranged to solve for the final isotopic (δ -value) of the rock after interacting with the fluid. The same terms were used from equation (1):

$$(2) \quad \begin{aligned} F/R &= \ln \left[\frac{\delta_{Fluid}^i + \Delta_{R-F} - \delta_{Rock}^i}{\delta_{fluid}^i - (\delta_{Rock}^f - \Delta_{R-F})} \right] \\ \delta_{Rock}^f &= e^{-F/R} \left[\delta_{Fluid}^i (e^{F/R} - 1) + \Delta_{R-F} (e^{F/R} - 1) + \delta_{Rock}^i \right] \end{aligned}$$

The whole-rock fractionation factor (Δ_{R-F}) has been calculated using standard fractionation equations for the rock's constituent minerals at a given temperature weighed to the typical modal mineralogy of the rock and the mole fraction of the element in each constituent mineral (Chamberlain et al. 1990; Zhao and Zheng 2003):

$$(5) \quad \Delta_{Rock-Fluid} = \sum X_{Mineral} \Delta_{Mineral-Fluid}$$

Where $X_{Mineral}$ is the molar fraction of the minerals comprising the rock in question and $\Delta_{Mineral-Fluid}$ is the fractionation factor between a mineral and fluid at a given temperature.

Taylor HP, 1978, Oxygen and hydrogen isotope studies of plutonic granitic rocks: Earth and Planetary Science Letters, v. 38, p. 177–210, doi: 10.1016/0012-821X(78)90131